

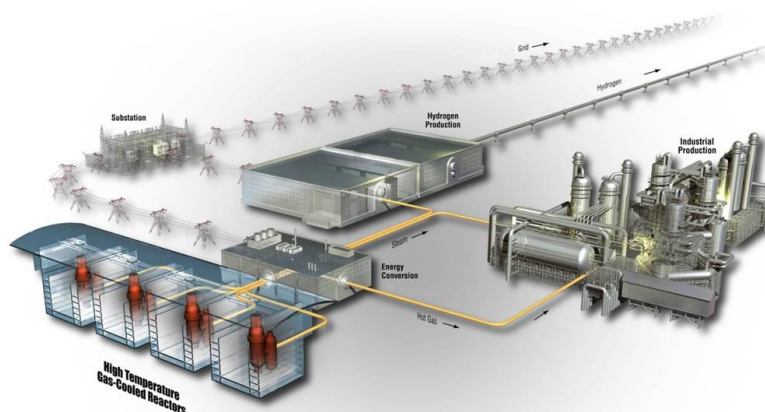


RELAP5-3D Modeling of High Temperature Test Facility Test PG-26

September 2020

Changing the World's Energy Future

Aaron S. Epiney



INL is a U.S. Department of Energy National Laboratory operated by Battelle

DISCLAIMER

This information was prepared as an account of work sponsored by an agency of the U.S. Government. Neither the U.S. Government nor any agency thereof, nor any of their employees, makes any warranty, expressed or implied, or assumes any legal liability or responsibility for the accuracy, completeness, or usefulness, of any information, apparatus, product, or process disclosed, or represents that its use would not infringe privately owned rights. References herein to any specific commercial product, process, or service by trade name, trade mark, manufacturer, or otherwise, does not necessarily constitute or imply its endorsement, recommendation, or favoring by the U.S. Government or any agency thereof. The views and opinions of authors expressed herein do not necessarily state or reflect those of the U.S. Government or any agency thereof.

RELAP5-3D Modeling of High Temperature Test Facility Test PG-26

Aaron S. Epiney

September 2020

**Idaho National Laboratory
Advanced Reactor Technologies
Idaho Falls, Idaho 83415**

<http://www.ART.INL.gov>

**Prepared for the
U.S. Department of Energy
Office of Nuclear Energy
Under DOE Idaho Operations Office
Contract DE-AC07-05ID14517**

INL ART Program

**RELAP5-3D Modeling of High Temperature Test
Facility Test PG-26**

INL/EXT-20-59902

September 2020

Technical Reviewer: (Confirmation of mathematical accuracy, and correctness of data and appropriateness of assumptions.)



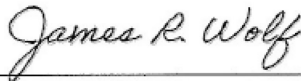
Carlo Parisi

RELAP5-3D Analyst

9/30/2020

Date

Approved by:



James Wolf

RELAP5-3D Program Manager

9/30/2020

Date



Michelle T. Sharp

INL Quality Assurance

9/30/2020

Date

ABSTRACT

The High Temperature Test Facility (HTTF) at Oregon State University (OSU) is a scaled integral effects experiment designed to investigate transient behavior in high-temperature gas-cooled nuclear reactors with prismatic fuel and reflector blocks. Several tests have been completed, and more are still planned to at the HTTF, including depressurized conduction cooldown (DCC) and pressurized conduction cooldown (PCC) transients. This report analyses test PG-26, a progression of the Double Ended Inlet-Outlet Crossover Duct Break transient that is referred to as a DCC. PG-26 has been performed at the HTTF between May 30 and June 30, 2019. Core initial conditions (i.e., before the DCC started) have been met using low power (<100 kW) and two of ten available electric heaters. The DCC transient was initiated during the 50th hour of the test. The break valves were opened, and hot helium from the core and cold helium from the reactor cavity simulation tank (RCST) started mixing. The gases flowed in a countercurrent fashion, where the top half of the hot duct contained hot helium that flowed in one direction and cold helium that flowed in the other direction in the bottom half of the duct. After the pressure and density reached equilibrium, the event entered a diffusion mode. The onset of a reverse natural circulation was not observed during the DCC period of the test.

Version 4.4.2ie of the RELAP5-3D computer code has been used to model the HTTF PG-26 test, and results have been compared to available high-quality measured data. The model used in this study is the quality-controlled HTTF RELAP5-3D model (HTTF base 2018-04-19 QA), originally developed by P. Bayless. The report includes RELAP5-3D results of the “base calculations” as well as some sensitivities to important uncertain model inputs, such as primary helium mass flow rate, core ceramic thermal properties, as well as heat evacuation and loop friction models.

Using the base RELAP5-3D model predicts a countercurrent helium flow in the hot duct observed at the beginning of the DCC, but instead of going into a molecular diffusion mode, the model predicts the onset of natural convection. Increasing friction in the core and hot duct prevents the natural convection from happening in some of the simulations. Although some temperatures are well predicted (and even overpredicted), the general tendency is to underpredict the ceramic and helium temperatures and heat removal rates during the DCC, resulting in many of the assessment findings being in minimal or insufficient agreement with the data. It is worth noting that the described discrepancies between measured data and RELAP5-3D predictions are not RELAP5-3D code limitations. More so, they reflect limitations in boundary condition and thermal property knowledge. While the RELAP5-3D calculations of the test provide some insights into what happens during the transient, and point to missing or potentially uncertain data to which the experimenters can direct their attention, the principal conclusion is that the PG-26 test data are insufficient for a system code assessment.

ACKNOWLEDGEMENTS

The author would like to thank the following people:

- Paul Bayless, retired INL thermal-hydraulics engineer, for his discussions and explanations of the quality-controlled HTTF RELAP-3D model that he originally developed and allowed me to use.
- Brian Woods, professor at Oregon State University and principal investigator for the HTTF as well as Tommy Moore, one of the HTTF operators present during the PG-26 test, for their insightful discussions and explanations of the HTTF facility and the different phenomena happening during the PG-26 test.

CONTENTS

ABSTRACT.....	iv
ACKNOWLEDGEMENTS.....	vi
ACRONYMS.....	xiv
1. Introduction.....	1
2. Experiment Facility and Test Description.....	2
2.1 High Temperature Test Facility	2
2.2 Test PG-26	3
2.2.1 Facility Initial State.....	4
2.2.2 Heater Power.....	4
2.2.3 Steam Generator.....	6
2.2.4 Reactor Cavity Cooling System.....	7
2.2.5 Depressurized Conduction Cooldown Transient Implementation	8
2.2.6 Helium Pressure Evolution	8
2.2.7 Temperature Evolution	9
3. Computer Code and Input Model Description	11
3.1 RELAP5-3D.....	11
3.2 HTTF Input Model.....	11
3.3 Automation Tools	16
3.3.1 Initial and Boundary Conditions	16
3.3.2 Postprocessing and Plotting	17
4. Simulations.....	18
4.1 Assessment Criteria.....	19
4.2 Helium Mass Flow	20
4.3 Base Case Simulations.....	21
4.3.1 Steady State + DCC	22
4.3.2 Whole Transient.....	34
4.4 Sensitivity Studies.....	43
4.4.1 Core Ceramic Thermal Properties.....	43
4.4.2 RCCS Heat Evacuation.....	48
4.4.3 Primary Loop Helium Friction.....	49
5. Conclusions.....	51
6. References.....	53

FIGURES

Figure 1. Diagram of the HTTF primary pressure vessel (right), RCST, and hot and cold ducts.	3
Figure 2. Core heater bank locations.	5
Figure 3. Measured heater power for the two heat banks used, bank 104 and 110. Note that the vertical line in the power of bank 110 at ~150,000 is an artefact.	6
Figure 4. Measured steam generator water level.	6
Figure 5. Measured RCCS water flow rate.	7
Figure 6. Measured RCCS inlet and outlet water temperatures.	7
Figure 7. Measured PCS and RCST pressure evolution.	9
Figure 8. Measured core ceramic (midcore around the inner and outer fuel rings) and helium (in the upper and lower part of the hot and cold ducts) temperatures.	9
Figure 9. Measured thermal stratification of helium in the lower (outlet) plenum.	10
Figure 10. Primary pressure vessel nodalization.	12
Figure 11. Primary pressure vessel radial nodalization.	13
Figure 12. Core ring layout.	13
Figure 13. Nodalization of components outside the primary pressure vessel.	16
Figure 14. Heater 110 power boundary condition: Measured data from PG-26, smoothed data, and resampled points input in the RELAP5-3D model.	18
Figure 15. Helium circulator performance curve at nominal speed (theoretical value in black and measured values in red): PSIG vs. ICFM.	20
Figure 16. DCC only, 5 g/s helium mass flow: left) core heat balance and right) core helium ΔT	25
Figure 17. DCC only, 10 g/s helium mass flow: left) core heat balance and right) core helium ΔT	25
Figure 18. DCC only, 15 g/s helium mass flow: left) Core heat balance and right) core helium ΔT	25
Figure 19. DCC only, 5 g/s helium mass flow: left) PCS helium mass flow rates and right) PCS and RCST pressure.	26
Figure 20. DCC only, 10 g/s helium mass flow: left) PCS helium mass flow rates and right) PCS and RCST pressure.	26
Figure 21. DCC only, 15 g/s helium mass flow: left) PCS helium mass flow rates and right) PCS and RCST pressure.	26
Figure 22. DCC only, 5 g/s helium mass flow: left) helium core inlet temperatures and right) helium core outlet temperatures.	27
Figure 23. DCC only, 10 g/s helium mass flow: left) helium core inlet temperatures and right) helium core outlet temperatures.	27
Figure 24. DCC only, 15 g/s helium mass flow: left) helium core inlet temperatures and right) helium core outlet temperatures.	27
Figure 25. DCC only, 5 g/s helium mass flow, top of the core (block 7): upper left) helium coolant temperatures, upper right) central reflector ceramic temperatures, lower left)	

ceramic temperatures in the fuel region, and lower right) side and permanent ceramic temperatures.....	28
Figure 26. DCC only, 10 g/s helium mass flow, top of the core (block 7): upper left) helium coolant temperatures, upper right) central reflector ceramic temperatures, lower left) ceramic temperatures in the fuel region, and lower right) side and permanent ceramic temperatures.....	28
Figure 27. DCC only, 15 g/s helium mass flow, top of the core (block 7): upper left) helium coolant temperatures, upper right) central reflector ceramic temperatures, lower left) ceramic temperatures in the fuel region, and lower right) side and permanent ceramic temperatures.....	29
Figure 28. DCC only, 5 g/s helium mass flow, middle of the core (block 5): upper left) helium coolant temperatures, upper right) central reflector ceramic temperatures, lower left) ceramic temperatures in the fuel region, and lower right) side and permanent ceramic temperatures.....	29
Figure 29. DCC only, 10 g/s helium mass flow, middle of the core (block 5): upper left) helium coolant temperatures, upper right) central reflector ceramic temperatures, lower left) ceramic temperatures in the fuel region, and lower right) side and permanent ceramic temperatures.....	30
Figure 30. DCC only, 15 g/s helium mass flow, middle of the core (block 5): upper left) helium coolant temperatures, upper right) central reflector ceramic temperatures, lower left) ceramic temperatures in the fuel region, and lower right) side and permanent ceramic temperatures.....	30
Figure 31. DCC only, 5 g/s helium mass flow, bottom of the core (block 3): upper left) helium coolant temperatures, upper right) central reflector ceramic temperatures, lower left) ceramic temperatures in the fuel region, and lower right) side and permanent ceramic temperatures.....	31
Figure 32. DCC only, 10 g/s helium mass flow, bottom of the core (block 3): upper left) helium coolant temperatures, upper right) central reflector ceramic temperatures, lower left) ceramic temperatures in the fuel region, and lower right) side and permanent ceramic temperatures.....	31
Figure 33. DCC only, 15 g/s helium mass flow, bottom of the core (block 3): upper left) helium coolant temperatures, upper right) central reflector ceramic temperatures, lower left) ceramic temperatures in the fuel region, and lower right) side and permanent ceramic temperatures.....	32
Figure 34. Whole transient, 5 g/s helium mass flow: left) core heat balance and right) core helium ΔT	35
Figure 35. Whole transient, 10 g/s helium mass flow: left) core heat balance and right) core helium ΔT	35
Figure 36. Whole transient, 15 g/s helium mass flow: left) core heat balance and right) core helium ΔT	35
Figure 37. Whole transient, 5 g/s helium mass flow: left) PCS helium mass flow rates and right) PCS and RCST pressure.	36
Figure 38. Whole transient, 10 g/s helium mass flow: left) PCS helium mass flow rates and right) PCS and RCST pressure.	36

Figure 39. Whole transient, 15 g/s helium mass flow: left) PCS helium mass flow rates and right) PCS and RCST pressure.	36
Figure 40. Whole transient, 5 g/s helium mass flow: left) helium core inlet temperatures and right) helium core outlet temperatures.	37
Figure 41. Whole transient, 10 g/s helium mass flow: left) helium core inlet temperatures and right) helium core outlet temperatures.	37
Figure 42. Whole transient, 15 g/s helium mass flow: left) helium core inlet temperatures and right) helium core outlet temperatures.	37
Figure 43. Whole transient, 5 g/s helium mass flow, top of the core (block 7): upper left) helium coolant temperatures, upper right) central reflector ceramic temperatures, lower left) ceramic temperatures in the fuel region, and lower right) side and permanent ceramic temperatures.	38
Figure 44. Whole transient, 10 g/s helium mass flow, top of the core (block 7): upper left) helium coolant temperatures, upper right) central reflector ceramic temperatures, lower left) ceramic temperatures in the fuel region, and lower right) side and permanent ceramic temperatures.	38
Figure 45. Whole transient, 15 g/s helium mass flow, top of the core (block 7): upper left) helium coolant temperatures, upper right) central reflector ceramic temperatures, lower left) ceramic temperatures in the fuel region, and lower right) side and permanent ceramic temperatures.	39
Figure 46. Whole transient, 5 g/s helium mass flow, middle of the core (block 5): upper left) helium coolant temperatures, upper right) central reflector ceramic temperatures, lower left) ceramic temperatures in the fuel region, and lower right) side and permanent ceramic temperatures.	39
Figure 47. Whole transient, 10 g/s helium mass flow, middle of the core (block 5): upper left) helium coolant temperatures, upper right) central reflector ceramic temperatures, lower left) ceramic temperatures in the fuel region, and lower right) side and permanent ceramic temperatures.	40
Figure 48. Whole transient, 15 g/s helium mass flow, middle of the core (block 5): upper left) helium coolant temperatures, upper right) central reflector ceramic temperatures, lower left) ceramic temperatures in the fuel region, and lower right) side and permanent ceramic temperatures.	40
Figure 49. Whole transient, 5 g/s helium mass flow, bottom of the core (block 3): upper left) helium coolant temperatures, upper right) central reflector ceramic temperatures, lower left) ceramic temperatures in the fuel region, and lower right) side and permanent ceramic temperatures.	41
Figure 50. Whole transient, 10 g/s helium mass flow, bottom of the core (block 3): upper left) helium coolant temperatures, upper right) central reflector ceramic temperatures, lower left) ceramic temperatures in the fuel region, and lower right) side and permanent ceramic temperatures.	41
Figure 51. Whole transient, 15 g/s helium mass flow, bottom of the core (block 3): upper left) helium coolant temperatures, upper right) central reflector ceramic temperatures, lower left) ceramic temperatures in the fuel region, and lower right) side and permanent ceramic temperatures.	42

Figure 52. Whole transient, 15 g/s helium mass flow, PCS helium mass flow rates : upper left) original c_p and λ , upper right) 1/10 c_p and original λ , lower left) original c_p and 1/5 λ , and lower right) 1/10 c_p and 1/5 λ	45
Figure 53. Whole transient, 15 g/s helium mass flow, PCS and RCST pressure : upper left) original c_p and λ , upper right) 1/10 c_p and original λ , lower left) original c_p and 1/5 λ , and lower right) 1/10 c_p and 1/5 λ	45
Figure 54. Whole transient, 15 g/s helium mass flow, middle of the core (block 5) helium coolant temperatures : upper left) original c_p and λ , upper right) 1/10 c_p and original λ , lower left) original c_p and 1/5 λ , and lower right) 1/10 c_p and 1/5 λ	46
Figure 55. Whole transient, 15 g/s helium mass flow, middle of the core (block 5) central reflector ceramic temperatures : upper left) original c_p and λ , upper right) 1/10 c_p and original λ , lower left) original c_p and 1/5 λ , and lower right) 1/10 c_p and 1/5 λ	46
Figure 56. Whole transient, 15 g/s helium mass flow, middle of the core (block 5) ceramic temperatures in the fuel region : upper left) original c_p and λ , upper right) 1/10 c_p and original λ , lower left) original c_p and 1/5 λ , and lower right) 1/10 c_p and 1/5 λ	47
Figure 57. Whole transient, 15 g/s helium mass flow, middle of the core (block 5) side and permanent ceramic temperatures : upper left) original c_p and λ , upper right) 1/10 c_p and original λ , lower left) original c_p and 1/5 λ , and lower right) 1/10 c_p and 1/5 λ	47
Figure 58. Whole transient, 15 g/s helium mass flow, RCCS mass flow : left) base case and right) “no RCCS” case.	48
Figure 59. Whole transient, 15 g/s helium mass flow, helium core inlet temperatures : left) base case and right) “no RCCS” case.	49
Figure 60. Whole transient, 15 g/s helium mass flow, middle of the core (block 5) ceramic temperatures in the fuel region : left) base case and right) “no RCCS” case.	49
Figure 61. Whole transient, 5 g/s helium mass flow, core pressure drops : left) base case and right) “more friction” case.	50
Figure 62. Whole transient, 5 g/s helium mass flow, PCS helium mass flow rates : left) base case and right) “more friction” case.	50
Figure 63. Whole transient, 5 g/s helium mass flow, middle of the core (block 5) helium coolant temperatures : left) base case and right) “more friction” case.	50
Figure 64. Whole transient, 15 g/s helium mass flow, core pressure drops : left) base case and right) “more friction” case.	51
Figure 65. Whole transient, 15 g/s helium mass flow, PCS helium mass flow rates : left) base case and right) “more friction” case.	51
Figure 66. Whole transient, 15 g/s helium mass flow, middle of the core (block 5) helium coolant temperatures : left) base case and right) “more friction” case.	51

TABLES

Table 1. Main events of the test.	4
Table 2. Steady-state temperatures (all temperatures in [K]) for the RELAP5-3D calculations with 5, 10, and 15 g/s primary helium mass flow rate compared to the measured data of test PG-26 at 179,500 s.	24
Table 3. Steady state + DCC: qualitative trends for the ceramic temperatures in the core.....	32
Table 4. Whole transient: qualitative trends for the ceramic temperatures in the core.....	42
Table 5. Core ceramic thermal property sensitivity cases.....	44

ACRONYMS

DCC	Depressurized Conduction Cooldown
HTTF	High Temperature Test Facility
ICFM	Inlet Cubic Feet per Minute
INL	Idaho National Laboratory
MHTGR	Modular High Temperature Gas-cooled Reactor
OSU	Oregon State University
PCC	Pressurized Conduction Cooldown
PCS	Primary Coolant System
PSIG	Pound-per-Square-Inch Gauge
RCCS	Reactor Cavity Cooling System
RCST	Reactor Cavity Simulation Tank
RELAP	Reactor Excursion and Leak Analysis Program
SCS	Secondary Coolant System

RELAP5-3D Modeling of High Temperature Test Facility Test PG-26

1. Introduction

The High Temperature Test Facility (HTTF) at Oregon State University (OSU) is a scaled integral effects experiment designed to investigate transient behavior in high-temperature gas-cooled nuclear reactors with prismatic fuel and reflector blocks [1]. It is a one-quarter-scale model of the General Atomics' Modular High Temperature Gas-cooled Reactor (MHTGR). The nominal working fluid is helium; however, other gases can be used as well. The ceramic core can be electrically heated with a heater power of maximum 600 kW. The facility is configured to simulate a variety of postulated accident and normal operations events in the MHTGR. The facility was primarily built to produce data for code and model validation that includes the main physics and phenomena happening during MHTGR transients but does not exactly reproduce MHTGR conditions (temperature and pressure distributions, etc.).

Several tests have been completed, and more are still planned to at the HTTF, including depressurized conduction cooldown (DCC) and pressurized conduction cooldown (PCC) transients. This report analyses test PG-26 using the RELAP5-3D system code [2]. The PG-26 test is a progression of the Double Ended Inlet-Outlet Crossover Duct Break transient [3]. This test is referred to as a DCC. Core initial conditions (i.e., before the DCC started) have been met using low power (<100 kW) and two of ten available heaters. Transient decay power during the DCC has been scaled to the MHTGR. The heaters were operated during hours 1 through 59 of the test. Heater banks 104 and 110 were operated, where the power output reached a peak of ~30 kW during the DCC. The desired peak power was not reached as the ceramic heat-up limits were being exceeded. During the test, the reactor cavity cooling system (RCCS) began operation during the 26th hour of the test and was operated continuously, barring one mechanical issue during the 35th hour. The RCCS tank fill valve failed to work and had to be replaced. During the test, the steam generator level was maintained between 60% and 80%. Produced steam started venting to the atmosphere outside the HTTF building approximately 32 hours into the test. The DCC transient was initiated during the 50th hour of the test. The break valves were opened, and hot helium from the core and cold helium from the reactor cavity simulation tank (RCST) started mixing. The gases flowed in a countercurrent fashion, where the top half of the hot duct contained hot helium that flowed in one direction and cold helium that flowed in the other direction in the bottom half of the duct. After the pressure and density reached equilibrium, the event entered a diffusion mode. The onset of a reverse natural circulation was not observed during the DCC period of the test. The PG-26 test began on May 30, 2019 and was completed on June 30, 2019.

Version 4.4.2ie of the RELAP5-3D computer code has been used to model the HTTF PG-26 test, and results have been compared to available high-quality measured data. A RELAP5-3D input model has been developed for the HTTF. The model includes hydrodynamic components, heat structures, trips, and control systems. The model used in this study is the quality-controlled HTTF RELAP5-3D model (HTTF base 2018-04-19 QA) developed by P. Bayless [4].

Section 2 provides a more detailed description of the HTTF facility and test PG-26. A brief description of the RELAP5-3D code and a more detailed description of the HTTF input model are provided in Section 3. Code predictions of significant parameters in the system are presented in Section 4. This section includes RELAP5-3D results of the “base calculations” as well as some sensitivities to important uncertain model inputs. Section 5 summarizes the results and presents the conclusions of the study. References are listed in Section 6.

2. Experiment Facility and Test Description

An overview of the HTTF is provided in the next section, followed by a detailed description of HTTF test PG-26.

2.1 High Temperature Test Facility

The HTTF is a helium-cooled, electrically heated integral experiment facility. The reference design for the facility is General Atomics' MHTGR [5], which uses prismatic graphite blocks in the core and reflectors. The HTTF primary pressure vessel and core are one-fourth scale in length and diameter. Most of the coolant channels in the core are full scale, with smaller diameter channels around the core periphery. The facility operates at low pressure, compared to the prototype reactor, and is designed primarily to investigate DCC transients.

The facility, described in detail in Brian Woods "OSU High Temperature Test Facility Technical Design Report" [1], includes several systems. The primary coolant system (PCS) has a pressure vessel, a concentric hot and cold duct, a steam generator, a gas circulator, and connecting pipes. Break valves in both the hot and cold legs connect to a large RCST, whose gas composition can be initialized to a range of values to simulate the different conditions that may exist outside the reactor vessel following a loss-of-coolant accident. Figure 1 presents a rendering of the primary pressure vessel, RCST, and hot and cold ducts.

Alumina ceramic blocks are used to simulate the core and top and bottom reflectors. Each block encompasses the radial region occupied by the central reflector, fuel, and side reflector in the MHTGR. Holes in the blocks provide channels for the heater rods, which consist of stacks of graphite rodlets. The rods are grouped into ten heater banks, each of which contains 21 heater rods. Smaller coolant holes are arranged in a hexagonal pattern around the heater rods. Larger holes cast in the central and side reflector regions represent the core bypass flow in these regions. Permanent or outer reflector blocks, made of a different ceramic material, are located between the core blocks and the core barrel. A graphite plate in the upper plenum covers the gaps on either side of the permanent reflector blocks so that the only flow through the core is in the holes cast in the core blocks.

The steam generator has 188 U-tubes. Feedwater is pumped from a supply tank into the downcomer on the secondary side, and any steam generated is vented to the atmosphere.

The principal feature of the RCCS is the cooling panels that surround the pressure vessel. Water flowing through the panels provides the heat sink for the PCS during most transients. Water is pumped from the same tank as the steam generator feedwater but is recirculated back to the tank after exiting the top of the cooling panels. The inlet flow can be controlled to provide a desired panel outlet temperature, and isolation valves on the panels can be closed to simulate a degraded heat sink. There is a cover above the space between the pressure vessel and the RCCS panels so that there is no direct natural circulation path between the building and the pressure vessel to provide unwanted cooling.

Two additional break lines are available, from the top of the primary pressure vessel to the top of the RCST and from the bottom of the pressure vessel to the bottom of the RCST.

The facility has over 500 instruments, which are described in Stephen Louria, "Instrumentation Plan for the OSU High Temperature Test Facility, Revision 4" [6]. Most of these are thermocouples in the core region to provide a temperature profile of the ceramic. There are also vertical thermocouple rakes in the upper and lower plenums and in the hot and cold ducts, to capture temperature variations associated with recirculating or unmixed flow streams. The core and reflector instrumentation are generally arranged in one-sixth azimuthal sectors. The primary measurement sector is opposite the outlet plenum connection to the hot duct (on the east side of the plenum), the secondary sector is adjacent to the hot duct (west side), and the tertiary sector is next to (south of) the secondary sector.

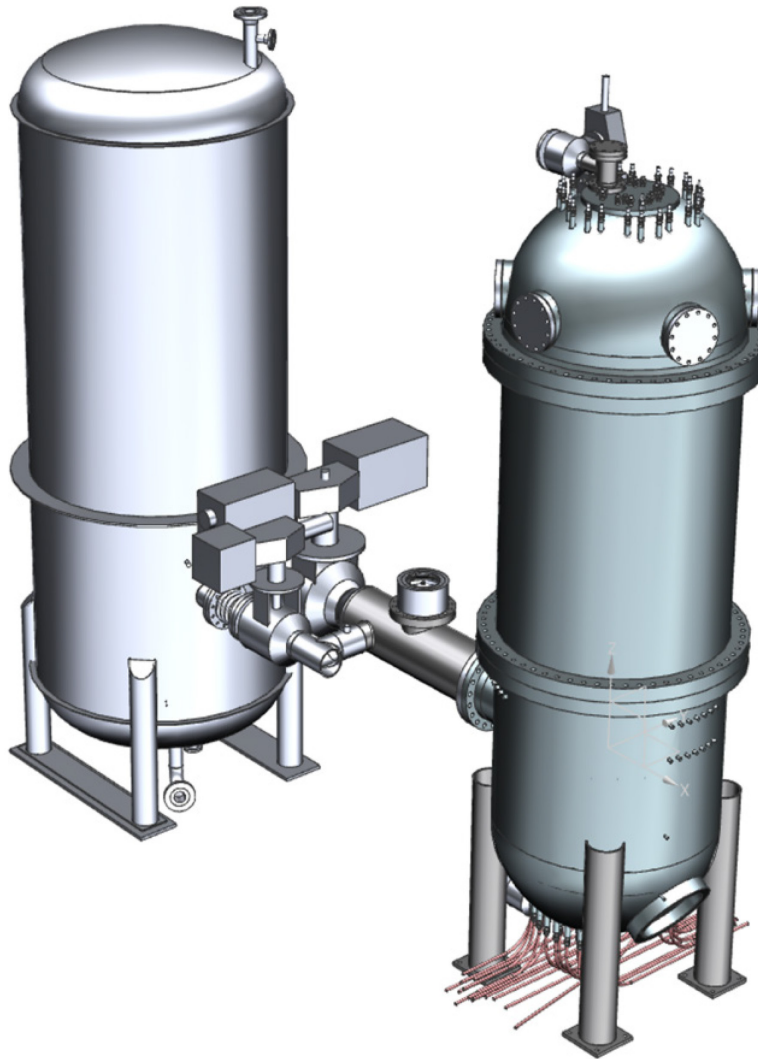


Figure 1. Diagram of the HTTF primary pressure vessel (right), RCST, and hot and cold ducts.

2.2 Test PG-26

Test PG-26 is a DCC transient that has been performed in the HTTF facility between May 30th, 2019 and June 3rd, 2019. The test is described in detail in Seth R. Cadell, “PG-26 Low Power (<350kW) Double Ended Inlet-Outlet Crossover Duct Break, 2 Heaters” [3], while this section provides a short summary. A core heat-up before the DCC has been performed using two electrical heaters at low power (i.e., a maximum of ~30 kW for 50 hours). Other than one valve failure, the facility heat-up went as expected. The DCC was initiated in the 50th hour of the test by opening the two break valves in the hot and cold ducts connecting the ducts to the RCST. The ceramics heated up quickly, and the simulated decay heat power levels were reduced to adhere to the heat-up limits of the ceramics. Additionally, the ceramics reached temperatures of near 1700 K where the thermocouples began failing, and, again, the heater power was reduced first to 26 kW and then to 22 kW. In the 59th hour, heater 110 quit operation. To limit any distortions from asymmetric heating, the other heater, 104, was shut off and secured as well. The facility cooled down, and data was collected until the 72nd hour. Table 1 summarizes the main events of the test.

Table 1. Main events of the test.

Date	Time in test [s]	Event
5/30/2019 18:19:18	0	Data acquisition started
5/30/2019 18:26:40	442	Helium circulator started
5/30/2019 18:31:33	735	Heater (core heat-up) started
5/31/2019 20:34:02	94,484	RCCS water pump started
6/1/2019 20:12:45	179,607	RCST pressure reduced
6/1/2019 20:18:41	179,963	PCS pressure reduced
6/1/2019 20:22:28	180,190	Helium circulator stopped
6/1/2019 20:23:11	180,233	DCC break valves opened
6/2/2019 17:31:46	256,348	Heaters shut off
6/2/2019 19:17:45	262,707	Data acquisition ended

2.2.1 Facility Initial State

Before the start of the test (i.e., prior to the data acquisition system start), the HTTF facility has been conditioned as follows:

- **Initial core temperature:** The ceramic core blocks take a long time to completely cool down to room temperature. To avoid having to wait unreasonably long times between tests, a new test can be started before the core blocks are completely cooled down. At the start of PG-26, the core ceramics were at around 400 K.
- **Pressure:** The PCS was pressurized to a little more than 2 bar with helium, while the RCST was pressurized to slightly above 1.3 bar, also using helium.
- **Cooling systems:** The cooling water system, including the RCCS tank and RCCS panels, were filled with water at an ambient pressure. The steam generator was filled with water to about 65%.
- **Flows:** All flows (i.e., primary helium as well as cooling water) were set to zero.

2.2.2 Heater Power

As mentioned, for PG-26, two electric heaters (104 and 110) in the facility were used to preheat the core for the first 50 hours of the test and, when the DCC was initiated, to simulate the scaled MHTGR decay heat. The heaters were run through hour 59 of the test, before heater 110 failed and heater 104 was shut off. It is worth noting that heater numberings have changed after to previous tests. Figure 2 shows the location of the two heater banks in the facility.

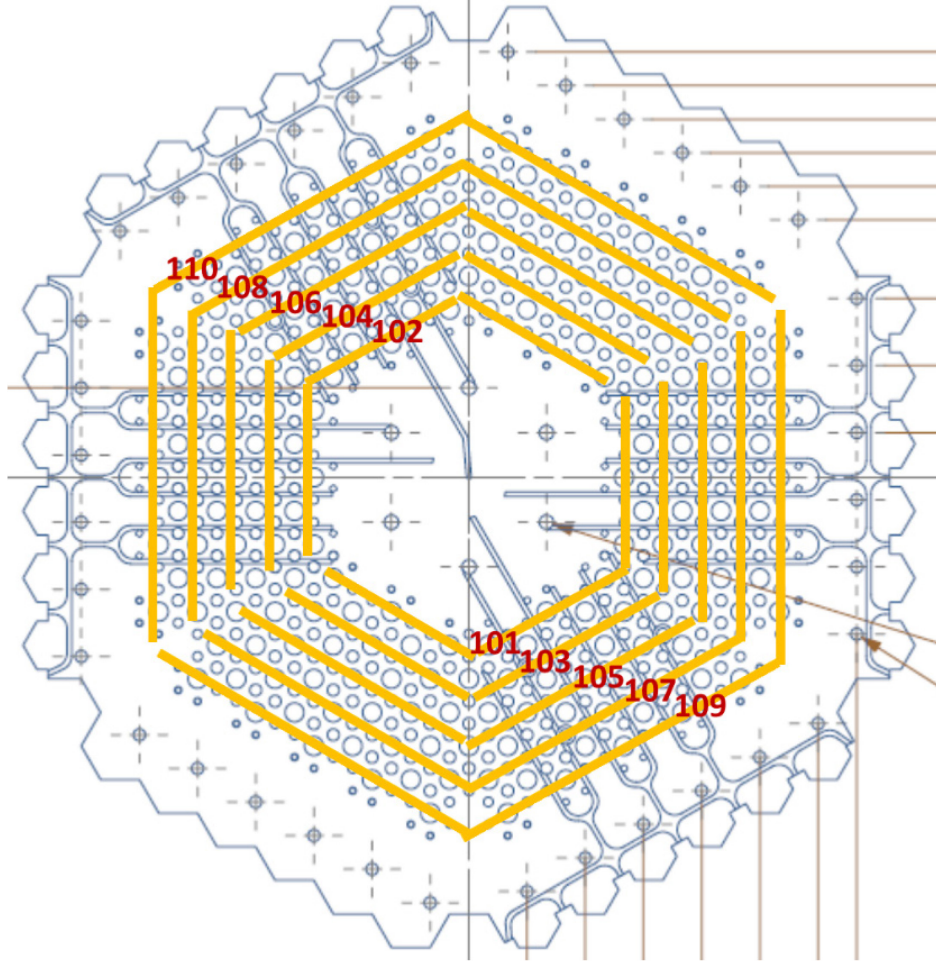


Figure 2. Core heater bank locations.

The HTTF heaters are not equipped to automatically follow a desired power history; instead, operators must manually control them while looking at available output readings. The heater power for each bank can be computed from the measured readings as follows:

$$p^{bank} [W] = C_{leg1}^{bank} V_{leg1}^{bank} + C_{leg2}^{bank} V_{leg2}^{bank}$$

where C_{legi}^{bank} is the current for the two legs ($i = 1$ and 2) in each heater bank and V_{legi}^{bank} is the voltage for the two legs ($i = 1$ and 2) in each heater bank.

The instrument labels for the current and voltage measurements for heaters 104 and 110 are as follows:

- **Heater 104:** CT-1041 and CT-1042 for the two current transducers, and VT-1041 and VT-1042 for the two voltage transducers for the two legs of heater bank 104.
- **Heater 110:** CT-1001 and CT-1002 for the two current transducers, and VT-1001 and VT-1002 for the two voltage transducers for the two legs of heater bank 110.

Figure 3 shows the heater power during the test for both heater banks used. Note that the desired peak power was not reached, as the ceramic heat-up limits were being exceeded, and power was manually reduced during the DCC period of the test.

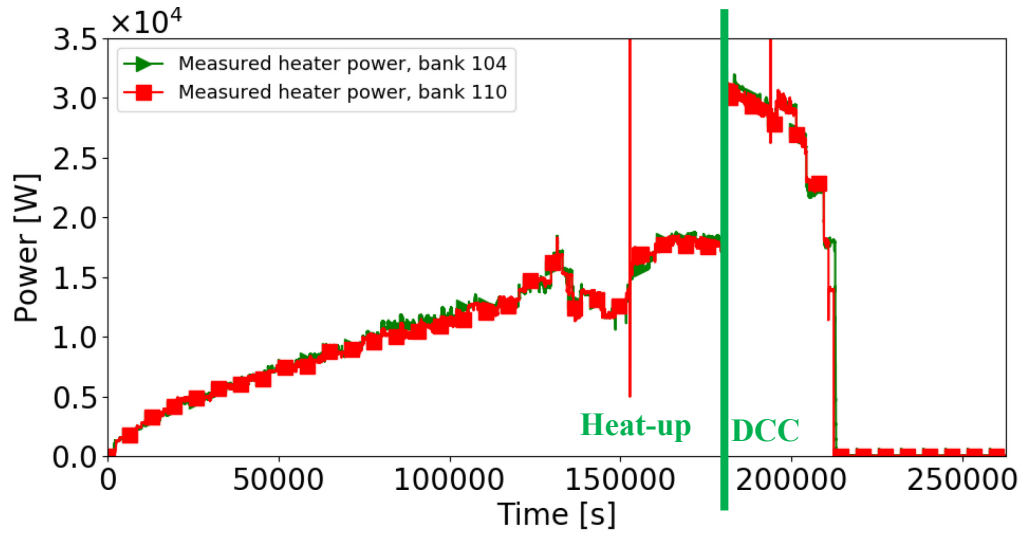


Figure 3. Measured heater power for the two heat banks used, bank 104 and 110. Note that the vertical line in the power of bank 110 at ~150,000 is an artefact.

2.2.3 Steam Generator

As mentioned, the steam generator was filled to ~65% with water at an ambient pressure and temperature prior to the test. During the test, water was added to keep the level between 60–80%. Figure 4 shows the steam generator level during the test. Around hour 32 of the test, the steam generator started venting steam to the atmosphere. After the DCC was initiated, there was no more helium flowing through the primary loop, and the steam generator was cooling down.

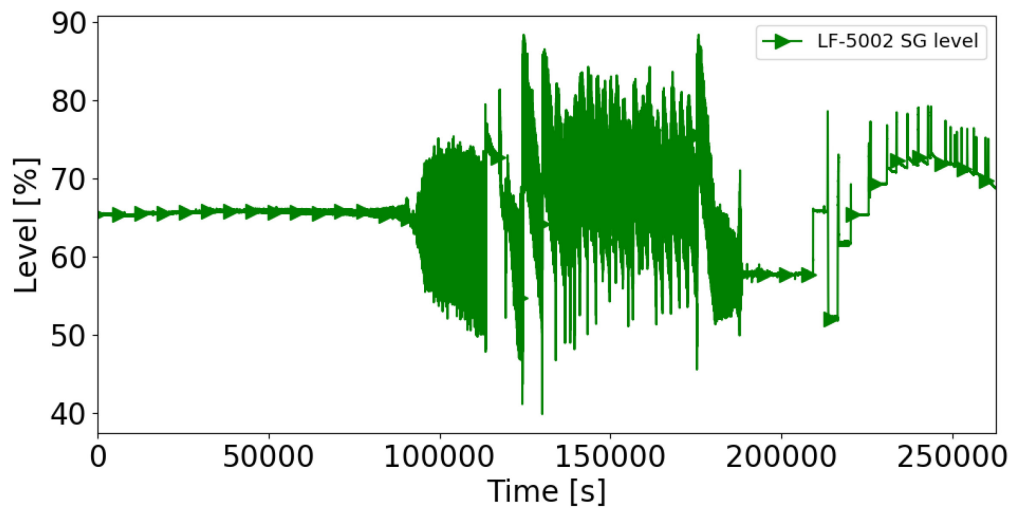


Figure 4. Measured steam generator water level.

2.2.4 Reactor Cavity Cooling System

The RCCS was activated 26 hours into the test. During the 35th hour of the test, the RCCS tank fill valve failed and had to be replaced. To perform that repair, the RCCS tank and cooling panels were drained, the valve replaced, and the RCCS tank and panels refilled. The repair took a little over an hour. After the repair, the RCCS was operated through the remainder of the test, including the DCC transient. Figure 5 shows the RCCS water flow rate, and Figure 6 shows the RCCS inlet and outlet water temperatures. One can see that the water temperature difference over the RCCS is very small during the whole test, indicating that nearly no heat is evacuated by the RCCS. However, during the test, a lot of the heat goes into heating up the core ceramics and vessel metal. The natural convection inside the cavity between the vessel and the RCCS panels is probably a large contributor to heat removal off the vessel wall (not measured), and air inside that cavity can escape since it is not airtight. This leads to a limited knowledge of heat escaping the system through the vessel wall during the test.

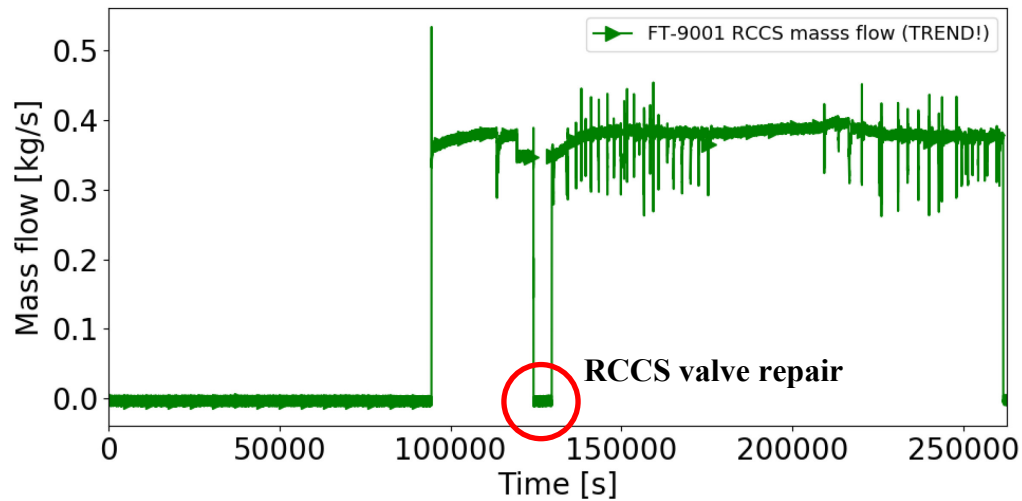


Figure 5. Measured RCCS water flow rate.

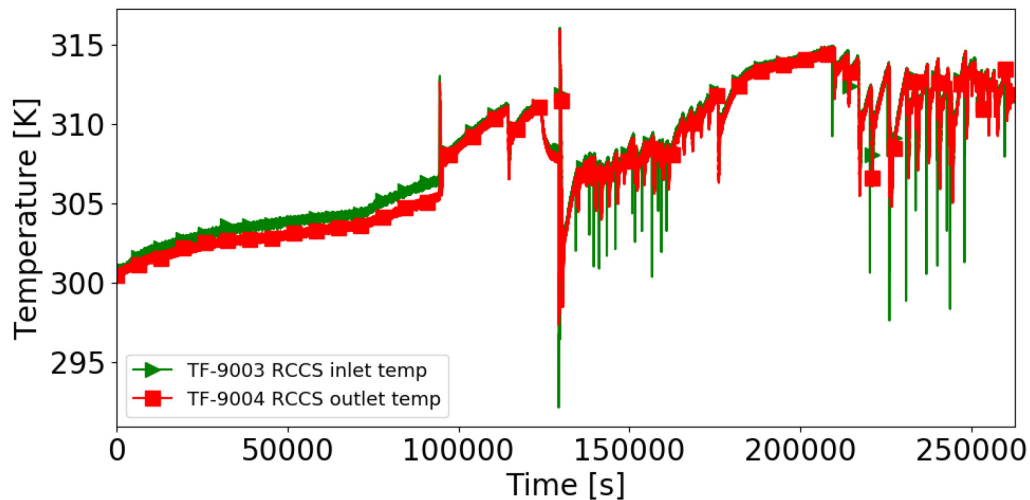


Figure 6. Measured RCCS inlet and outlet water temperatures.

2.2.5 Depressurized Conduction Cooldown Transient Implementation

The core was heated to operating temperatures (i.e., a core average temperature between 820 K and 860 K and a core peak temperature between 1080 K and 1090 K). Before the DCC transient was initiated, the core was kept in a state respecting these conditions for at least 2 hours. Additionally, during this time, no measured temperature channel increased at a rate bigger than 10 K/h. The implementation of the DCC started on June 1, 2019 at 20:12 hours, following the DCC sequence:

- The pressure in the RCST was decreased to a value between 1.05 and 1.07 bar by manually opening the RCST vent valve.
- The PCS pressure was decreased to a value between 1.07 and 1.09 bar by manually opening the primary vent valve.
- The primary helium circulator was stopped.
- Finally, the break valves connecting the hot and cold ducts to the RCST were opened at 20:23 hours on June 1, 2019.
- Once the break valves are open, the two HTTF heaters used to preheat the core followed a scaled MHTGR decay heat curve. During the decay heat transient, the power was decreased manually twice because the limits on the ceramic heat-up rate were reached.

2.2.6 Helium Pressure Evolution

Figure 7 shows the PCS and RCST pressure evolution during the entire test (i.e., the heat-up and the DCC phase). The following observations can be made:

- There was a small helium leak from the PCS into the RCST during the heat-up phase of the test (see the rise of RCST pressure during heat-up in Figure 7). To keep the pressure in the PCS somewhat constant, cold helium from helium bottles was periodically injected by the operators (see the sawtooth behavior of PCS pressure during heat-up in Figure 7). While attempting to reseal the leaking valve between the PCS and RCST, the operators over-pressured the primary loop at one point during the transient for a short period of time and subsequently blew down the overpressure into the RCST manually. One can see the helium blowdown from the PCS led to a sudden increase in pressure in the RCST. After the blowdown finished, the pressure in the RCST still increased but at a much slower rate than before, indicating that the operators' actions reduced the leakage.
- Before the DCC starts (i.e., before the break valves are opened that connect the primary pressure vessel with the RCST), the manual blowdown of pressure in the PCS and RCST to about 1 bar can be seen in Figure 7. One can also see the common evolution of the PCS and RCST pressures after the break valves are opened. The slow pressure swing of the helium is due to the heat up from the simulated decay heat and then, after the heaters have been shut off, it is due to the slow cooldown of the gas.

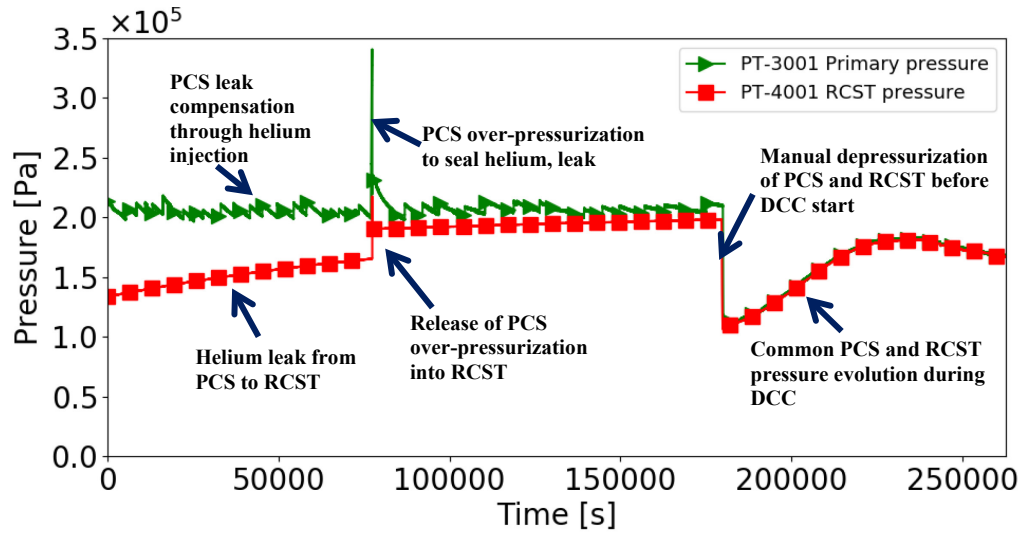


Figure 7. Measured PCS and RCST pressure evolution.

2.2.7 Temperature Evolution

Figure 8 shows the temperature evolution during PG-26 for selected measurement channels. The figure shows a) the core ceramic temperatures at the midcore axial level (core block 5) in the regions of the inner and outer fuel rings, b) the helium core outlet temperature in the upper and lower parts of the hot duct, and c) the helium core inlet temperature in the upper and lower parts of the cold duct.

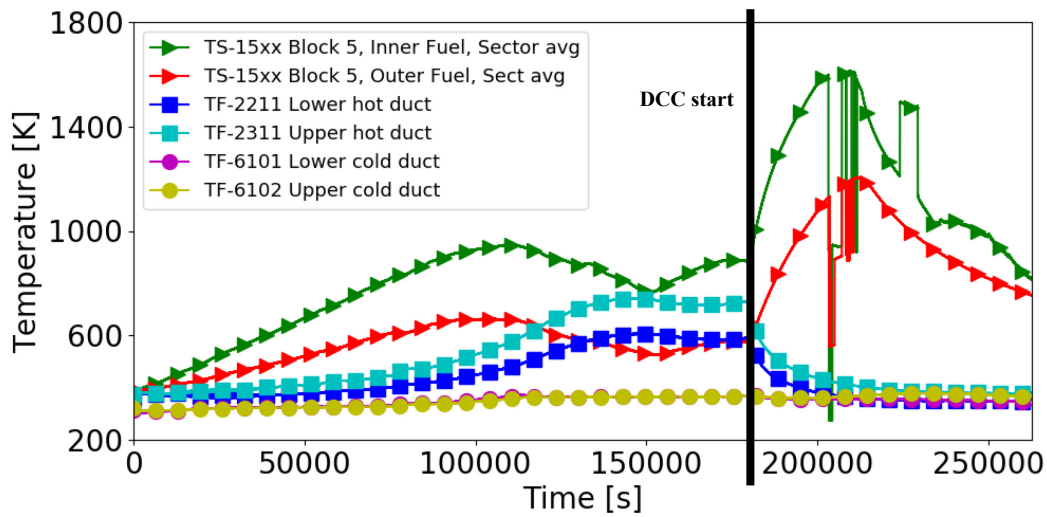


Figure 8. Measured core ceramic (midcore around the inner and outer fuel rings) and helium (in the upper and lower part of the hot and cold ducts) temperatures.

From Figure 8, the following observations can be made:

- The core ceramic temperatures go down during the core heat-up from $\sim 120,000$ s to $150,000$ s. This is due to the steam generator behavior and heater power. The steam generator started producing steam around $80,000$ s and pressurized up to about $110,000$ s. At that time, the steam generator pressure was reduced, and the inventory was refilled with cold city water. This reduced the steam generator temperature, which stabilized the core inlet gas temperature. From the start of the test to $\sim 110,000$ s, the cold duct temperature rises steadily from ~ 300 K to ~ 360 K, where it stabilizes for the remainder of the heat-up transient.
- After the DCC starts, the hot helium flowed into the RCST as the cold helium flowed into the primary loop. The gases flowed in a countercurrent fashion, where the hot helium in the top half of the hot duct flowed in one direction and the cold helium in the bottom half of the duct flowed in the other direction. After the pressure and density reached equilibrium, the event entered a diffusion mode. The onset of reverse of natural circulation was not observed during the DCC period of the test. It is worth noting that no helium flow measurements were taken during the test and that conclusions are drawn from interpreting temperature measurements only.

Another phenomenon that happened during the PG-26 test was thermal stratification. As an example, Figure 9 shows the helium temperatures measured for all thermocouples in the lower (outlet) plenum of the vessel. These thermocouples are distributed radially, azimuthally, and axially in the lower plenum. The figure also shows the average gas temperature in the lower plenum and the measured helium temperature in the hot duct, which is directly leaving the lower plenum. One can see that thermal stratification plays an important role in determining the temperatures for helium flows leaving the plenum as well as for determining the structure temperatures encompassing the helium plenum.

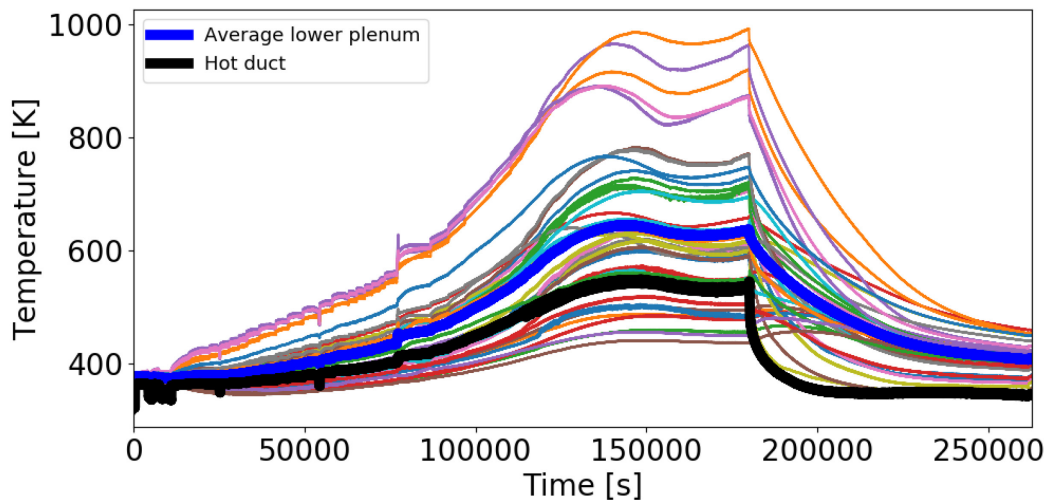


Figure 9. Measured thermal stratification of helium in the lower (outlet) plenum.

3. Computer Code and Input Model Description

The general characteristics of the RELAP5-3D computer code are provided, followed by a description of the HTTF input model.

3.1 RELAP5-3D

The RELAP5 series of codes has been developed at Idaho National Laboratory; RELAP5-3D is the latest code version in the series, see “RELAP5-3D Code Manual, Volumes I-V” [2]. While RELAP5 was originally developed to model accidents and operational transients in light-water reactor systems, the general nature of the code allows it to be used to simulate a wide variety of hydraulic and thermal transients in both nuclear and non-nuclear systems that can be stationary or moving. More than 25 working fluids are available in the code, including water, gases, liquid metals, refrigerants, and molten salts; eleven noncondensable gases are also available.

RELAP5-3D uses a two-fluid, nonequilibrium, six-equation hydrodynamic model. This model provides continuity, momentum, and energy equations for both the liquid and vapor phases within a control volume. Noncondensable gases and boron in solution in the liquid are also modeled. The energy equation contains source terms that couple the hydrodynamic model to the heat structure conduction model by a convective heat transfer formulation.

RELAP5-3D has a fully integrated, multidimensional thermal-hydraulic and neutron kinetics modeling capability. Several specific component models are available in the code in addition to the basic control volumes and junctions, allowing the user more flexibility in modeling fluid systems. These include models for branching, turbines, pumps, compressors, accumulators, valves, separators, and jet mixers.

The code uses special process models to treat phenomena that involve large spatial gradients or that are sufficiently complex that empirical models are required. Special process models in the code address critical flow, countercurrent flow limitation (flooding), horizontal stratification and entrainment, crossflow, reactor kinetics, cladding oxidation and deformation, and molecular diffusion. The code also contains trip and control system models that can be used to simulate automatic or operator-initiated actions during a transient. The control systems can also be used to calculate parameters of interest (such as peak fuel temperature) to aid in the analysis of the code calculation.

System hardware is modeled using heat structures. Heat structures use a one- (radial) or two-dimensional (radial and axial) conduction solution internally and can have a variety of boundary conditions applied on the surface. Energy can be transferred directly between heat structures using an enclosure model that models either radiation or conduction. An energy source term allows heat to be generated within a structure; direct (gamma/neutron) heating of the adjacent fluid volumes can also be modeled. A reflood model is also available that can be applied to the heat structures where needed. Thermophysical properties for the heat structures are normally input by the user.

Version 4.4.2ie of the code was used for the analyses.

3.2 HTTF Input Model

A RELAP5-3D input model has been developed for the HTTF. The model includes hydrodynamic components, heat structures, trips, and control systems. Systems modeled are the PCS, secondary coolant system (SCS), RCCS, potable water system that supplies both the SCS and the RCCS, and reactor cavity. The RCST is considered part of the PCS. The model used in this study is the quality-controlled HTTF RELAP5-3D model (HTTF base 2018-04-19 QA) developed by P. Bayless. A detailed description of the

model is provided in Paul D. Bayless' "RELAP5-3D Input Model for the High Temperature Test Facility" [4].

The primary pressure vessel nodalization is shown in Figure 10. Flow enters from the cold duct (Component 270), passes through the core support structure under the outlet plenum bottom plate (Component 105), then flows up between the primary pressure vessel and core barrel (Component 115) to the inlet plenum (Component 120). The flow then passes down through various flow channels in the core (Components 140, 145, and 150) and reflectors (Components 132 and 162), recombines in the outlet plenum (Component 175), and flows out into the hot duct (Component 200 and 206).

The heated region of the core is divided into ten equal-length axial segments, one for each block. The upper and lower reflectors each have two axial regions. This axial nodalization extends through each of the radial components in the vessel and in the RCCS.

The primary pressure vessel is divided into several different radial regions, as illustrated in Figure 11. The central reflector is divided into three regions: a central solid cylinder, a middle ring that contains the six 0.75-in.-diameter gap simulation channels and the ceramic that is directly influenced by the holes, and a solid outer ring that is adjacent to the core. The core is also divided into three rings, as it is designed on the hexagonal block pattern of the modular high-temperature gas-cooled reactor, which has three fueled rings. Figure 12 shows which blocks are included in each of the rings in a 60-degree sector; the boundaries of the inner and outer rings were extended beyond the full hexagonal block geometry to include all the coolant channels.

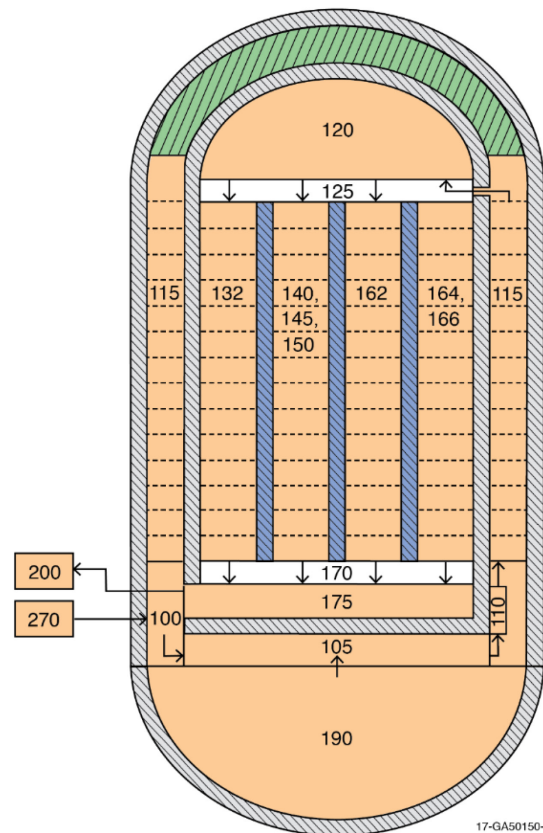


Figure 10. Primary pressure vessel nodalization.

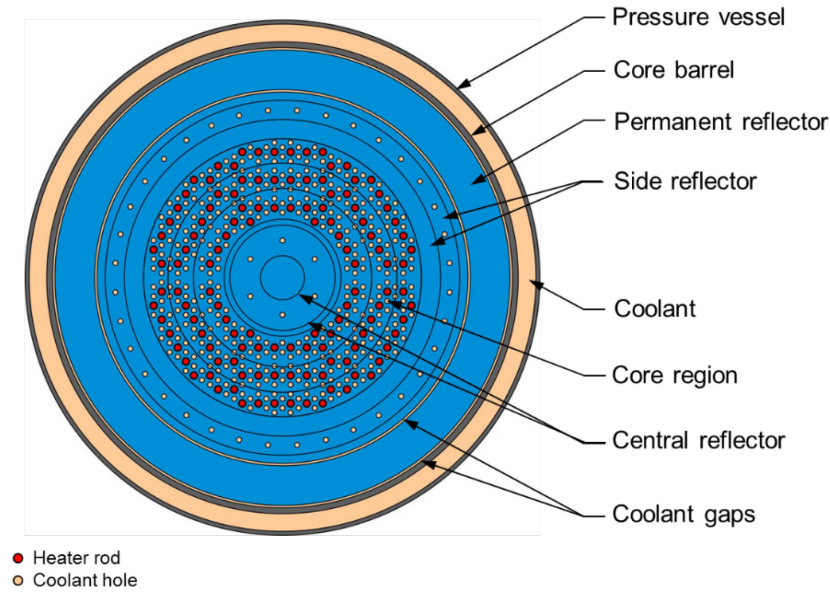


Figure 11. Primary pressure vessel radial nodalization.

The inner ring includes 23 hexagonal blocks, 56 heater rods, and 138 coolant channels; the middle ring models 24 blocks, 72 heater rods, and 144 coolant channels; and the outer ring includes 39 blocks, 82 heater rods, and 234 coolant channels. The side reflector is divided into three regions: an inner solid ring next to the outer core ring, a middle ring that contains the thirty-six 0.625-in.-diameter gap simulation channels and associated ceramic, and a solid outer ring. The next radial structure is the outer or permanent reflector, which has a coolant gap on either side (Components 164 and 166); these gaps do not have axial flow through them, as the top is covered by a plate (the upper plenum floor), leaving them open only to the outlet plenum. Continuing outward, the core barrel is next, followed by the coolant upcomer region between the core barrel and the pressure vessel wall, and, finally, the primary pressure vessel itself.

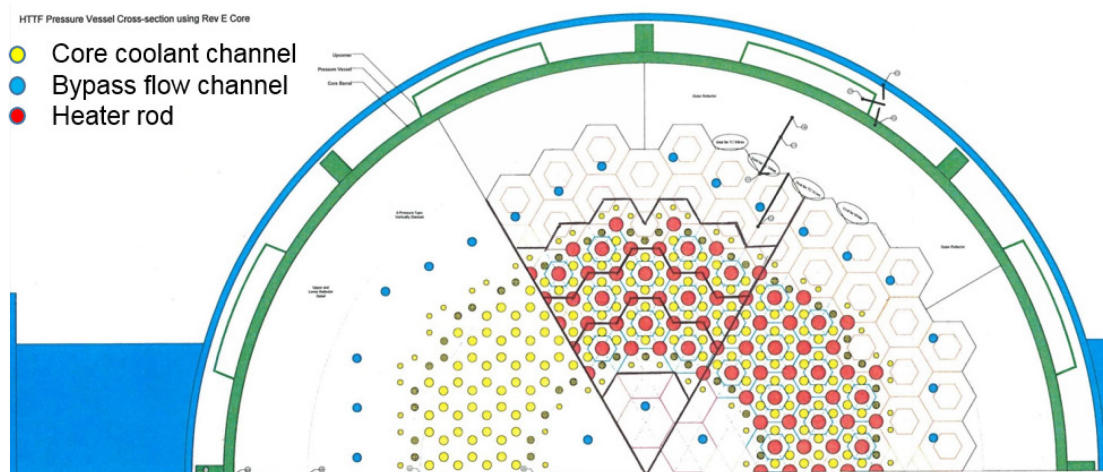


Figure 12. Core ring layout.

The nodalization of the PCS is shown in Figure 13. Hot gas exits the primary pressure vessel into the hot duct (Components 200 and 206), then flows up through a check valve (Component 217) and into the steam generator inlet plenum and tubes (Components 220 and 225). The cooled gas flows out of the steam generator outlet plenum (Component 228) into piping (Component 230) that leads to the gas circulator. The circulator is modeled using a branch (Component 235) and a time-dependent junction (Component 237). From the circulator, the flow proceeds through an isolation valve (Component 245), into a crossover pipe (Component 260), into an annulus around the hot duct (the cold duct, Component 270), and then back into the primary pressure vessel.

One phenomenon of interest in the PG-26 test was the single-phase countercurrent helium flow in the hot duct during the DCC. During the DCC phase of the test, hot (less dense) gas was flowing from the pressure vessel outlet plenum to the RCST along the top of the pipe and colder (denser) gas was returning from the RCST to the outlet plenum along the bottom of the pipe. RELAP5-3D cannot simulate this directly within a single 1D pipe. Therefore, the nodalization of the outlet plenum and hot duct have been changed compared to the quality-controlled HTTF model base 2018-04-19 QA. The hot duct has been split into top and bottom halves using two 1D pipes in RELAP5-3D (Components 200 and 206). Each of the cells in the two pipes are connected by crossflow junctions to allow the pressure to equalize along the pipe. The pipe heat structures are also split into top and bottom halves. The outlet plenum is modeled with four components (Components 175, 180, 183 and 185), with the objective to allow the plenum to fill with the returning gas before it interacts with the hotter gas in the core.

Break valves are located on the ends of the hot duct (two valves, one for the upper and one for the lower half of the hot duct (Components 205 and 207)) and the circulator discharge pipe (Component 255), connecting them to the RCST. These valves are closed during steady-state operation. The RCST (Component 280) is modeled as a two-volume pipe; the bottom volume represents the stagnant portion of the tank below the break valves, and the top volume includes the portion of the tank that will mix with the break effluent. Safety relief valves and a depressurization line are connected to the cold leg piping between the gas circulator and the loop isolation valve. These are modeled as a single line in the RELAP5-3D input model.

The nodalization of the SCS is also provided in Figure 13. The feedwater pump (Component 320), which is modeled using a time-dependent junction, draws suction from a water storage day tank and pumps it into the steam generator downcomer (Component 340). The downcomer extends up to near the top of the tube sheet. The water is then boiled on the outside of the tubes (Component 350) as it flows upward to the steam dome at the top of the steam generator (Component 355). The steam then turns back downward before exiting out the side of the steam generator. The steam then flows through a pressure control valve (Component 370) in the steam line before flowing through more piping and being vented to the atmosphere. This downstream piping is not included in the RELAP5-3D input model. A safety relief valve (Component 395) is connected to a nozzle (Component 390) on the top of the steam generator. The piping downstream of the relief valve is not included in the input model.

The principal component in the potable water supply system is the water storage day tank (Component 450). This tank is the water source for both the SCS and the RCCS. The tank water level is maintained within a specified range. When the level gets too low, the supply line valve (Component 410) opens, allowing water from the public water system (Component 400) to flow into the tank through an inlet pipe (Component 420). When the level rises to a certain level, the supply line valve is closed. The tank also has an interior drain/vent line (Component 490) that extends from the bottom of the tank to near the top; it is modeled as being open to the atmosphere below the tank. An outlet line (Component 460) is connected to the bottom of the tank; both the feedwater and RCCS pumps take suction from this pipe.

The reactor cavity (Component 900, not shown) is modeled as a large air-filled volume at atmospheric pressure and is located between the primary pressure vessel and the RCCS panels (Component 950). The RCCS draws flow from the water storage tank and pumps it through a series of

pipes (Components 930, 940, and 945) into the cooling panels surrounding the primary pressure vessel. The pump (Component 920) is modeled using a time-dependent junction. Water exiting the top of the panels is collected (Component 955) and returned (Component 960) to the water storage tank.

Heat structures are used to model the metallic and ceramic structures important to heat storage and transfer in the facility. These consist of the primary pressure vessel and its internal structures, including the heater rods; the PCS pipe walls; the steam generator tubes, internals, and shell; the gas circulator structure; the RCCS panels; and the RCST. Heat structure numbers generally match the numbers of the volume components to which they are attached.

The Gnielinski correlation is being used for forced convection in the core coolant channels, with Dittus-Boelter being used elsewhere. Two-dimensional conduction (radial and axial) is used in all vertical structures. Insulation is modeled on the outside of the PCS piping, steam generator, gas circulator, RCST, and back side of the RCCS panels; a natural convection heat transfer coefficient ($15\text{W/m}^2\cdot\text{K}$) and sink temperature are applied to the outside of the insulation. The insulation between the hot and cold ducts, and between the upper plenum shield and the pressure vessel upper head, is also included in the model.

The core region is modeled with two heat structures in each channel. The first structure is centered on a coolant channel and models the ceramic material. The second structure represents the heater rods and is modeled as a solid cylinder that radiates heat to the outer surface of the ceramic structure. Heater rods are likely to touch the ceramic surface on some portions of the heaters. However, the conduction heat transfer through these portions is considered negligible compared to the radiation heat transfer in this model. Both structures have a common boundary volume that represents the gas gap between the heater rods and the ceramic. The power to the heaters in the three core rings is provided by control variables and is assumed to be distributed uniformly over the heater rod length. Ten general tables, one for each of the heater rod banks, provide the power to individual banks; these are then apportioned to the three core rings based on how many of the heater rods in each bank are located in each core ring.

Conduction enclosures are used to transfer heat radially across the core ceramic blocks and to transfer heat axially between the core blocks and the top and bottom reflectors. Radiation enclosures are used to transfer the heat radially from the core blocks to the outer reflector, from the outer reflector to the core barrel, from the core barrel to the primary pressure vessel, and from the pressure vessel to the RCCS panels. As mentioned above, radiation enclosures are also used between the heater rods and the surrounding core ceramic. Radiation view factors were calculated assuming only one-dimensional (radial) heat transfer for these enclosures. Radiation was also modeled from the upper plenum floor to the upper plenum shield and control rod guide tubes and from the lower plenum roof to the bottom plate, the outlet plenum side reflector, and the support posts.

Trips and controls are used to operate the active components in the facility. Some control variables are used to calculate parameters corresponding to facility measurements, such as differential pressures across components. Others are used to calculate parameters that may be useful for analyzing the code simulations.

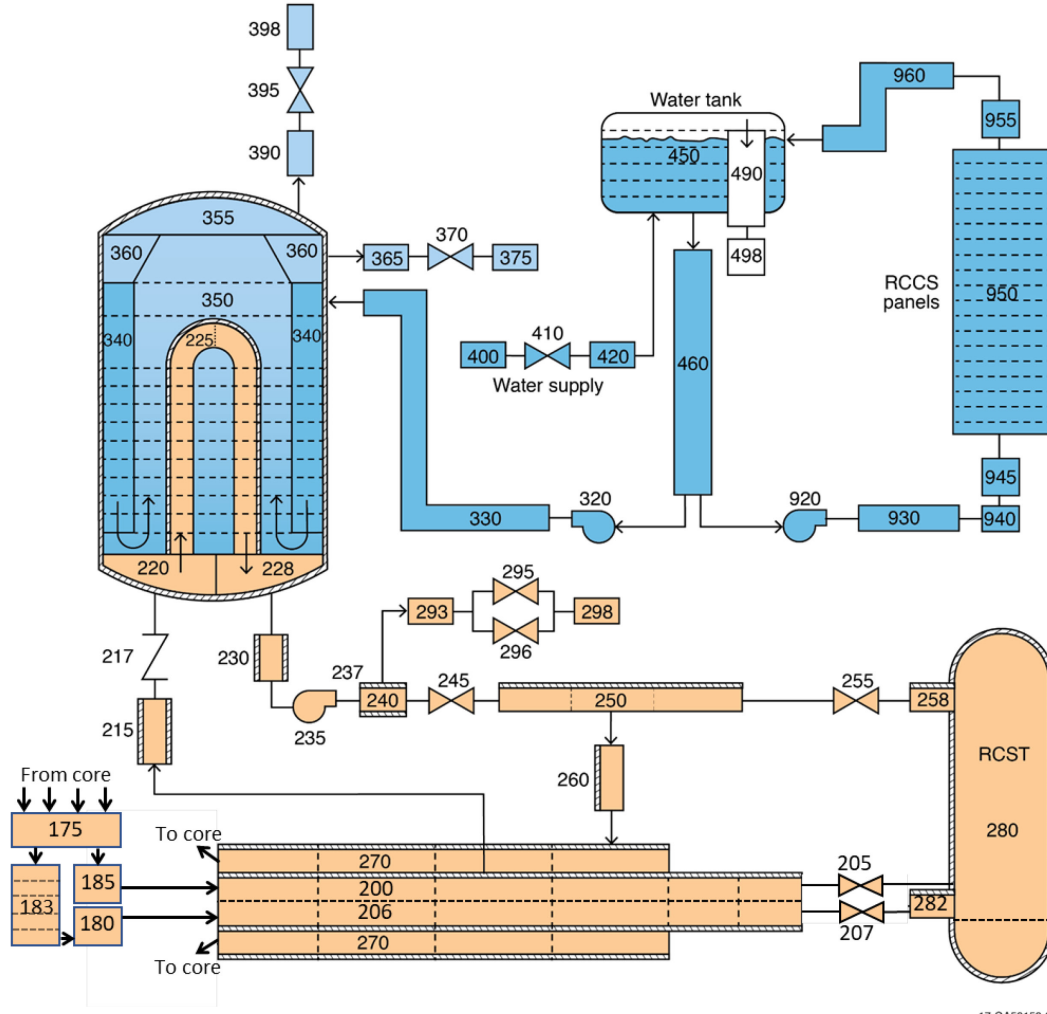


Figure 13. Nodalization of components outside the primary pressure vessel.

3.3 Automation Tools

As mentioned, the HTTF facility is equipped with over 500 instruments. To facilitate handling this amount of data, an input creation and a postprocessing tools have been created. Both tools have been written in Python 3.7.

3.3.1 Initial and Boundary Conditions

The first developed tool helps create RELAP5-3D inputs for the PG-26 test. The tool creates initial and boundary conditions for the PG-26 test from measured data and puts them in the RELAP5-3D input file. First, to create initial conditions, the tool reads the following inputs:

- A mapping table establishing a correspondence between the HTTF measured instrument nomenclature and the RELAP5-3D model channel names.
- A set of rules on how to apply the measured values to the RELAP5-3D model. These rules include instructions on how to convert units from measured data (°C, kPa, etc.) to the RELAP5-3D input

requirements (K, Pa, etc.) as well as instructions on how to interpolate measured data to generate initial conditions for RELAP5-3D channels that don't have a corresponding measurement.

- The time during the test at which the RELAP5-3D input deck will be initialized.
- The tool reads a template RELAP5-3D input deck for the HTTF, (typically the quality-controlled base 2018-04-19 QA, including the “split hot duct,” (see model description above)) and changes the initial conditions for all heat structures (temperature) and fluid volumes (temperature and pressure) in the deck to the measured values at a given time (user input) during the PG-26 test. Note that, since there were no helium flow rates measured in the HTTF, the initial helium velocities are set to zero. The tool allows users to initialize the RELAP5-3D input at different times during the test (e.g. at the start of the test or shortly before the DCC starts). This is useful to get an estimate of the energy stored in the core at the beginning of the RELAP5-3D calculation. The core was still cooling down from a previous test with temperatures around 400K when the PG-26 test started, so there was no real steady state that could be used to compute the initial conditions for the RELAP5-3D transient calculation.

Second, the developed tool can read time-dependent boundary conditions from the HTTF measured data and put them into tables in the RELAP5-3D input. The HTTF measurements are recorded every 0.5 s, which leads to a total of ~500,000 measured time points during the PG-26 test. However, a RELAP5-3D table can only accommodate 100 data points. The tool reduces the measured points to 100, preserving the integral (i.e., the surface under the curve, as well as the biggest changes in the data). The methodology to reduce the number of points for the RELAP5-3D input is as follows:

- Reduce noise in measured data. The measured data is smoothed using a moving average filter with a 30-minute rolling window. The smoothening allows the user to better identify changes in the slope of the actual data (i.e., points sampled capture changes in data not changes in noise, which might be big even if the noise itself is small).
- 50 points are randomly sampled in the smoothed data.
- 50 points are selected at the biggest changes in slope of the smoothed data (i.e., at the 50 biggest values of the absolute values of the second derivative). This makes sure that on/off type and other step changes in the data are captured.
- The new 100-point curve is rescaled to preserve the integral of the original data.

All boundary conditions used in the RELAP5-3D simulations have been processed and input using this methodology. Different calculations presented in this report will use different boundary conditions (explained later in the result section), but, as an example, Figure 14 shows the treatment of the power boundary condition for heater 110. The plot shows the measured 500,000 data points, the smoothed data, and the 100 points input into RELAP5-3D. The renormalization to preserve the integral of the original data assures that the total energy deposited during the test is captured in the reduced 100-point curve.

3.3.2 Postprocessing and Plotting

A second python tool has been developed for postprocessing and plotting the RELAP5-3D simulation results. Like the first tool, the postprocessor reads the mapping table that establishes the correspondence between the HTTF measured instrument nomenclature and the RELAP5-3D model channel names as well as the ruleset for converting units from the measured data to the RELAP5-3D output units. From the mapping table, the tool first generates and runs RELAP5-3D “strip” input files that extract the RELAP5-3D outputs that have corresponding measured data from the RELAP5-3D binary output file into a csv. The script then converts the units and plots measured data for each HTTF instrument together with the corresponding RELAP5-3D computed values.

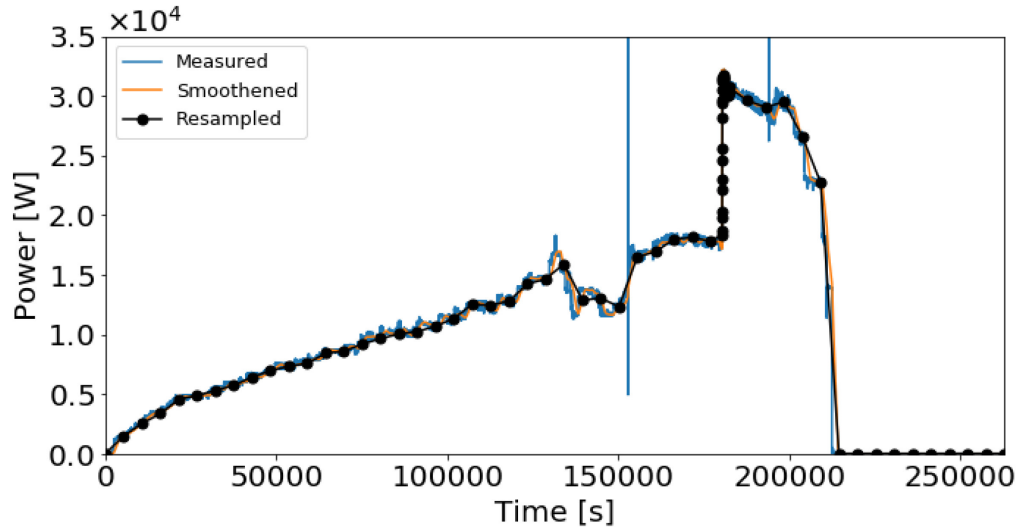


Figure 14. Heater 110 power boundary condition: Measured data from PG-26, smoothed data, and resampled points input in the RELAP5-3D model.

4. Simulations

The main goal of the PG-26 test is to investigate the facility behavior during a DCC transient test. The main figures of interest are:

- Depressurized core cooling under decay heat conditions. That includes radial and axial conduction and the radiation of heat from the core to the pressure vessel and out into the RCCS or directly into the environment.
- Gas behavior during the cooldown, such as the gas mixing phenomena between the hot and cold helium in the PCS and RCST, like molecular diffusion, the establishment of natural convection, and possible flow reversal.

To capture the phenomena happening during the DCC portion of the transient, the core state (stored energy, temperature distribution, etc.) at the beginning of the transient must be known. To get initial conditions before the DCC start, two approaches for the RELAP5-3D simulations have been considered:

- **Steady state + DCC:** In this approach, the facility state right before the DCC starts is modeled as RELAP5-3D steady-state, and only the DCC itself is modeled as RELAP5-3D transient. The goal is to get a well-defined facility state modeled before the transient of interest starts. The difficulty with this approach is that the HTTF did not reach a fully developed steady state (temperature distribution). The HTTF operating procedure indicates that a hot steady state is reached when the following conditions have been held for a minimum of 2 hours: a) peak temperature is between 780°C (1053 K) and 820°C (1093 K), b) average core temperature is between 550°C (823 K) to 590°C (863 K), and c) no temperature measurement channel increases at a rate greater than 10 K/h. Looking at the test data in particular, the steam generator behavior did not reach a true steady state during the test. Another difficulty with this approach is that the RELAP5-3D steady state must be performed while the blower is still running (to be able to get a zero energy-balance). That means that the transient calculation will have to go through the blower rundown and manual depressurization of the PCS and RCST before the DCC start.
- **Whole transient:** This approach considers running the whole test (i.e., the heat-up as well as the DCC) as a RELAP5-3D transient. As mentioned, the HTTF did not reach a well-defined steady state

before the initiation of the DCC transient and simulating the heat-up phase might lead to a better characterization of the core and primary system before the DCC. One difficulty with this approach is that to save time, the HTTF facility is not completely cooled down to room temperature between tests. At the start of PG-26, the core structures were still $\sim 100^{\circ}\text{C}$ (373 K) and cooling down (i.e. not at steady state but in a transient).

4.1 Assessment Criteria

This research made judgments on the adequacy of the code models, using a standardized and consistent set of criteria that has been previously applied in the assessment of the United States Nuclear Regulatory Commission-sponsored codes [7–9]. The terminology is defined below.

Excellent Agreement—Applies when the code exhibits no deficiencies in modeling a given behavior. Major and minor phenomena and trends are correctly predicted. The calculated results are judged to agree closely with the data. The calculation will, with few exceptions, lie within the uncertainty bands of the data. The code may be used with confidence in similar applications. (The term “major phenomena” refers to the phenomena that influence key parameters, such as fuel rod cladding temperature, pressure, differential pressure, mass flow rate, and mass distribution. Predicting major trends means that the prediction shows the significant features of the data. Significant features include the magnitude of a given parameter through the transient, slopes, and inflection points that mark significant changes in the parameter.)

Reasonable Agreement—Applies when the code exhibits minor deficiencies. Overall, the code provides an acceptable prediction. All major trends and phenomena are correctly predicted. Differences between calculation and data are greater than deemed necessary for excellent agreement. The calculation will frequently lie outside but near the uncertainty bands of the data. However, the correct conclusions about trends and phenomena would be reached if the code were used in similar applications. The code models and/or facility model nodes should be reviewed to see if improvements can be made.

Minimal Agreement—Applies when the code exhibits significant deficiencies. Overall, the code provides a prediction that is only conditionally acceptable. Some major trends or phenomena are not predicted correctly, and some calculated values lie considerably outside the uncertainty bands of the data. Incorrect conclusions about trends and phenomena may be reached if the code were used in similar applications, and an appropriate warning needs to be issued to users. Selected code models and/or facility model nodes need to be reviewed, modified, and assessed before the code can be used with confidence in similar applications.

Insufficient Agreement—Applies when the code exhibits major deficiencies. The code provides an unacceptable prediction of the test. Major trends are not predicted correctly. Most calculated values lie outside the uncertainty bands of the data. Incorrect conclusions about trends and phenomena are probable if the code is used in similar applications, and an appropriate warning needs to be issued to users. Selected code models and/or facility model nodes need to be reviewed, modified, and assessed before the code can be used with confidence in similar applications.

Assessment judgments of “excellent” or “reasonable” are considered to indicate an acceptable code performance. While there is a quantitative aspect to the assessment characterizations, the judgments made in this report remain mostly qualitative.

4.2 Helium Mass Flow

The HTTF facility is not equipped to directly measure the helium flow rate in the PCS. However, to get the right energy balance and core conditions before the DCC transient, knowledge of the helium mass flow rate is needed. For the presented simulations, this section describes the method of estimating the helium mass flow rate.

The PG-26 test protocol indicates that the primary helium blower has been run at 29% speed during the test. A measured circulator performance curve (for nominal speed) is available for the primary helium blower (Brian G. Woods, email to the author, May 15, 2020). Figure 15 shows the circulator pound-per-square-inch gauge (PSIG) vs. inlet cubic feet per minute (ICFM), with the black line representing theoretical values and the red line measured values.

To scale the measured circulator curve down to 29% speed, the approximations that the volumetric flow is proportional to the speed and the pressure is quadratic to the speed have been used.

To estimate the helium density during the heat-up portion of the transient, the measured pressure (instrument PT-6201, ~2 bar) and measured temperature (instrument TF-6201, ~380 K) at the circulator inlet have been used. These values lead to a helium density of ~250 g/m³ at the circulator inlet. Furthermore, the measured pressure difference over the circulator (PT-6202 - PT-6201) is about ~2.5 kPa.

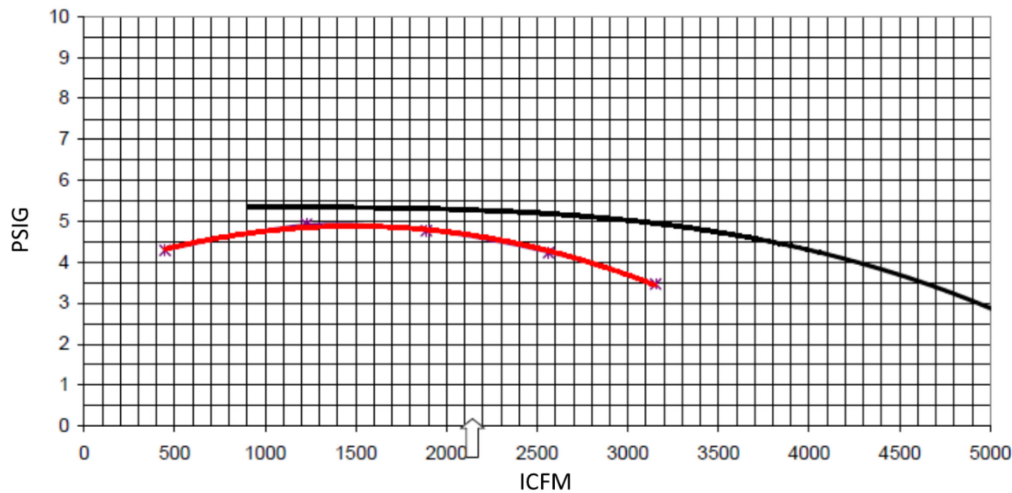


Figure 15. Helium circulator performance curve at nominal speed (theoretical value in black and measured values in red): PSIG vs. ICFM.

Knowing the circulator speed, the helium density and pressure loss over the circulator during the test allows us to estimate the helium mass flow rate as follows:

- Convert units of measured ΔP_{circ} (29% speed) = 2,500 Pa = 0.363 PSIG.
- The measured ΔP_{circ} is for 29% circulator speed. To be able to use the circulator curve in Figure 15, the ΔP_{circ} has to be scaled-up to nominal circulator speed:
 - $\frac{\Delta P_{\text{circ}}(29\% \text{ speed})}{\Delta P_{\text{circ}}(100\% \text{ speed})} = \left(\frac{29\% \text{ speed}}{100\% \text{ speed}} \right)^2 \Rightarrow \frac{0.363 \text{ PSIG}}{\Delta P_{\text{circ}}(100\% \text{ speed})} = \left(\frac{0.29}{1.0} \right)^2$
 - $\Delta P_{\text{circ}}(100\% \text{ speed}) = 4.32 \text{ PSIG}$

- On the red curve in Figure 15, for $\Delta P_{circ}(100\% \text{ speed}) = 4.32 \text{ PSIG}$, there are two possible volumetric flow rates \dot{v} (for 100% speed):
 - $\dot{v}(4.32 \text{ PSIG}, 100\% \text{ speed})(4.32 \text{ PSIG}, 100\% \text{ speed}) = 2570 \text{ ICFM}$ or 450 ICFM
- The two possible volumetric flow rates can be scaled back down to 29% circulator speed:
 - $\frac{\dot{v}(29\% \text{ speed})}{\dot{v}(100\% \text{ speed})} = \frac{29\% \text{ speed}}{100\% \text{ speed}}$
 - $\dot{v}(29\% \text{ speed})(29\% \text{ speed}) = 745 \text{ ICFM}$ or 130 ICFM
- Convert units of \dot{v} :
 - $745 \text{ ICFM} \cong 0.3516 \text{ m}^3/\text{s}$ and $130 \text{ ICFM} \cong 0.0613 \text{ m}^3/\text{s}$
- Finally, using the helium density, the mass flow rate during PG-26 can be estimated:
 - $\dot{m}(29\% \text{ speed}) = 0.3516 \frac{\text{m}^3}{\text{s}} 250 \frac{\text{g}}{\text{m}^3} = 88 \frac{\text{g}}{\text{s}}$ or $0.0613 \frac{\text{m}^3}{\text{s}} 250 \frac{\text{g}}{\text{m}^3} = 15 \frac{\text{g}}{\text{s}}$

The circulator power consumption during the test is needed to select which of the two possible mass flow rates is the correct one. The description of the PG-26 test does not include that information. However, a calorimetric calculation across the core indicates a mass flow rate during PG-26 that is even lower than the $15 \frac{\text{g}}{\text{s}}$ estimated from the circulator curve.

A sensitivity study for the helium mass flow rate has been performed for the presented simulations (“steady state + DCC” and “whole transient”) (i.e., 5, 10, and 15 g/s of helium mass flow have been considered in all calculations).

4.3 Base Case Simulations

This section presents the base case RELAP5-3D calculations for the PG-26 test. As discussed in Section 2, the core temperature reduction during the heat-up phase is believed to be due to the steam generator operation. The steam generator pressurized during the first part of the heat-up transient until it reached conditions close to saturation. Steam was then released, and the steam generator inventory was refilled with cold city water. This led to a stabilization of the core helium inlet temperature (which was rising before) and a reduction in core structure temperatures. Accurate steam generator behavior is hard to replicate in the RELAP5-3D model because not all the boundary conditions of the steam generator are known. To simplify the problem and focus on the primary system and DCC transient, the steam generator has been excluded from the model and boundary conditions have been placed at the steam generator inlet and helium circulator outlet for the presented calculations.

Measurement uncertainties are small [6] compared to the discrepancies between measured results and RELAP5-3D simulation results. Uncertainty bands are therefore not included in the plots.

The base case RELAP5-3D calculations for both the “steady state + DCC” and “whole transient” cases include the following time-dependent boundary conditions and events:

- **Primary pressure:** A time-dependent outlet pressure boundary condition has been placed at the steam generator inlet. Helium coming from the core is going through this boundary condition and leaves the system. The boundary condition follows the measured pressure of instrument PT-6001 during the heat-up transient. The measured data has been preprocessed for the RELAP5-3D input as discussed in Section 3.3.1. The boundary condition includes a) the sawtooth behavior of the PCS pressure during the heat-up that comes from helium leaking into the RCST and the manual injection of helium into the PCS and b) the over-pressurization of the PCS while trying to reseal the leaking helium valve between the PCS and RCST (see Figure 7). The manual depressurization of the primary

helium loop before the DCC is also modeled with this boundary condition. As soon as the break valves open and the DCC starts, any helium flow from or to the boundary condition has been stopped, and the pressure in the combined PCS-RSCT system can evolve freely.

- **Primary temperature and mass flow rate:** A time-dependent helium inlet boundary condition is placed at the helium circulator outlet. The boundary condition follows the measured helium temperature of instrument TF-6202 during the heat-up transient. The measured data has been preprocessed for the RELAP5-3D input, as discussed in Section 3.3.1. The measured temperature at the helium circulator outlet included a) any effects from the steam generator on the core inlet temperature, b) the cooling effect of the circulator cooling water on the primary helium temperature, and c) helium temperature changes from the cold helium injections to stabilize the PCS pressure. The helium mass flow rate is imposed as 5, 10, and 15 g/s, as discussed in Section 4.2. The mass flow rate is reduced to zero at the time when the circulators has been stopped during the test shortly before the break valves are opened.
- **RCST pressure:** As mentioned, the pressure in the RCST was rising during the heat-up of the core due to a leaking valve between the PCS and the RCST (see Section 2.2.6 and Figure 7). A controller has been added to the RELAP5-3D model that operates the break valve between the PCS (hot duct) and RCST, allowing helium to flow from the PCS to the RCST. The controller adjusts the valve position so that the pressure inside the RCST follows the measured pressure from instrument PT-4001. The measured data has been preprocessed for the RELAP5-3D input, as discussed in Section 3.3.1. The controller is stopped before the manual depressurization of the RCST happens. The depressurization of the RCST before the DCC start is modeled with a dedicated (outlet) pressure boundary condition that has been connected to the RCST. Helium can leave the system through this boundary condition during the manual depressurization of the RCST. As soon as the break valves open and the DCC starts, any helium flowing from or to the boundary condition has been stopped, and the pressure in the combined PCS-RSCT system can evolve freely.
- **Heaters:** The RELAP5-3D model of the HTTF allows users to input time-dependent heater powers for all ten heaters of the facility independently. Heater power can be computed from the measured voltage (VT) and current (CT) in the heater rods (see Section 2.2.2). Only two heaters were used during PG-26 (banks 4 and 10). The computed power data for these heaters has been preprocessed for the RELAP5-3D input, as discussed in Section 3.3.1.
- **RCCS:** A time-dependent water inlet boundary condition is placed at the RCCS inlet. The boundary condition follows the measured RCCS inlet water temperature of instrument TF-9003 and the measured RCCS inlet water mass flow rate of instrument FT-9001 during the whole transient. The measured data has been preprocessed for the RELAP5-3D input, as discussed in Section 3.3.1.
- **Valves:** As described in the PG-26 test protocol, the valve between the hot duct and the RCST (SV-3001) and the valve between the cold duct and the RCST (SV-6001) have been opened to initiate the DCC transient. In addition, the valve after the helium circulator (SV-6201) has been closed when the transient starts, and the flow path through the steam generator has been blocked.

4.3.1 Steady State + DCC

As mentioned, the first approach for modeling the PG-26 test is to compute a steady state with RELAP5-3D and then restart the calculation into a RELAP5-3D transient. The goal is to get a well-defined facility state modeled before the DCC transient starts. The RELAP5-3D steady state must be performed while the blower is still running (to be able to get a zero energy-balance). That means that the subsequent transient calculation will have to go through the blower rundown and manual depressurization of the primary and RCST before the DCC starts. The steady state was run 179,500 s into the test. The developed automation tools (see Section 3.3) extracted all initial and boundary conditions from measured

data for the specified steady-state time. Table 2 compares the steady-state results with measured data (for the 5, 10, and 15 g/s primary helium mass flow rate), while Figure 16 through Figure 33 show the transient results of the RELAP5-3D calculations. As mentioned, the calculations start from an assumed steady state at 179,500 s and go through the manual depressurizations of the PCS and RCST, the blower rundown, and break valve opening that initiate the DCC. In all figures, colored lines represent measured data, and black lines are RELAP5-3D calculation results.

For the “steady state + DCC” RELAP5-3D calculation of PG-26, the following observations were made:

- The **core helium temperature difference** (see Table 2 and Figure 16–Figure 18) is computed from the vessel entrance in the cold duct to the vessel outlet in the hot duct (instruments TF-3001 and TF-6001 and RELAP5-3D channels tempg-200010000 and tempg-270040000). For the steady-state calculation, the helium core temperature difference is significantly higher than the measured value. Even though the difference reduces from ~400 K to ~300 K going from 5 g/s to 15 g/s helium mass flow rate, it is still significantly bigger than the 166 K measured value. One can see that, during the DCC transient, the core helium temperature difference drops below 100 K; however, the temperature difference does not become negative as it does for the measured value. This value is judged to be in **minimal agreement**.
- Having a closer look at the **core inlet and outlet helium temperatures** (see Figure 22–Figure 24), one can see that, in the RELAP5-3D simulations, the helium temperature rise in the core itself (i.e., between block 7 and block 3) (see the top left plots in Figure 25–Figure 33) is smaller than for the measured values. However, the helium is much more preheated, compared to the measured data, in the lower vessel before it enters the riser section. The RELAP5-3D calculations assume a steady-state condition, (i.e., the energy put in the system and leaving the system are in balance). The much higher energy flow from the metallic vessel structures into the helium could indicate that a well-defined steady state is not yet reached in the facility. A second observation from Figure 22 through Figure 24 is that the hot duct temperature difference between the upper and lower part of the duct during the heat-up phase is higher than in the RELAP5-3D simulation. Furthermore, comparing the core helium temperature difference estimated from the core inlet and outlet temperatures to the one reported in Figure 16–Figure 18, one can see that the core outlet temperature used to compute the core helium temperature difference (TF-3001, see “Hot duct” in Figure 9) is lower than the two reported hot duct temperatures (TF-2211 and TF-2311) in Figure 22–Figure 24. These two observations are in line with the strong thermal stratification observed in the lower plenum (see Figure 9) in the measured data. The thermal stratification of helium is something the RELAP5-3D 0D elements used to model the lower plenum cannot predict. Using the RELAP5-3D 3D component to model the lower plenum might improve the result. These values are judged to be in **minimal agreement**.
- Qualitative trends for the **ceramic solid temperatures in the core** are summarized in Table 3 for the steady state, the peak temperature during the DCC, and the DCC cooling rate once the heaters have been stopped (i.e., after the temperature peak). The table compares the RELAP5-3D temperature predictions with the region averaged (radially and azimuthally [sectors] averaged through the region) measured temperatures.

Table 2. Steady-state temperatures (all temperatures in [K]) for the RELAP5-3D calculations with 5, 10, and 15 g/s primary helium mass flow rate compared to the measured data of test PG-26 at 179,500 s.

	RELAP5-3D 5 g/s	RELAP5-3D 10 g/s	RELAP5-3D 15 g/s	Measured
Core helium ΔT	402	374	318	166
RCCS water ΔT	14	9	6	0
Upper core (block 7)				
Helium temperature inner/middle/outer fuel ring	1112/1097/1016	885/879/823	732/730/688	715/517/427
Ceramic temperature inner/outer central reflector region	1108/1111	881/885	728/734	604/618
Ceramic temperature inner/middle/outer fuel region	1114/1101/1017	889/886/826	739/739/693	691/680/457
Ceramic temperature side/permanent reflector region	964/829	792/703	670/608	427/403
Midcore (block 5)				
Helium temperature inner/middle/outer fuel ring	1149/1133/1046	934/926/863	783/779/730	881/714/529
Ceramic temperature inner/outer central reflector region	1147/1149	931/934	780/784	794/807
Ceramic temperature inner/middle/outer fuel region	1151/1137/1047	937/932/866	788/786/734	884/903/573
Ceramic temperature side/permanent reflector region	989/845	827/723	706/628	497/430
Lower core (block 3)				
Helium temperature inner/middle/outer fuel ring	1170/1152/1060	967/957/889	819/814/760	1030/791/565
Ceramic temperature inner/outer central reflector region	1168/1170	964/967	817/820	952/964
Ceramic temperature inner/middle/outer fuel region	1172/1156/1061	969/962/891	823/820/762	1034/939/603
Ceramic temperature side/permanent reflector region	999/844	847/729	729/637	540/450

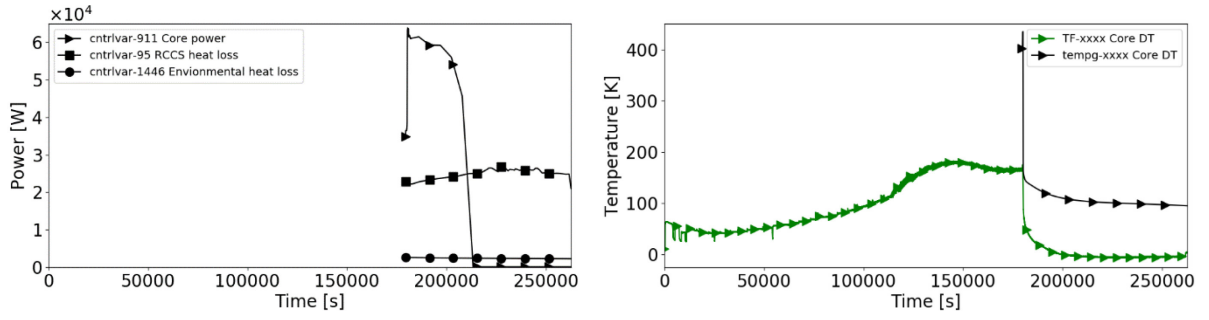


Figure 16. DCC only, **5 g/s** helium mass flow: left) core heat balance and right) core helium ΔT .

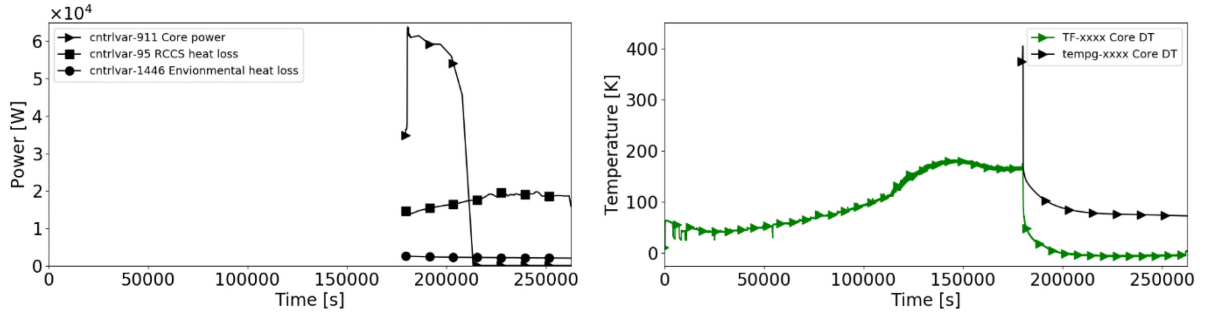


Figure 17. DCC only, **10 g/s** helium mass flow: left) core heat balance and right) core helium ΔT .

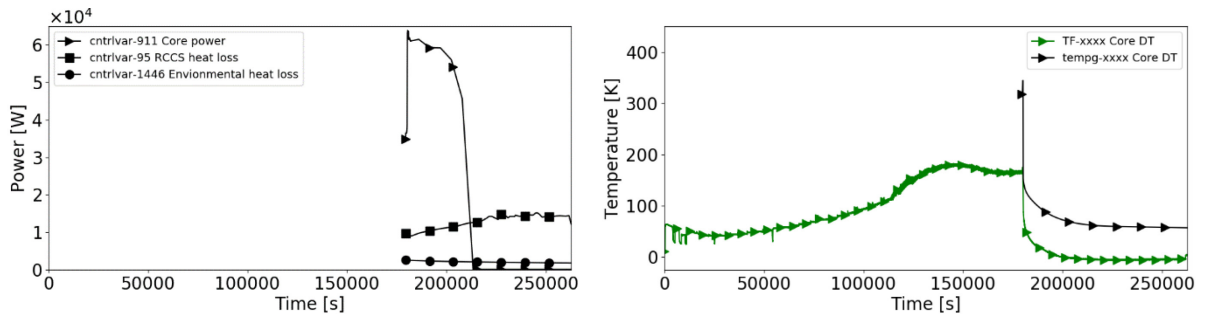


Figure 18. DCC only, **15 g/s** helium mass flow: left) Core heat balance and right) core helium ΔT .

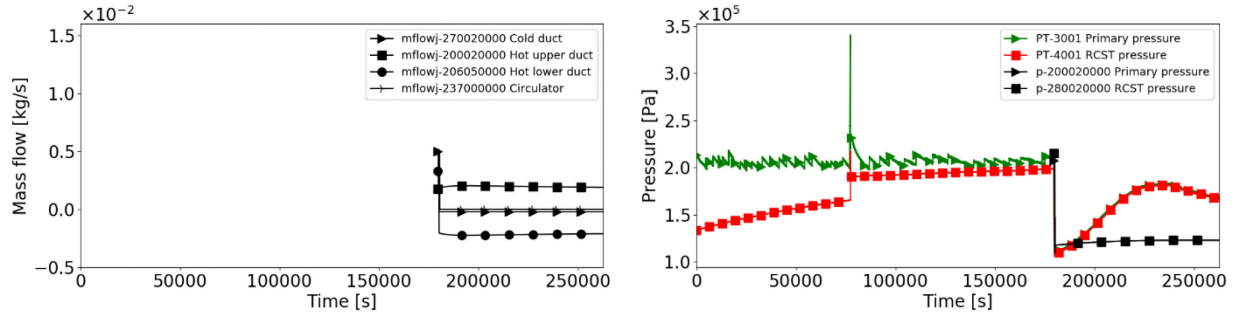


Figure 19. DCC only, **5 g/s** helium mass flow: left) PCS helium mass flow rates and right) PCS and RCST pressure.

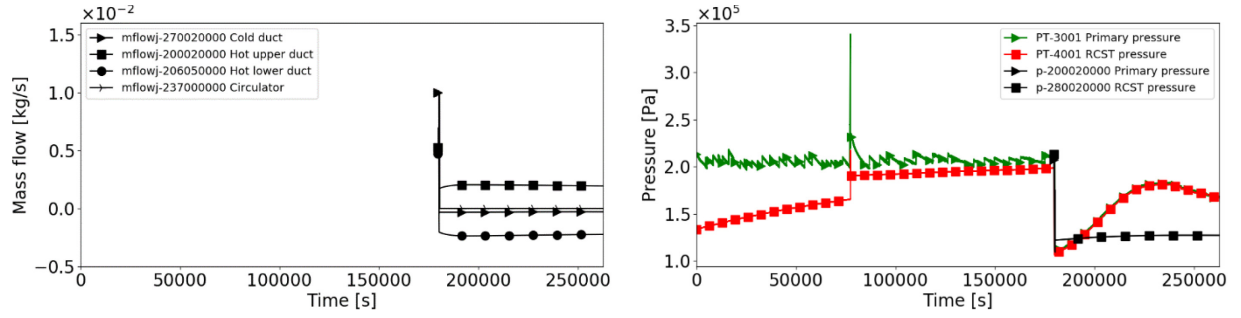


Figure 20. DCC only, **10 g/s** helium mass flow: left) PCS helium mass flow rates and right) PCS and RCST pressure.

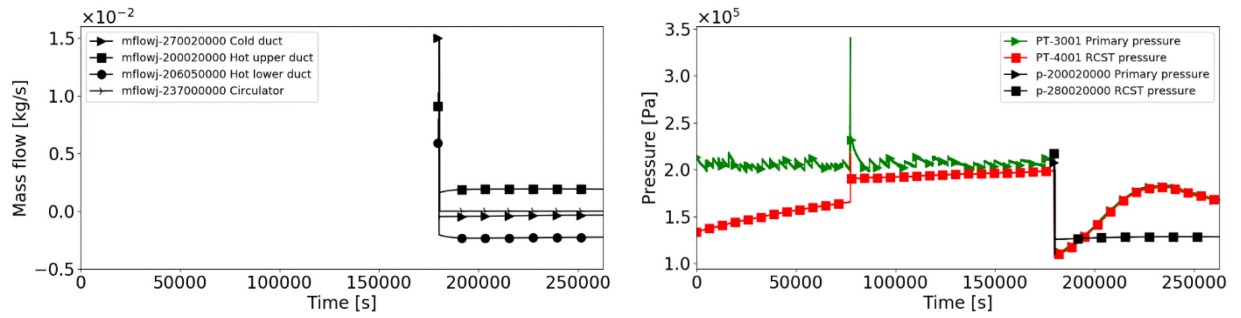


Figure 21. DCC only, **15 g/s** helium mass flow: left) PCS helium mass flow rates and right) PCS and RCST pressure.

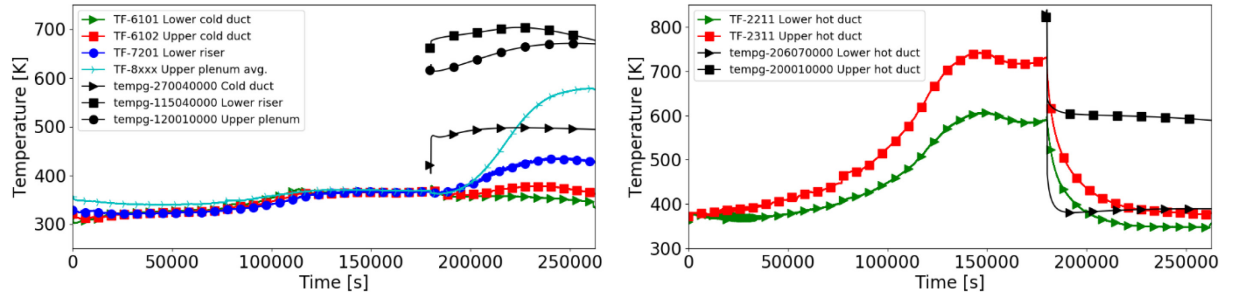


Figure 22. DCC only, **5 g/s** helium mass flow: left) helium core inlet temperatures and right) helium core outlet temperatures.

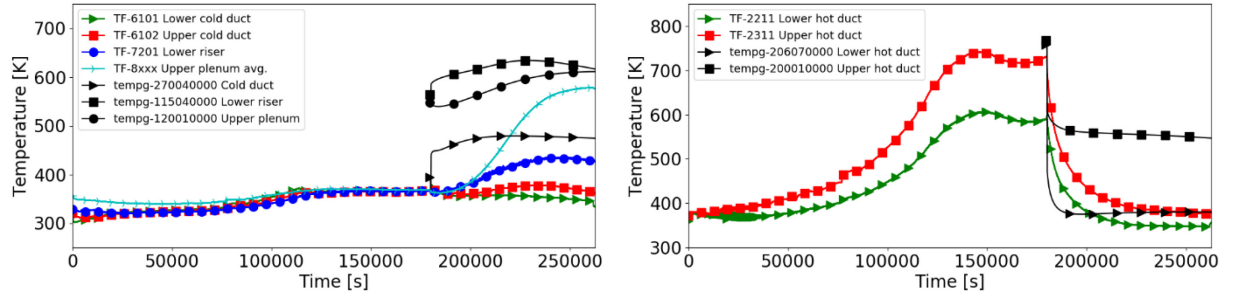


Figure 23. DCC only, **10 g/s** helium mass flow: left) helium core inlet temperatures and right) helium core outlet temperatures.

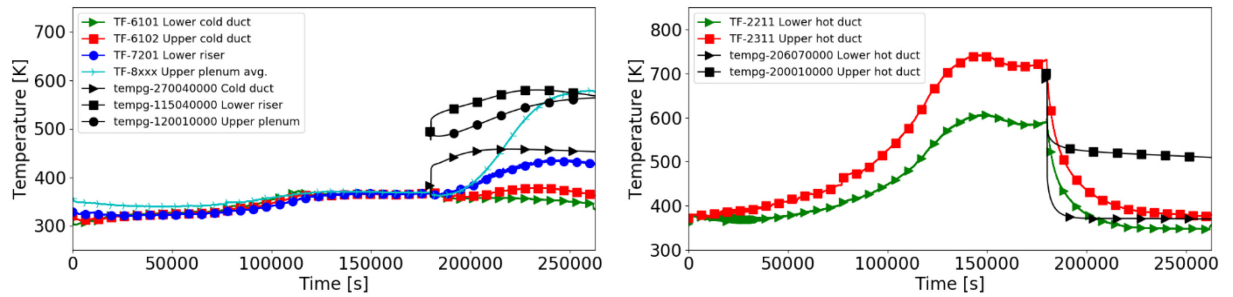


Figure 24. DCC only, **15 g/s** helium mass flow: left) helium core inlet temperatures and right) helium core outlet temperatures.

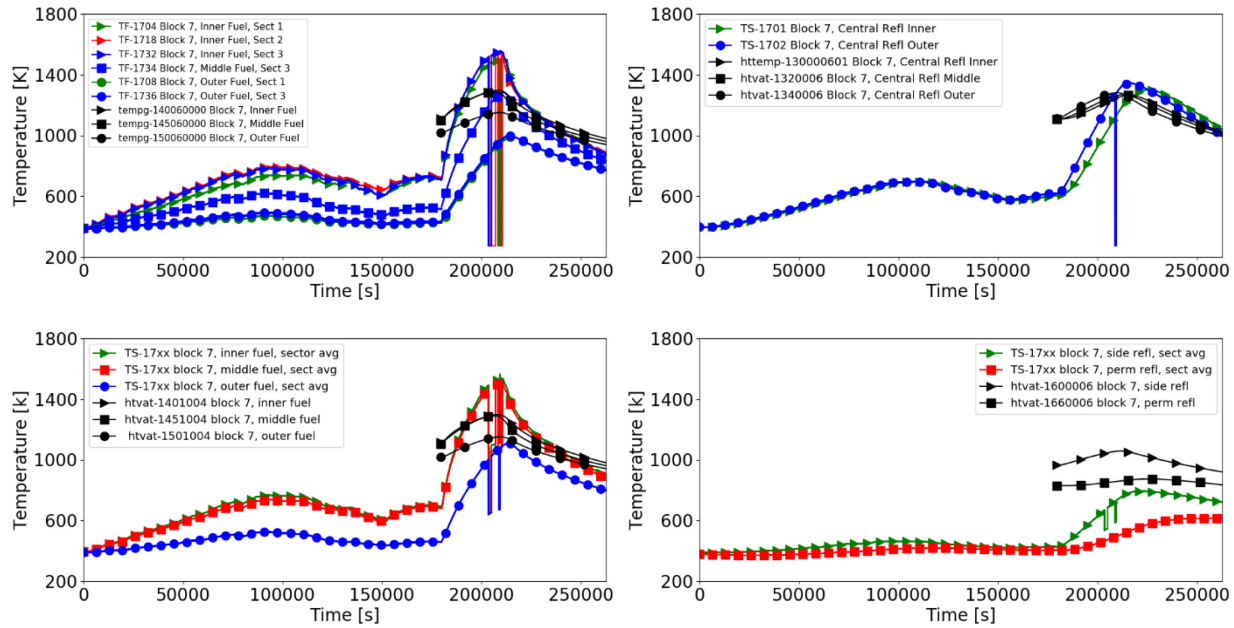


Figure 25. DCC only, **5 g/s** helium mass flow, **top of the core** (block 7): upper left) helium coolant temperatures, upper right) central reflector ceramic temperatures, lower left) ceramic temperatures in the fuel region, and lower right) side and permanent ceramic temperatures.

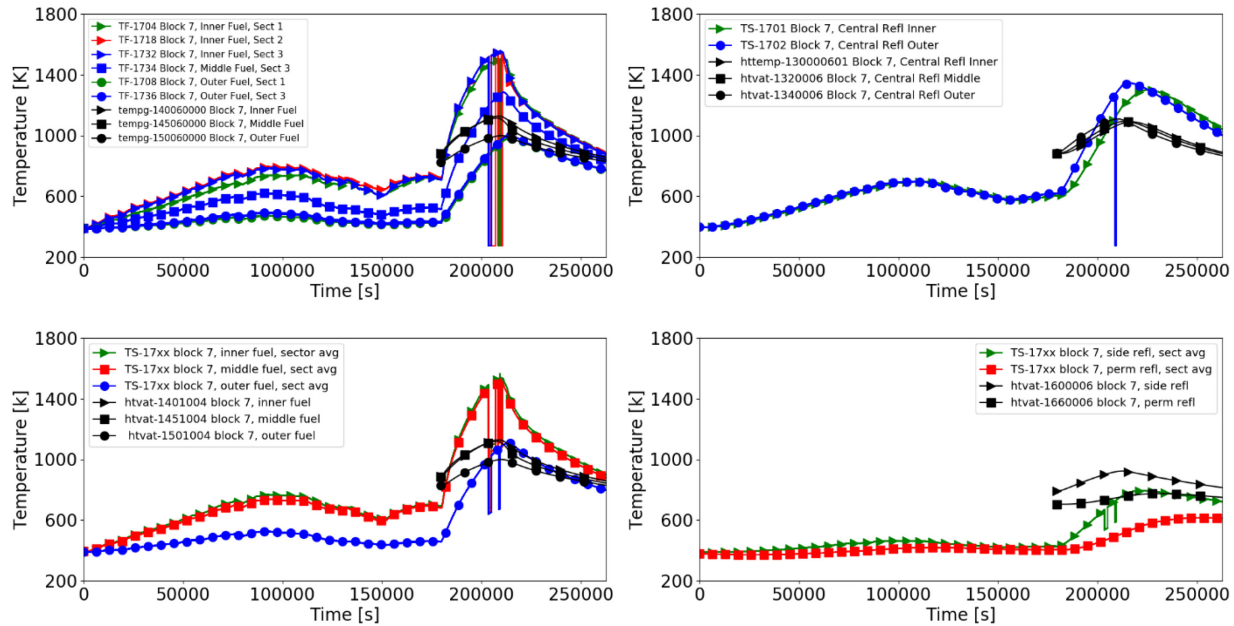


Figure 26. DCC only, **10 g/s** helium mass flow, **top of the core** (block 7): upper left) helium coolant temperatures, upper right) central reflector ceramic temperatures, lower left) ceramic temperatures in the fuel region, and lower right) side and permanent ceramic temperatures.

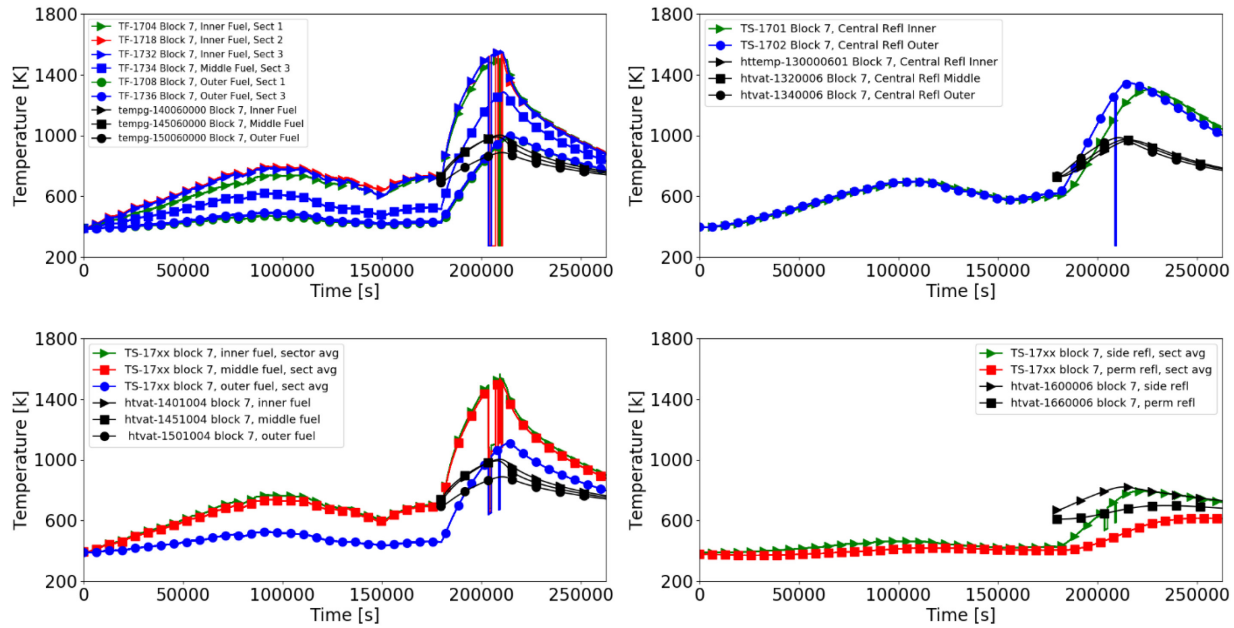


Figure 27. DCC only, **15 g/s** helium mass flow, **top of the core** (block 7): upper left) helium coolant temperatures, upper right) central reflector ceramic temperatures, lower left) ceramic temperatures in the fuel region, and lower right) side and permanent ceramic temperatures.

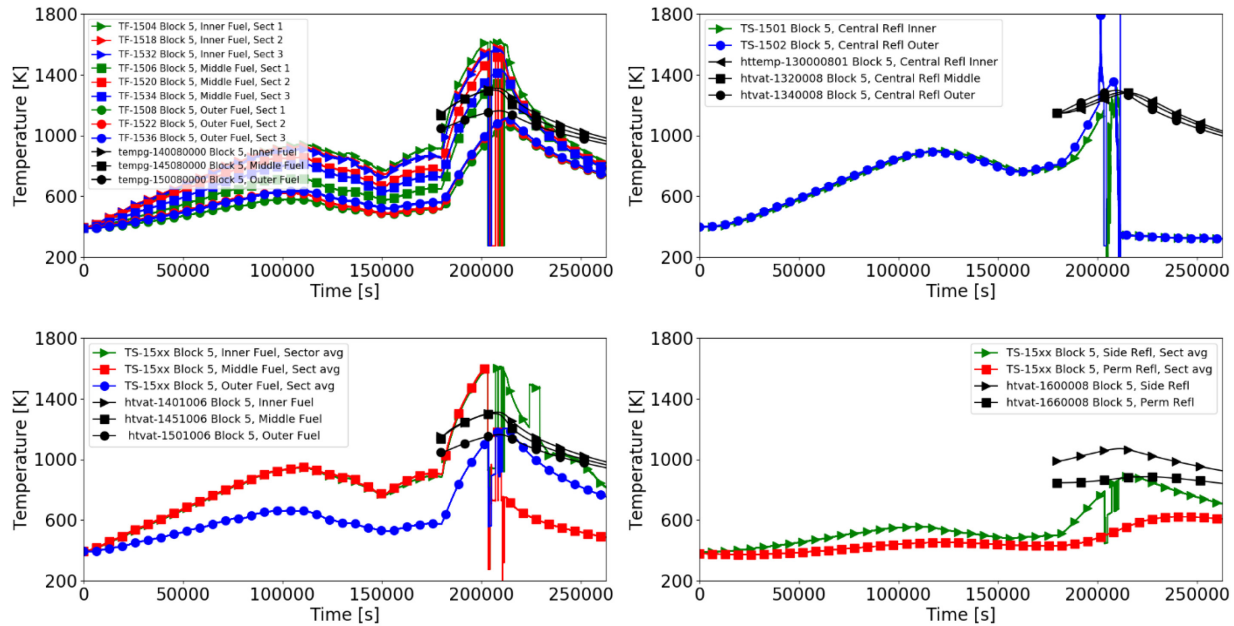


Figure 28. DCC only, **5 g/s** helium mass flow, **middle of the core** (block 5): upper left) helium coolant temperatures, upper right) central reflector ceramic temperatures, lower left) ceramic temperatures in the fuel region, and lower right) side and permanent ceramic temperatures.

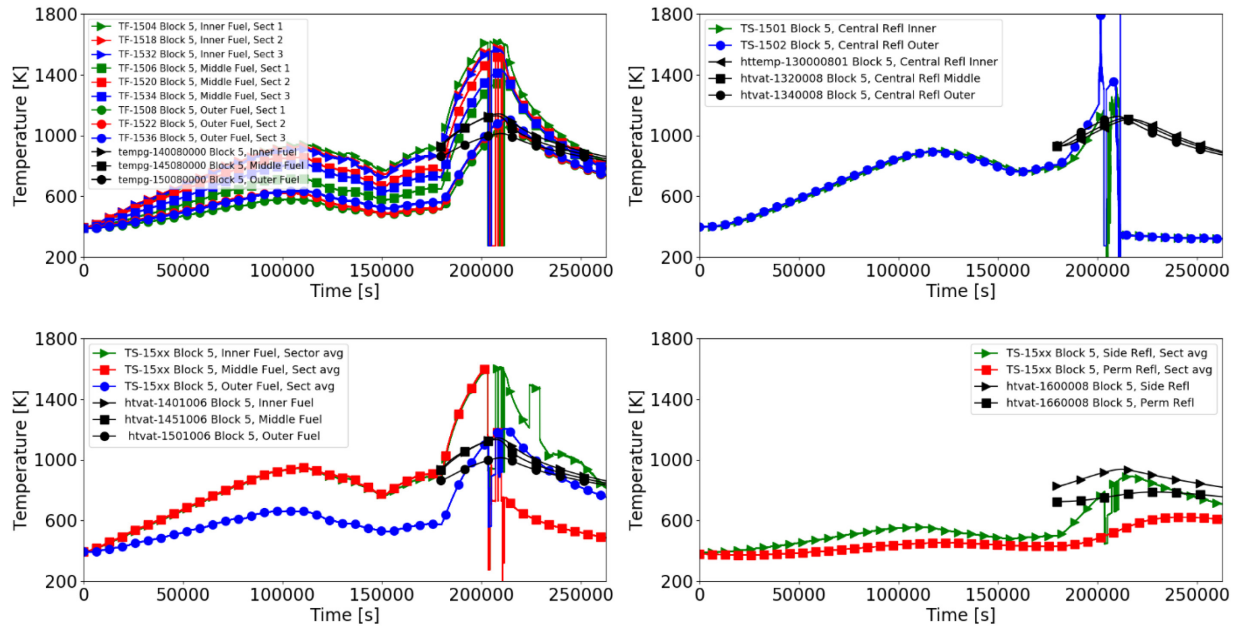


Figure 29. DCC only, **10 g/s** helium mass flow, **middle of the core** (block 5): upper left) helium coolant temperatures, upper right) central reflector ceramic temperatures, lower left) ceramic temperatures in the fuel region, and lower right) side and permanent ceramic temperatures.

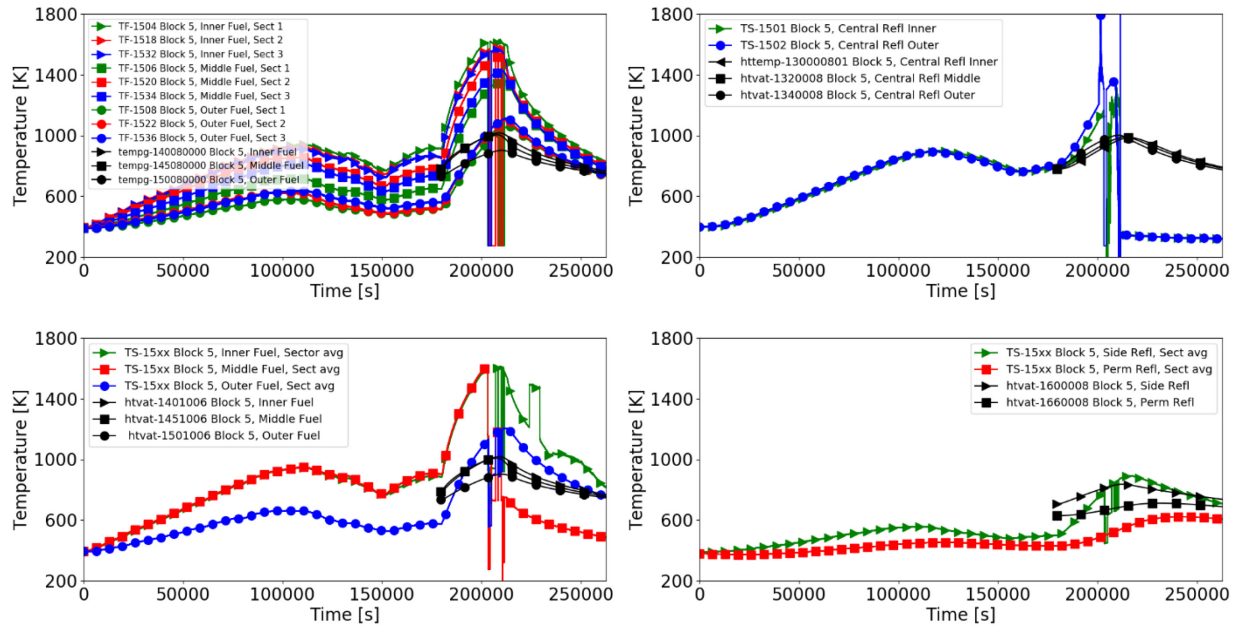


Figure 30. DCC only, **15 g/s** helium mass flow, **middle of the core** (block 5): upper left) helium coolant temperatures, upper right) central reflector ceramic temperatures, lower left) ceramic temperatures in the fuel region, and lower right) side and permanent ceramic temperatures.

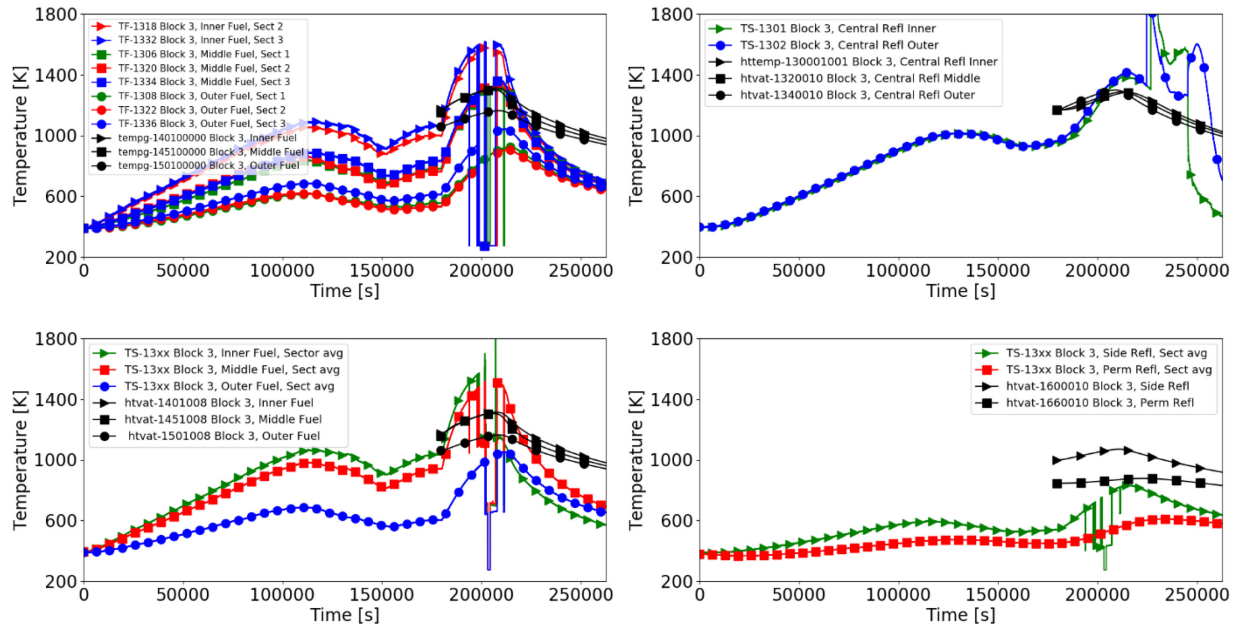


Figure 31. DCC only, **5 g/s** helium mass flow, **bottom of the core** (block 3): upper left) helium coolant temperatures, upper right) central reflector ceramic temperatures, lower left) ceramic temperatures in the fuel region, and lower right) side and permanent ceramic temperatures.

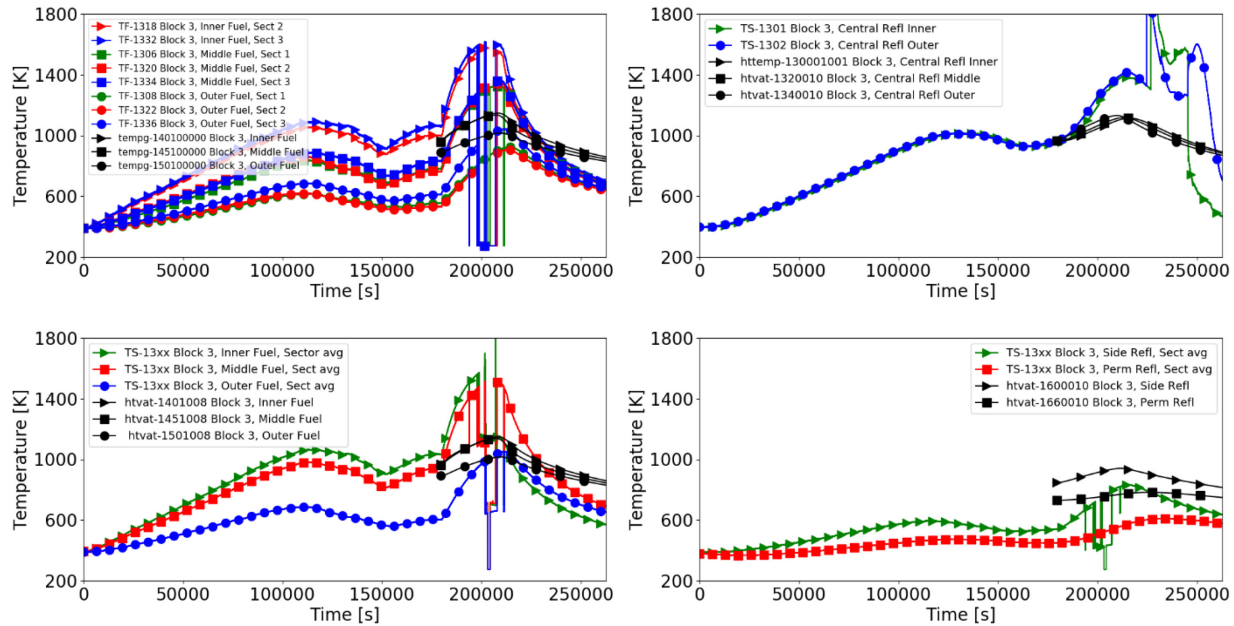


Figure 32. DCC only, **10 g/s** helium mass flow, **bottom of the core** (block 3): upper left) helium coolant temperatures, upper right) central reflector ceramic temperatures, lower left) ceramic temperatures in the fuel region, and lower right) side and permanent ceramic temperatures.

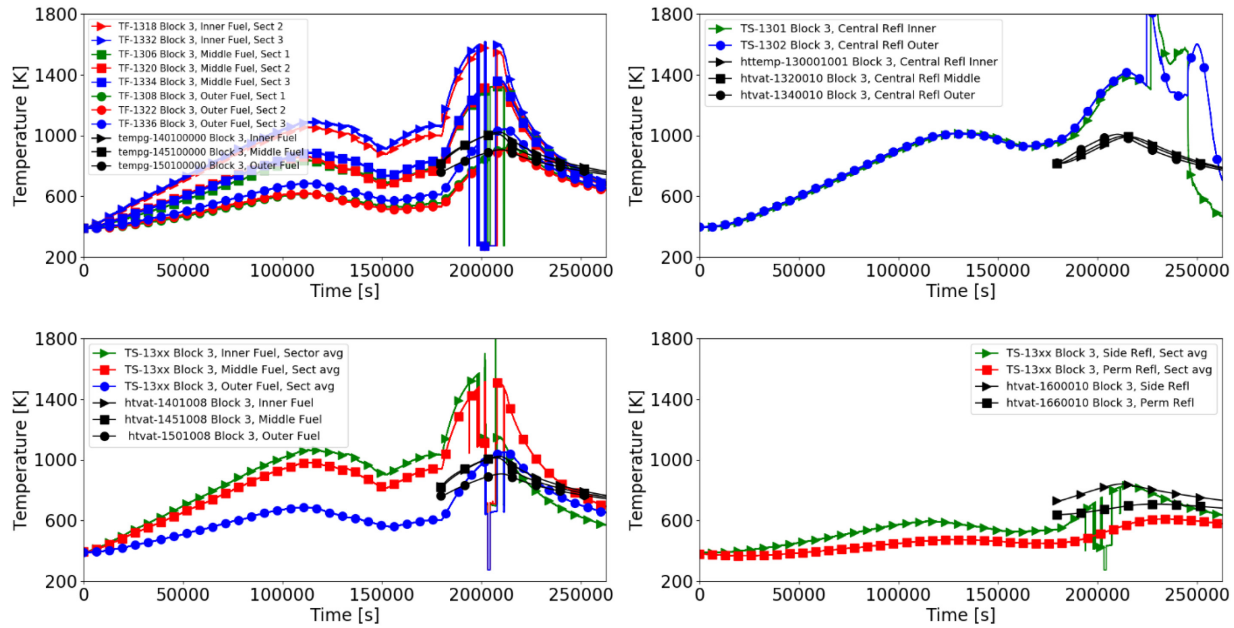


Figure 33. DCC only, **15 g/s** helium mass flow, **bottom of the core** (block 3): upper left) helium coolant temperatures, upper right) central reflector ceramic temperatures, lower left) ceramic temperatures in the fuel region, and lower right) side and permanent ceramic temperatures.

Table 3 shows the agreement for the central reflector, fuel region, and side reflector at the top (block 7), middle (block 5), and bottom (block 3) of the core. The indicators in the table for temperature (“Steady state” and “Peak during DCC”) and temperature slope (“Cooling during DCC”) are as follows:

- ↑↑ indicates RELAP5-3D significantly overpredicts the measured values (more than +50%),
- ↑ indicates RELAP5-3D somewhat overpredicts the measured values (between +10% and +50%),
- indicates RELAP5-3D is in close agreement with the measured values (between -10% and +10%),
- ↓ indicates RELAP5-3D somewhat underpredicts the values (between -10% and -50%) , and
- ↓↓ indicates RELAP5-3D significantly underpredicts the measured values (more than -50%).

Table 3. Steady state + DCC: qualitative trends for the ceramic temperatures in the core.

		Central refl.			Fuel region			Side refl.		
		Top	Mid	Bot	Top	Mid	Bot	Top	Mid	Bot
Steady state	5 g/s	↑↑	↑	↑	↑↑	↑	↑	↑↑	↑↑	↑↑
	10 g/s	↑	↑	■	↑	↑	■	↑↑	↑↑	↑↑
	15 g/s	↑	■	↓	↑	■	■	↑↑	↑	↑
Peak during DCC	5 g/s	■	■	↓	■	■	■	↑	↑	↑
	10 g/s	↓	↓	↓	↓	↓	↓↓	↑	■	↑
	15 g/s	↓	↓↓	↓↓	↓	↓	↓↓	■	■	■
Cooling during DCC	5 g/s	■	n/a	n/a	↓	↓↓	↓↓	↑↑	↓	↓
	10 g/s	↓	n/a	n/a	↓	↓↓	↓↓	↑↑	↓	■
	15 g/s	↓	n/a	n/a	↓↓	↓↓	↓↓	↑	■	↓

- One can see that the **steady state temperatures** are generally overpredicted. The helium mass flow rate of 15 g/s leads to the best average temperature prediction. The side reflector temperature is significantly overpredicted, indicating that RELAP5-3D predicts more heat transported out radially compared to measured data. Overall, these values are judged to be in **minimal agreement**.
- During the DCC transient, the ceramic solid temperature reduction is slower in the RELAP5-3D calculation compared to the measured data. These values are judged to be in **minimal agreement**. Looking at the energy balance, during the DCC, no heat can escape through the steam generator (isolated), and measured data indicates that no heat escaped through the RCCS (ΔT RCCS is zero in the measured data). This leaves two possibilities where the heat can go: a) it leaks directly into the environment through the RCST and cross-duct walls or b) the temperature reduction comes from the heat redistribution (averaging) inside the core ceramics. The RELAP5-3D simulations indicate that the heat leakage through the component walls is very small (see Figure 14–Figure 16). The author suspects that a) more heat than what was measured is escaping through natural convection in the air volume between the primary vessel and the RCCS panels, since this air volume is not sealed tightly and air can escape the space and b) if heat redistribution in the core lowers solid temperatures faster than in the RELAP5-3D simulation, the ceramic thermal properties, in particular the specific heat capacity (c_p), might be overestimated in the calculations.
- Looking at the **radial temperature distribution** in the core fuel region (and associated helium coolant channels), one can see a significant temperature difference between the inner, middle, and outer fuel rings (see top and bottom left plots in Figure 25–Figure 33) in the measured data that the RELAP5-3D model does not predict. One possible reason is that the ceramic thermal properties, in particular the thermal conductivity (λ), are overestimated in the RELAP5-3D model. These values are judged to be in **minimal agreement**.
- The **phenomenology during the DCC transient** can be interpreted from Figure 19 through Figure 21. The plots show the pressure evolution and the helium mass flow rate at different points in the system. The RELAP5-3D calculation starts at the steady-state and, as mentioned, goes through the blower rundown and manual depressurization before the break valves are opened and the DCC starts. During the time that the heaters are still running, one can see the **equalized PCS/RCST pressure** rise in the measured data. As soon as the heaters are shut off ($\sim 220,000$ s), the measured combined pressure starts to decrease slowly. This phenomenon was not observed in the RELAP5-3D calculation, where the equalized PCS/RCST pressure stays relatively constant. These values are judged to be in **insufficient agreement**. Looking at the core outlet helium temperatures, assuming flow stagnation at the core inlet and upper plenum (see Figure 22–Figure 24), one can see that the drop in core outlet temperature in the RELAP5-3D calculation compared to data is less pronounced and that the temperature difference between the upper and lower hot duct is larger. In fact, the calculated RELAP5-3D mass flow rates indicate that natural convection establishes through the following flow path: lower (outlet) plenum \rightarrow upper hot duct \rightarrow RCST \rightarrow lower hot duct \rightarrow lower outlet plenum (with a much smaller flow through the core). These two observations, no pressure rise and the establishment of natural convection, indicate that heat might be evacuated faster in the RELAP5-3D calculation compared to the measured data. However, the generally slower core ceramic cooling rates indicate the contrary (see slope underprediction in “Cooling during DCC in Table 3). One possible reason that the model does not predict a faster core cooldown while possibly overpredicting heat evacuation is that the core can actually store less heat than modeled (i.e., as already suspected from other observations, the specific heat capacity (c_p) of the core ceramic might be overestimated in the calculations).
- It is worth noting that the onset of a reverse **natural convection** through the core is observed in the RELAP5-3D calculation. This is in **insufficient agreement** with the test interpretation. The fact that the RELAP5-3D calculation predicts a countercurrent natural circulation flow path through the hot duct and the core that was not observed during the test indicates that friction in the core and hot duct might be underpredicted in the RELAP5-3D calculation.

4.3.2 Whole Transient

This section presents the results for the “whole transient” solutions. As mentioned, to possibly get better initial conditions before the DCC transient compared to the “steady state + DCC” calculations, the heat-up phase of the test has been modeled as well. At the beginning of PG-26, the HTTF core was still cooling down from a previous test (i.e., the facility had not reached a cold steady-state yet and was still in a transient). Consequently, no RELAP5-3D steady-state calculation can be performed to determine the facility conditions before the heat-up. The RELAP5-3D transient was started with initial conditions as close as possible to the core state at time zero (the automation script transferred all available measured data from the beginning of the test into the RELAP5-3D input deck). Figure 34–Figure 51 show the results of the RELAP5-3D calculations. As for the “steady-state + DCC” calculations, colored lines represent measured data while black lines are RELAP5-3D calculation results.

For the “whole transient” RELAP5-3D calculation of PG-26, the following observations are made:

- The **core helium temperature difference** (see Figure 34–Figure 36) is well matched during the heat-up transient. The best match is achieved for the 15 g/s helium mass flow case. This data is judged to be in **reasonable agreement**. During the DCC transient, the core helium temperature difference drops to close to zero K (for the 15 g/s helium mass flow case). The fact that the core helium temperature difference is much better captured in the “whole transient” calculations compared to the “steady-state + DCC” indicates that the facility is (as suspected) not at steady state before the DCC starts.
- Looking at the **helium core inlet and outlet temperatures** (see Figure 40–Figure 42), one can see that the helium is much less preheated (compared to the “steady-state + DCC” case) in the lower vessel before it entered the riser section. In fact, cold duct, riser, and upper plenum helium temperatures for the 15 g/s helium mass flow case match the measured data well. The fact that the “whole transient” run captures helium pre-heating in the lower vessel structures better than the “steady-state + DCC” is another indication that the facility did not reach a true steady-state before the DCC transient. The **core inlet temperature** is judged to be in **reasonable agreement during the heat-up portion of the transient**. Looking at the 15 g/s case core inlet helium temperatures during the DCC portion of the test, one can see that the (assumed to be stagnant) helium heat-up in the upper plenum is less pronounced than in the measured data. Furthermore, the temperature decrease in measured data in the cold duct and riser is not captured in the RELAP5-3D simulations. Together with the fact that the core solid structure cooldown in the RELAP5-3D simulations is slower than in the measure data, these observations are indications that the amount of heat released from the core into the helium and associated temperature change in the material is different in the RELAP5-3D simulation and the measured data. The **core inlet temperature** is judged to be in **minimal agreement during the DCC portion of the transient**. Another observation from Figure 40 through Figure 42 is that the temperature difference between the upper and lower part of the hot duct is not captured in the RELAP5-3D simulation. As already discussed for the “steady-state + DCC” case, this could be explained with the thermal stratification of the helium in the lower outlet plenum that cannot be captured with the 0D nodalization of this structure currently in the RELAP5-3D model of HTTF. The **core outlet temperature** is judged to be in **minimal agreement**.
- Qualitative trends for the **ceramic solid core temperatures** are presented in Table 4 for the “whole transient” case. The table shows qualitative trends for temperature predictions at the end of the heat-up transient (at 175,000 s), the peak temperature during the DCC, and the cooling rate once the heaters have been stopped (~220,000 s). The table compares the RELAP5-3D temperature predictions with the region averaged (Radially and azimuthally [sectors] averaged through the region) measured temperatures.

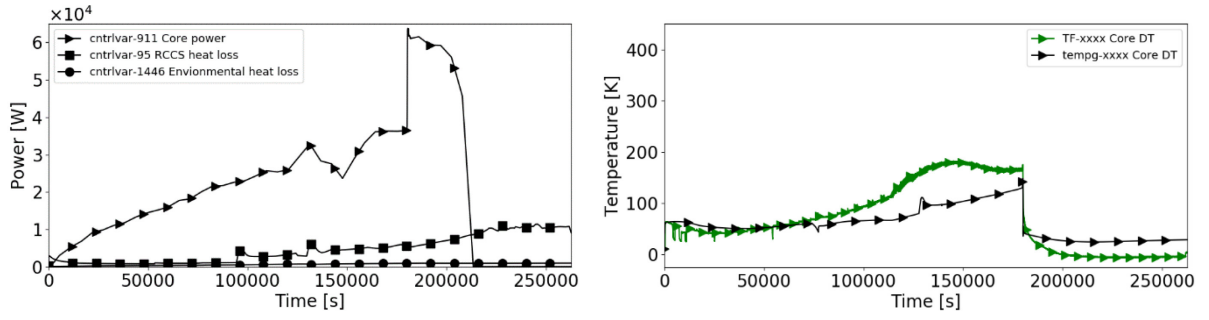


Figure 34. Whole transient, **5 g/s** helium mass flow: left) core heat balance and right) core helium ΔT .

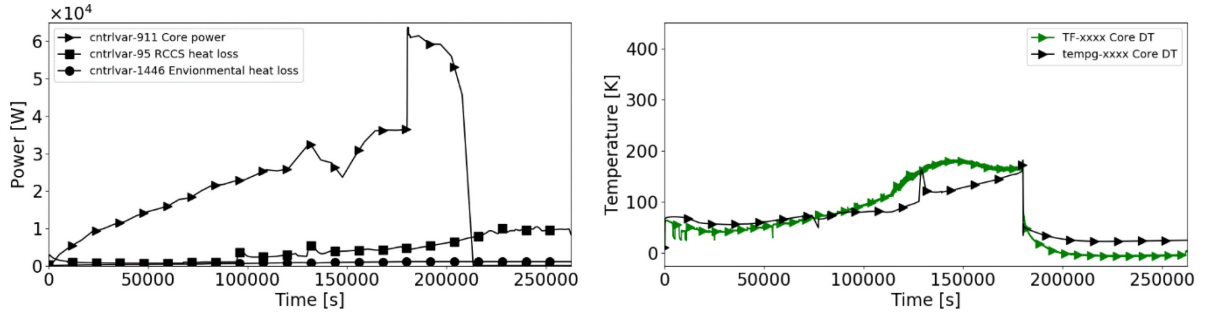


Figure 35. Whole transient, **10 g/s** helium mass flow: left) core heat balance and right) core helium ΔT .

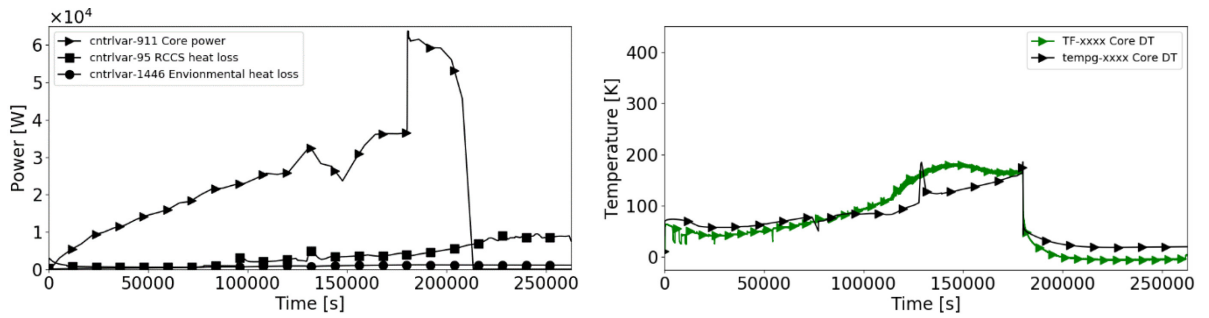


Figure 36. Whole transient, **15 g/s** helium mass flow: left) core heat balance and right) core helium ΔT .

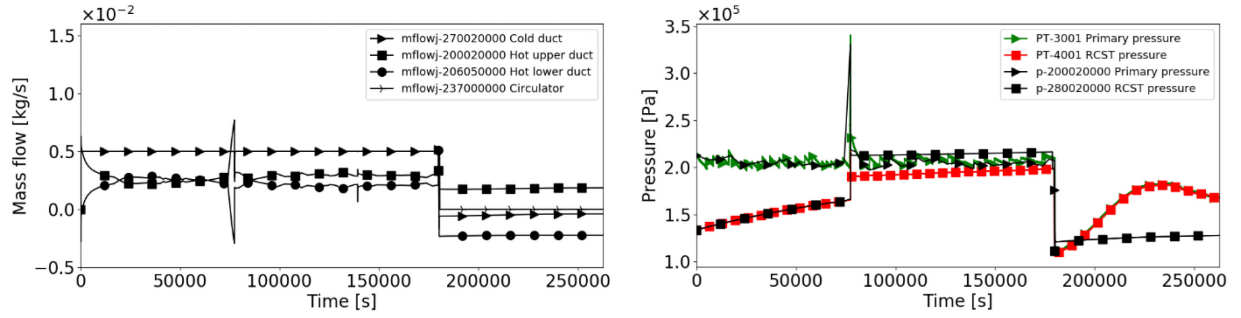


Figure 37. Whole transient, 5 g/s helium mass flow: left) PCS helium mass flow rates and right) PCS and RCST pressure.

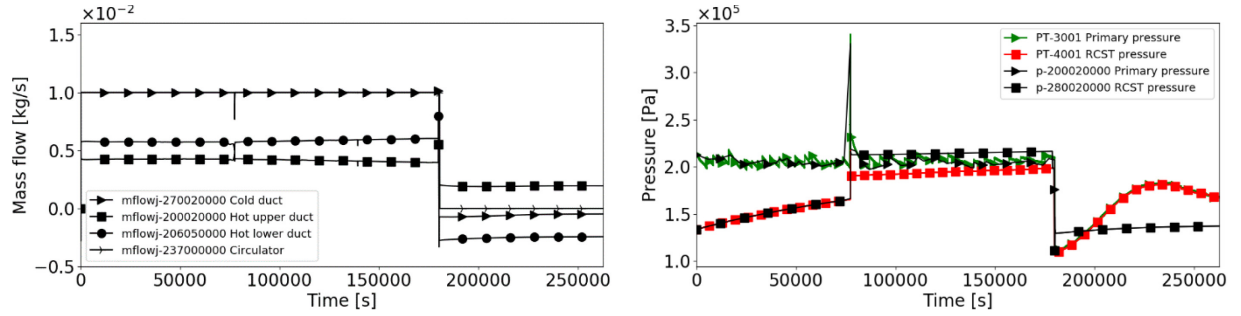


Figure 38. Whole transient, 10 g/s helium mass flow: left) PCS helium mass flow rates and right) PCS and RCST pressure.

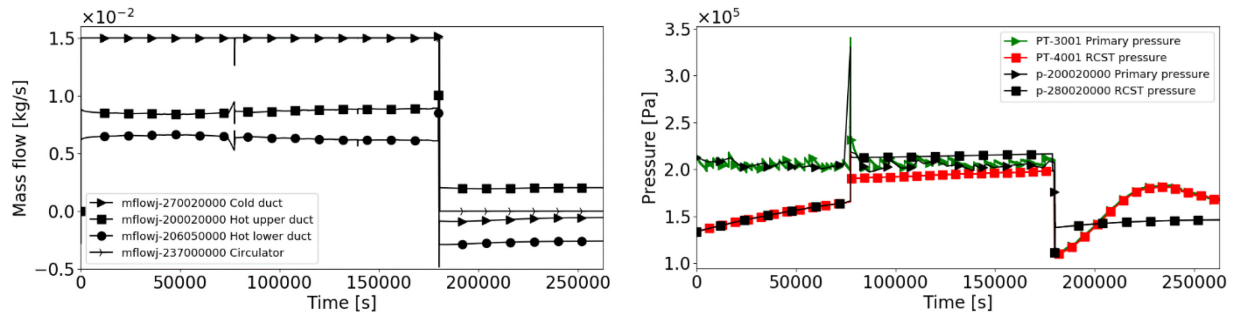


Figure 39. Whole transient, 15 g/s helium mass flow: left) PCS helium mass flow rates and right) PCS and RCST pressure.

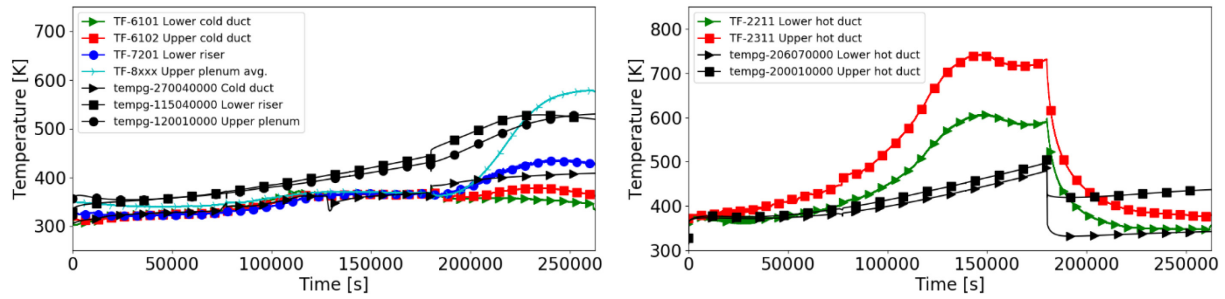


Figure 40. Whole transient, 5 g/s helium mass flow: left) helium core inlet temperatures and right) helium core outlet temperatures.

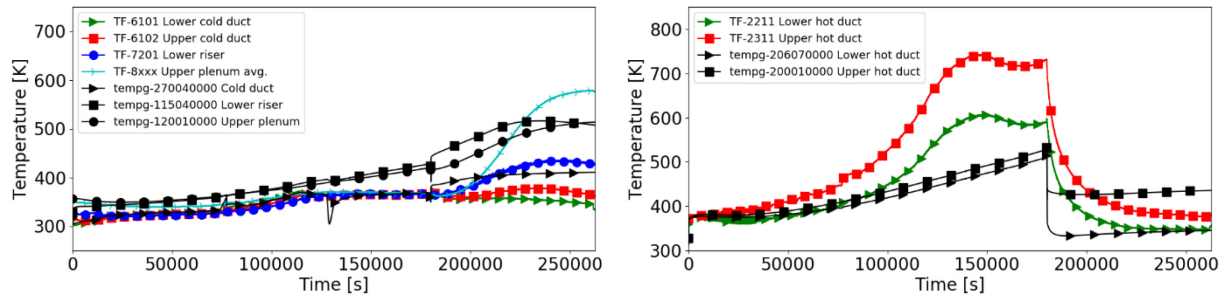


Figure 41. Whole transient, 10 g/s helium mass flow: left) helium core inlet temperatures and right) helium core outlet temperatures.

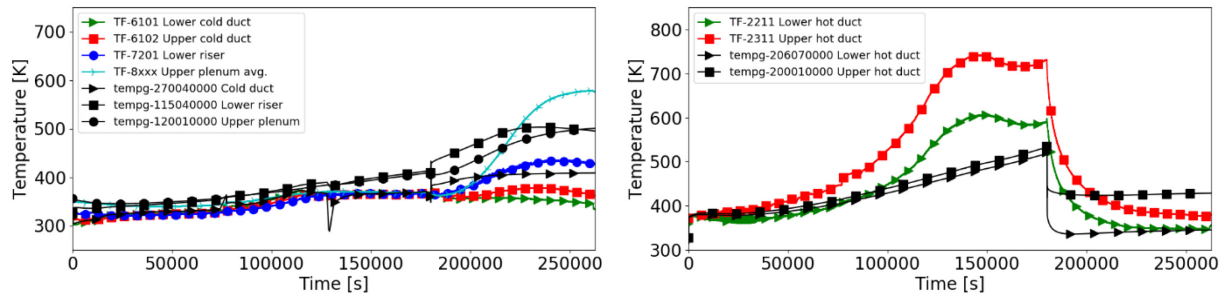


Figure 42. Whole transient, 15 g/s helium mass flow: left) helium core inlet temperatures and right) helium core outlet temperatures.

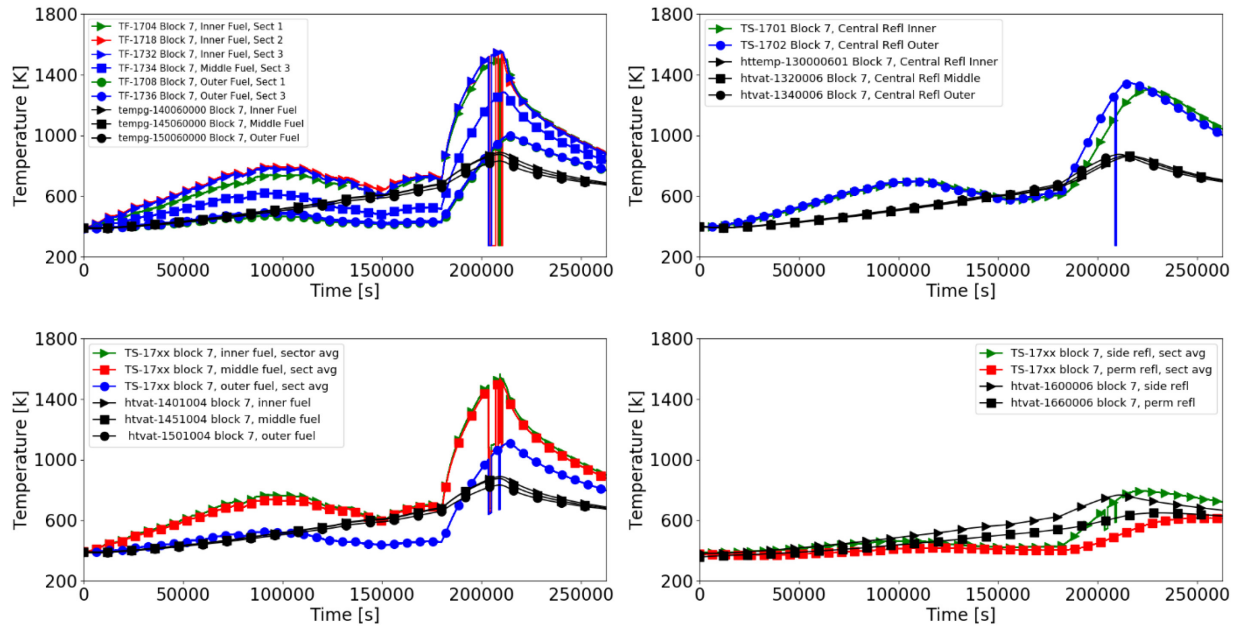


Figure 43. Whole transient, **5 g/s** helium mass flow, **top of the core (block 7)**: upper left) helium coolant temperatures, upper right) central reflector ceramic temperatures, lower left) ceramic temperatures in the fuel region, and lower right) side and permanent ceramic temperatures.

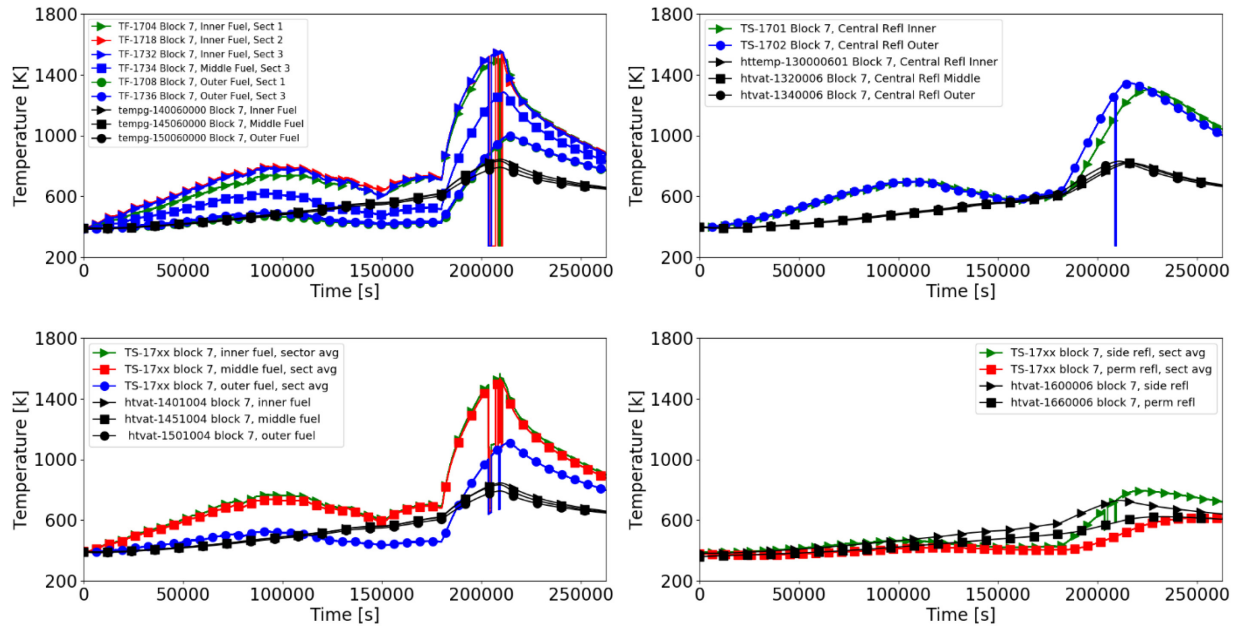


Figure 44. Whole transient, **10 g/s** helium mass flow, **top of the core (block 7)**: upper left) helium coolant temperatures, upper right) central reflector ceramic temperatures, lower left) ceramic temperatures in the fuel region, and lower right) side and permanent ceramic temperatures.

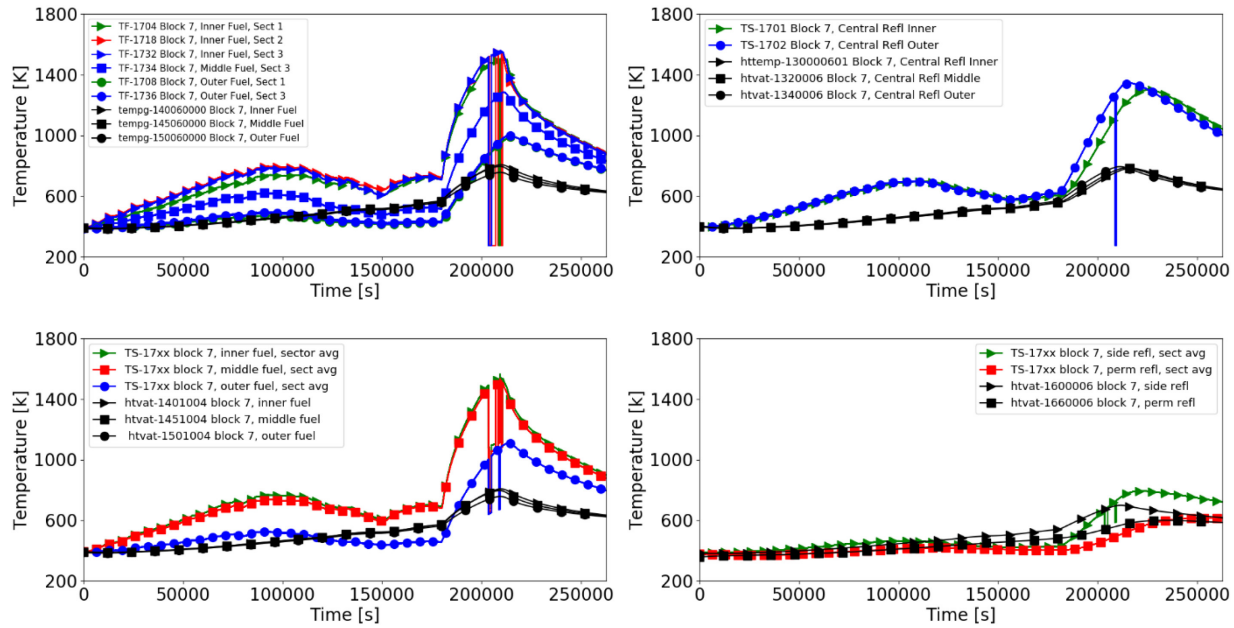


Figure 45. Whole transient, **15 g/s** helium mass flow, **top of the core** (block 7): upper left) helium coolant temperatures, upper right) central reflector ceramic temperatures, lower left) ceramic temperatures in the fuel region, and lower right) side and permanent ceramic temperatures.

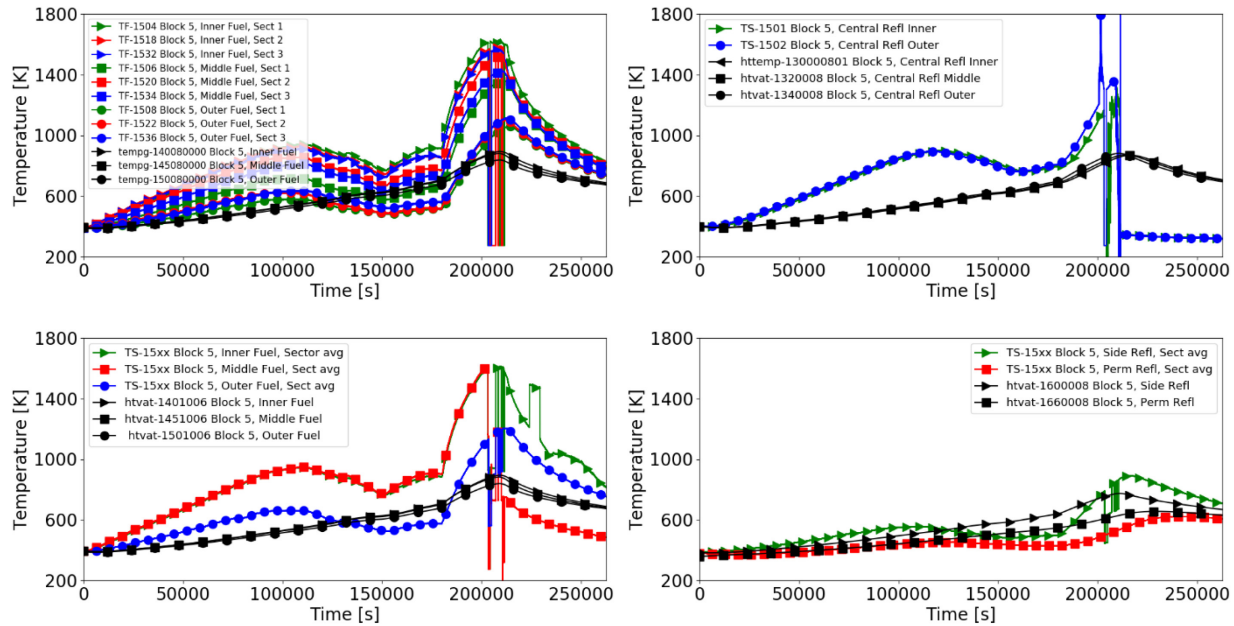


Figure 46. Whole transient, **5 g/s** helium mass flow, **middle of the core** (block 5): upper left) helium coolant temperatures, upper right) central reflector ceramic temperatures, lower left) ceramic temperatures in the fuel region, and lower right) side and permanent ceramic temperatures.

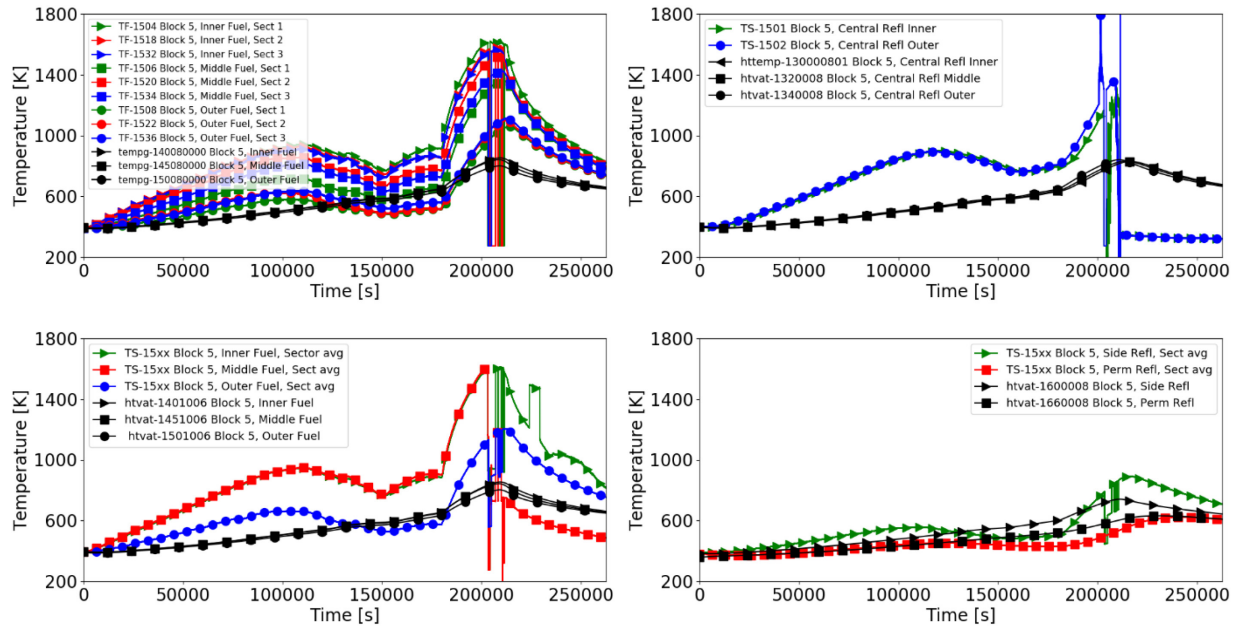


Figure 47. Whole transient, **10 g/s** helium mass flow, **middle of the core** (block 5): upper left) helium coolant temperatures, upper right) central reflector ceramic temperatures, lower left) ceramic temperatures in the fuel region, and lower right) side and permanent ceramic temperatures.

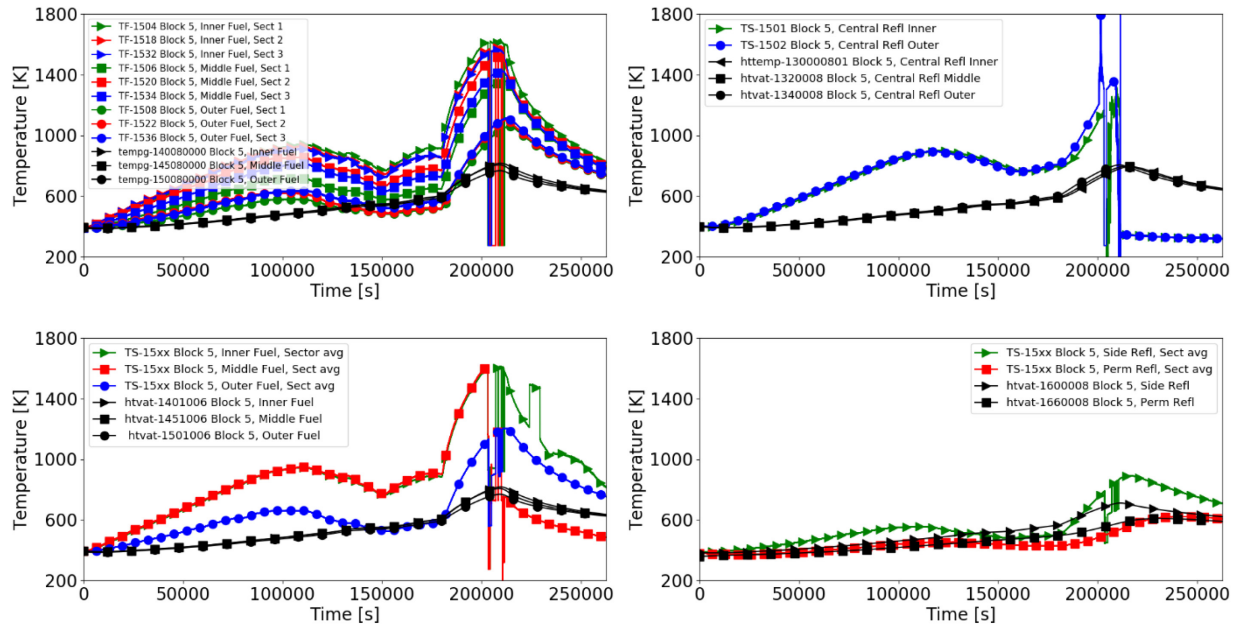


Figure 48. Whole transient, **15 g/s** helium mass flow, **middle of the core** (block 5): upper left) helium coolant temperatures, upper right) central reflector ceramic temperatures, lower left) ceramic temperatures in the fuel region, and lower right) side and permanent ceramic temperatures.

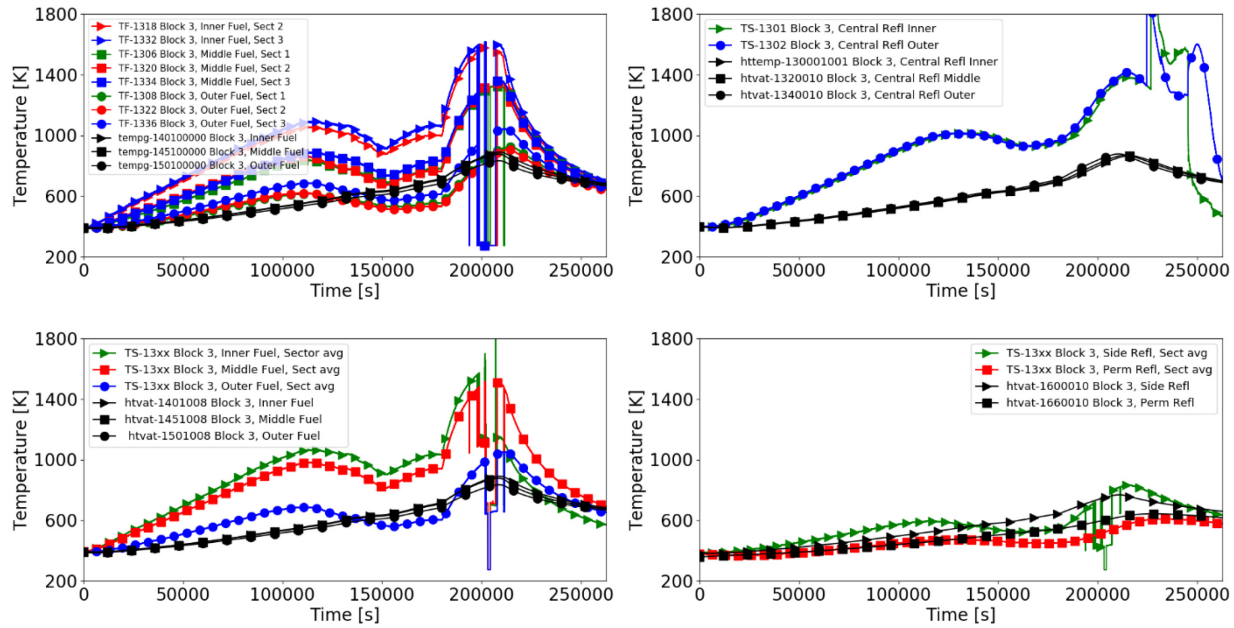


Figure 49. Whole transient, **5 g/s** helium mass flow, **bottom of the core** (block 3): upper left) helium coolant temperatures, upper right) central reflector ceramic temperatures, lower left) ceramic temperatures in the fuel region, and lower right) side and permanent ceramic temperatures.

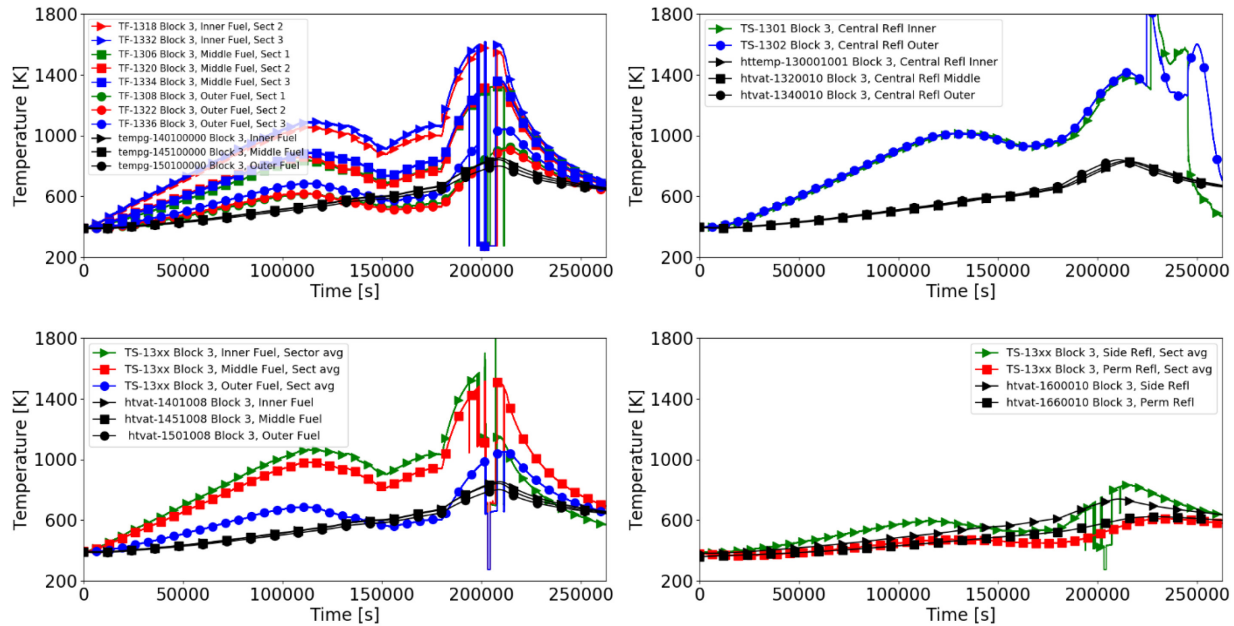


Figure 50. Whole transient, **10 g/s** helium mass flow, **bottom of the core** (block 3): upper left) helium coolant temperatures, upper right) central reflector ceramic temperatures, lower left) ceramic temperatures in the fuel region, and lower right) side and permanent ceramic temperatures.

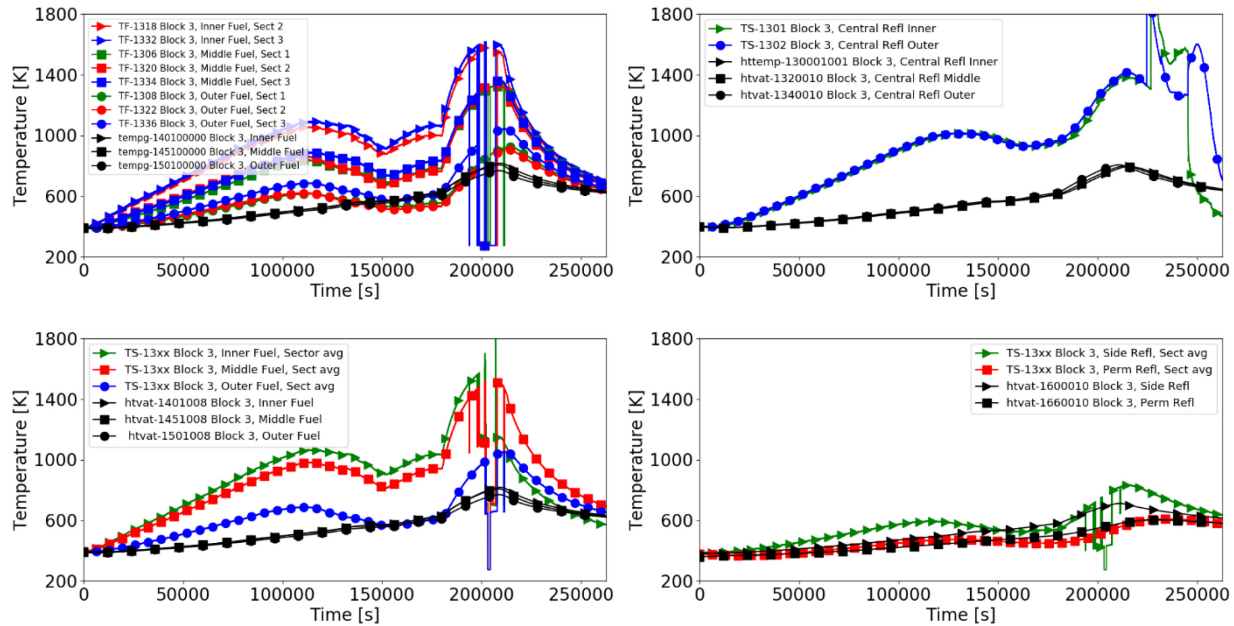


Figure 51. Whole transient, **15 g/s** helium mass flow, **bottom of the core** (block 3): upper left) helium coolant temperatures, upper right) central reflector ceramic temperatures, lower left) ceramic temperatures in the fuel region, and lower right) side and permanent ceramic temperatures.

Table 4 shows the agreement for the central reflector, fuel region, and side reflector at the top (block 7), middle (block 5), and bottom (block 3) of the core. The indicators in the table for temperature (“Steady state” and “Peak during DCC”) and temperature slope (“Cooling during DCC”) are as follows:

- ↑↑ indicates RELAP5-3D significantly overpredicts the measured values (more than +50%),
- ↑ indicates RELAP5-3D somewhat overpredicts the measured values (between +10% and +50%),
- indicates RELAP5-3D is in close agreement with the measured values (between -10% and +10%),
- ↓ indicates RELAP5-3D somewhat underpredicts the values (between -10% and -50%), and
- ↓↓ indicates RELAP5-3D significantly underpredicts the measured values (more than -50%).

Table 4. Whole transient: qualitative trends for the ceramic temperatures in the core.

		Central refl.			Fuel region			Side refl.		
		Top	Mid	Bot	Top	Mid	Bot	Top	Mid	Bot
Heat-up @175000s	5 g/s	■	↓	↓	↑	■	■	↑	↑	↑
	10 g/s	■	↓	↓	■	■	■	↑	↑	↑
	15 g/s	■	↓	↓	■	↓	↓	↑	↑	■
Peak during DCC	5 g/s	↓	↓↓	↓↓	↓	↓	↓↓	■	↓	■
	10 g/s	↓	↓↓	↓↓	↓	↓	↓↓	■	↓	↓
	15 g/s	↓	↓↓	↓↓	↓	↓	↓↓	↓	↓	↓
Cooling during DCC	5 g/s	↓	n/a	n/a	↓	↓↓	↓↓	↑	■	↓
	10 g/s	↓↓	n/a	n/a	↓↓	↓↓	↓↓	↑	■	↓
	15 g/s	↓↓	n/a	n/a	↓↓	↓↓	↓↓	↑	■	↓

- Contrary to the “steady-state + DCC” case, one can see that that **solid temperatures before the DCC starts** are generally underpredicted for the “whole transient” case. For the central reflector and fuel region, increasing the helium mass flow rate in the core from 5 g/s to 15 g/s leads to further underpredictions of the temperatures. The 5 g/s mass flow case is in best agreement with the measured data. Because all temperatures are “shifted down” compared to the “steady-state + DCC” case, the side and permanent reflector temperatures are better captured during the heat-up portion of the test, indicating that RELAP5-3D predicts that there is less heat transported out radially compared to the “steady-state + DCC,” which also explained the lower helium upper plenum temperatures. Overall, these values are judged to be in **minimal agreement**.
- Another observation from Figure 40 through Figure 51 is that the measured data shows a **ceramic temperature reduction from ~100,000 s to ~150,000 s** during the heat-up (especially in the central reflector and fuel regions), which is not captured by the RELAP5-3D model. It is believed that this temperature reduction is due to the change in heater power together with the reduced inlet helium temperature stemming from the venting and replenishing of the steam generator that happens around these times (see Section 2.2.7). Both effects should be reflected in the RELAP5-3D model through the heater power and primary helium inlet temperature boundary conditions used, and it remains unclear why this behavior is not captured in the simulations. This data is judged to be in **insufficient agreement**.
- During the DCC transient, like in the “steady-state + DCC” case, **peak ceramic solid temperatures and temperature reduction rates** are slower in the RELAP5-3D calculation compared to the measured data. The reasonings made for the “steady-state + DCC” case can be applied to the “whole transient” case. These values are judged to be in **minimal agreement**.
- For the **radial temperature distribution** in the core fuel region (and associated helium coolant channels) and the **phenomenology during the DCC transient**, the same observations as for the “steady-state + DCC” case can be made. They are still in **minimal** and **insufficient agreement**, respectively.

4.4 Sensitivity Studies

During the discussion of the base calculations, the biggest disagreements between the measured data and RELAP-3D simulation results have been speculated to come from differences in the energy balance and loop friction. This section presents some sensitivities to investigate these hypotheses. All presented sensitivities consider the “whole transient” with 15 g/s primary helium flow as the reference case.

4.4.1 Core Ceramic Thermal Properties

During the discussion of the base case results, it has been speculated that both the specific heat capacity (c_p) as well as the thermal conductivity (λ) of the core ceramic might be overestimated in the calculations. The first sensitivity study considers the core ceramic thermal properties. Four cases are compared as shown in Table 5.

Table 5. Core ceramic thermal property sensitivity cases.

Case	Specific heat (c_p)	Thermal conductivity (λ)	Comment
1	Reference	Reference	This is the reference as shown in the base case calculations.
2	1/10	Reference	
3	Reference	1/5	
4	1/10	1/5	

Figure 52 through Figure 57 compare the helium mass flow rate in the PCS, the pressure in the PCS and RCST, and the helium and solid temperatures at a midcore height in core block 5 for the four combinations of ceramic specific heat (c_p) and thermal conductivity (λ), as indicated above. The temperatures of the other core blocks behave similarly and are not shown. From the sensitivity study of the core ceramic thermal properties, the following observations are made:

- Decreasing c_p and λ increases the ceramic **temperatures** in the core ceramics and, consequently, in the helium **during the DCC** portion of the test. The fourth case, where c_p is decreased by a factor of 10 and λ is decreased by a factor of 5, reproduces the height and duration of the temperature peaks in the core ceramics well. This confirms the hypothesis that less energy can be stored in the core ceramics per degree Kelvin than is indicated in the base thermal properties for the ceramic. These values are judged to be improved to **reasonable agreement**.
- Looking at the **ceramic and helium temperatures during the heat-up phase of the transient**, one can see that the radial temperature distribution in the fuel region (see Figure 56) and associated helium temperatures (see Figure 54) are still not reproduced by the RELAP5-3D simulations when lowering the core ceramic c_p and λ . Possible explanations that merit further investigation in future studies are that:
 - the helium flow distribution in the core channels is not captured well by the RELAP5-3D simulation. The distribution in the facility could be affected by different radial expansions of the core blocks and therefore different flow channel obstructions in the radial direction.
 - the ceramic thermal properties (in particular the thermal conductivity) are not just a function of temperature, but also a function of the dryness of the ceramic, which might change radially through the core. As one can see, the central reflector temperatures are still underpredicted (they may be the least dry) while the side reflectors are better captured (they may be the driest). These values are still judged to be in **minimal agreement**.
- As mentioned, the measured data shows a **ceramic temperature reduction from ~100,000 s to ~150,000 s** during the heat-up. Lowering the thermal properties of the core ceramics shows a slight stabilization and reduction of these temperatures in the RELAP5-3D model as well. This indicates that the ceramics thermal properties are at least partially responsible for not capturing this phenomenon during the base calculations. However, the decreasing trend is still not captured by the simulation. This data is judged to be improved to **minimal agreement**.
- The higher helium temperatures lead to a slight **pressure swing during the DCC portion** of the transient (see Figure 53). However, the calculated swing is still much lower compared to the measured data. These values are still judged to be in **insufficient agreement**.
- The helium flow behavior during the DCC (gas mixing and natural convection in the core and lower plenum) has not changed compared to the base calculation. They are still in **insufficient agreement**.

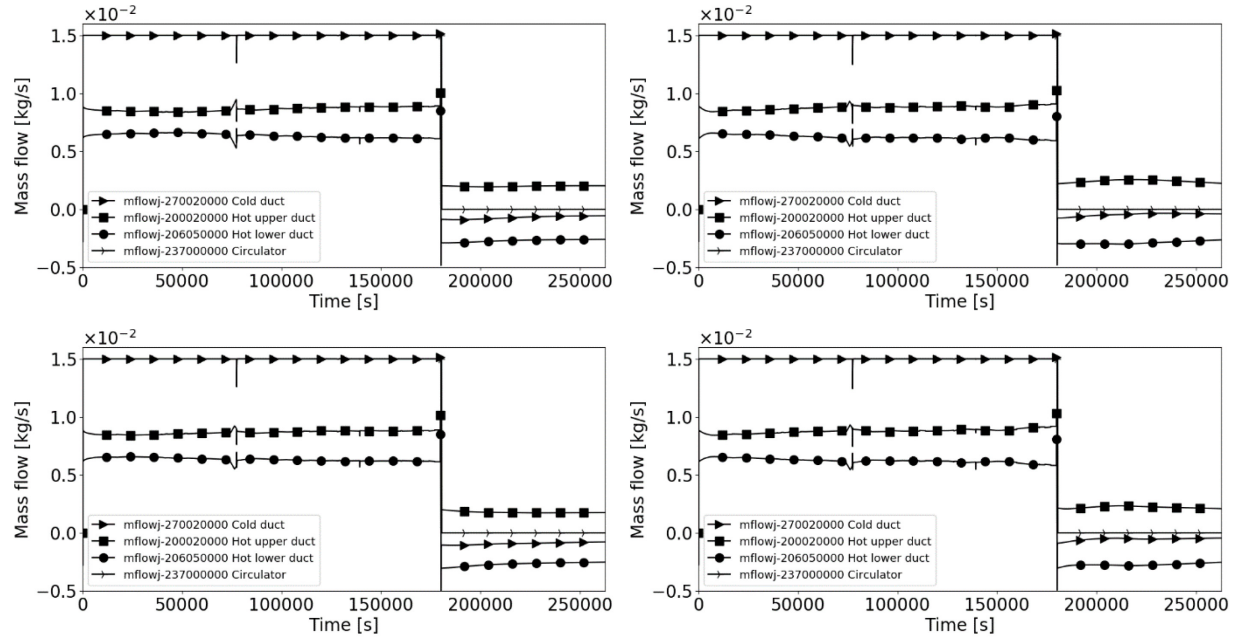


Figure 52. Whole transient, 15 g/s helium mass flow, **PCS helium mass flow rates**: upper left) original c_p and λ , upper right) $1/10 c_p$ and original λ , lower left) original c_p and $1/5 \lambda$, and lower right) $1/10 c_p$ and $1/5 \lambda$.

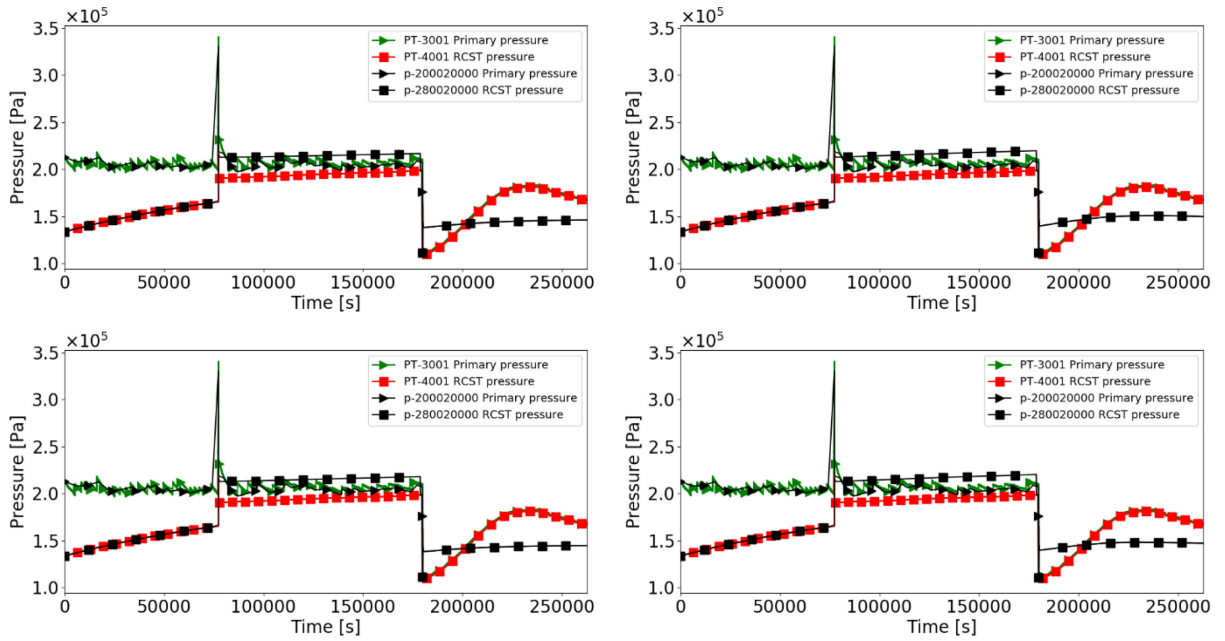


Figure 53. Whole transient, 15 g/s helium mass flow, **PCS and RCST pressure**: upper left) original c_p and λ , upper right) $1/10 c_p$ and original λ , lower left) original c_p and $1/5 \lambda$, and lower right) $1/10 c_p$ and $1/5 \lambda$.

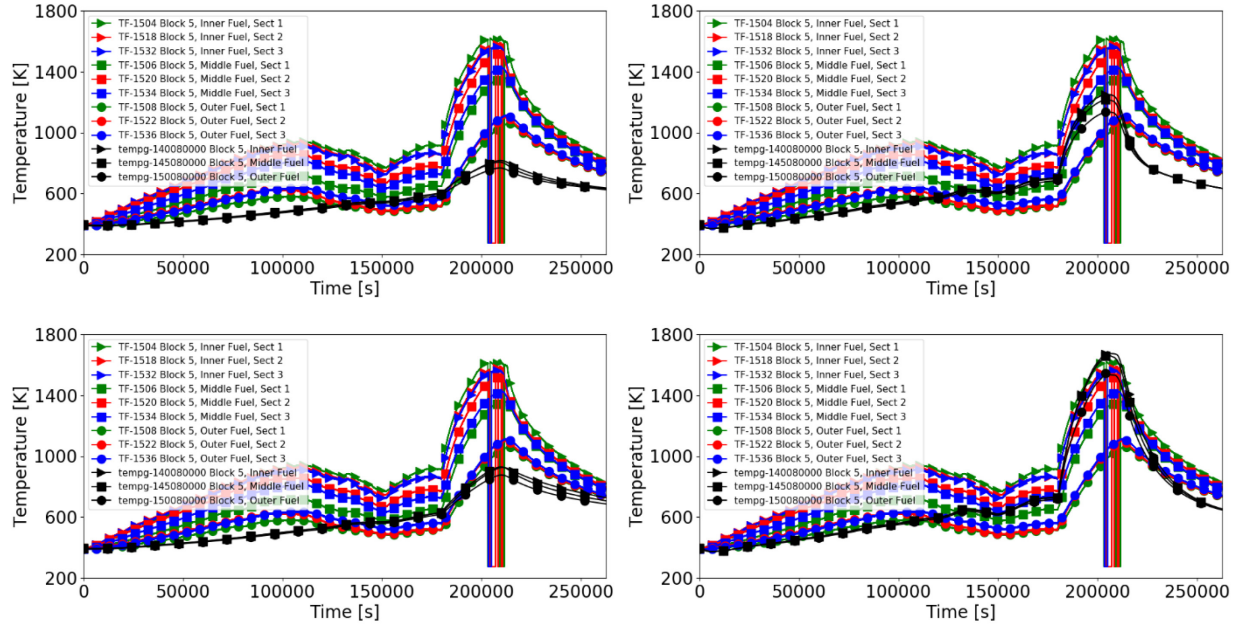


Figure 54. Whole transient, 15 g/s helium mass flow, **middle of the core (block 5) helium coolant temperatures**: upper left) original c_p and λ , upper right) $1/10 c_p$ and original λ , lower left) original c_p and $1/5 \lambda$, and lower right) $1/10 c_p$ and $1/5 \lambda$.

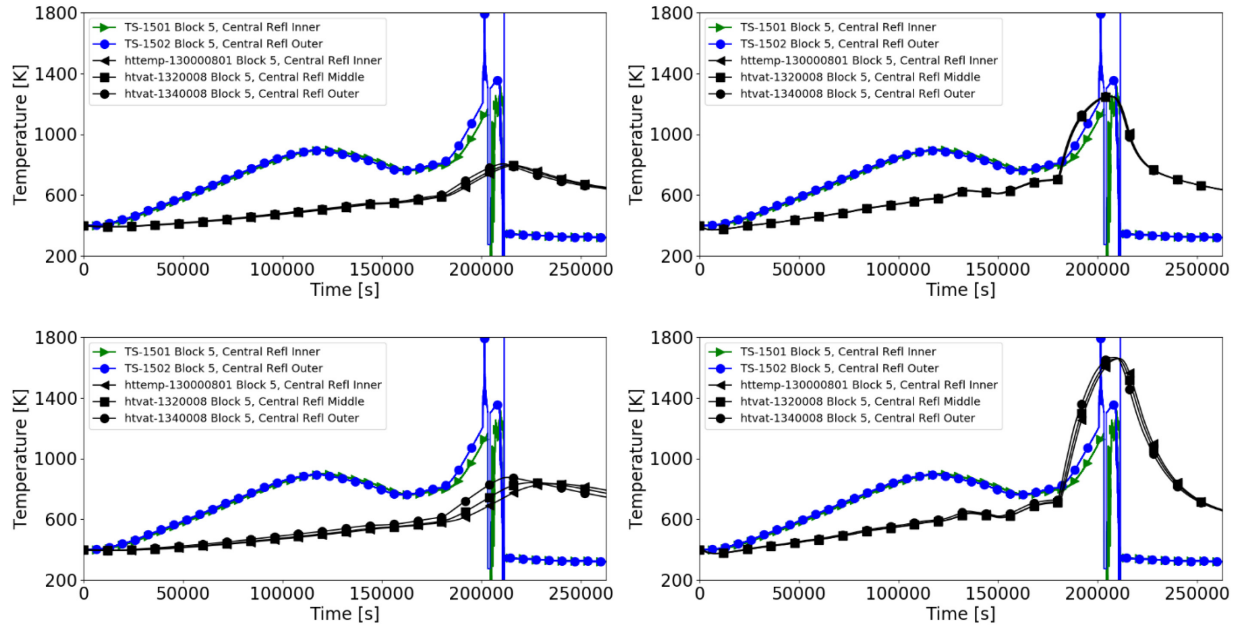


Figure 55. Whole transient, 15 g/s helium mass flow, **middle of the core (block 5) central reflector ceramic temperatures**: upper left) original c_p and λ , upper right) $1/10 c_p$ and original λ , lower left) original c_p and $1/5 \lambda$, and lower right) $1/10 c_p$ and $1/5 \lambda$.

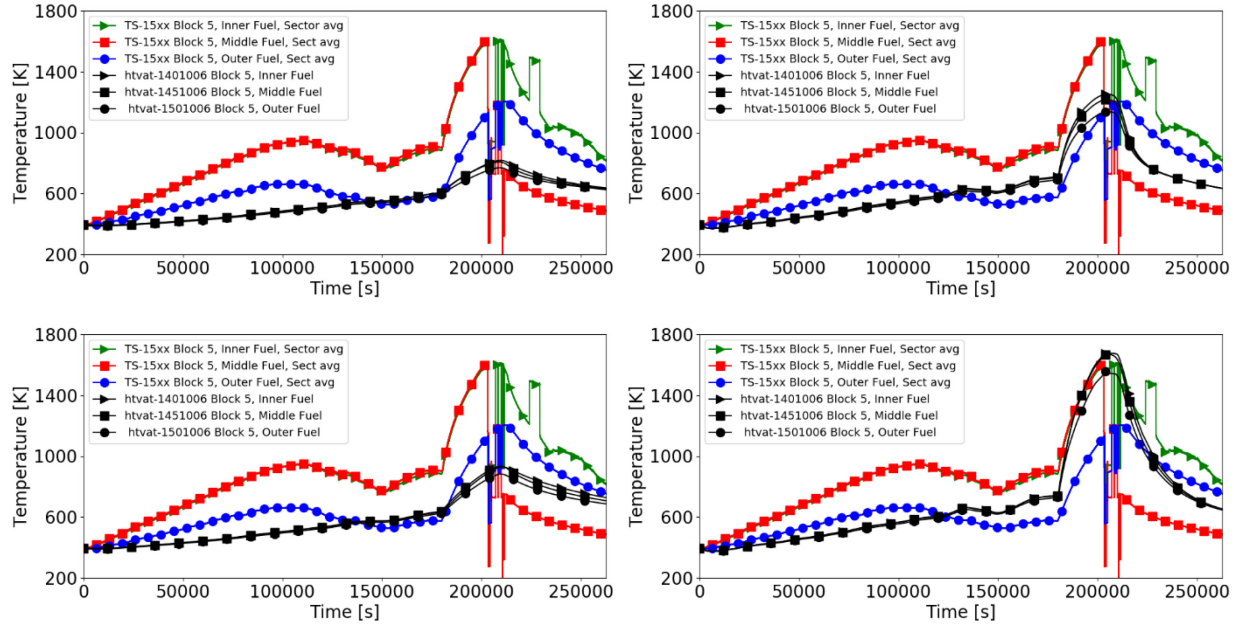


Figure 56. Whole transient, 15 g/s helium mass flow, **middle of the core (block 5) ceramic temperatures in the fuel region**: upper left) original c_p and λ , upper right) $1/10 c_p$ and original λ , lower left) original c_p and $1/5 \lambda$, and lower right) $1/10 c_p$ and $1/5 \lambda$.

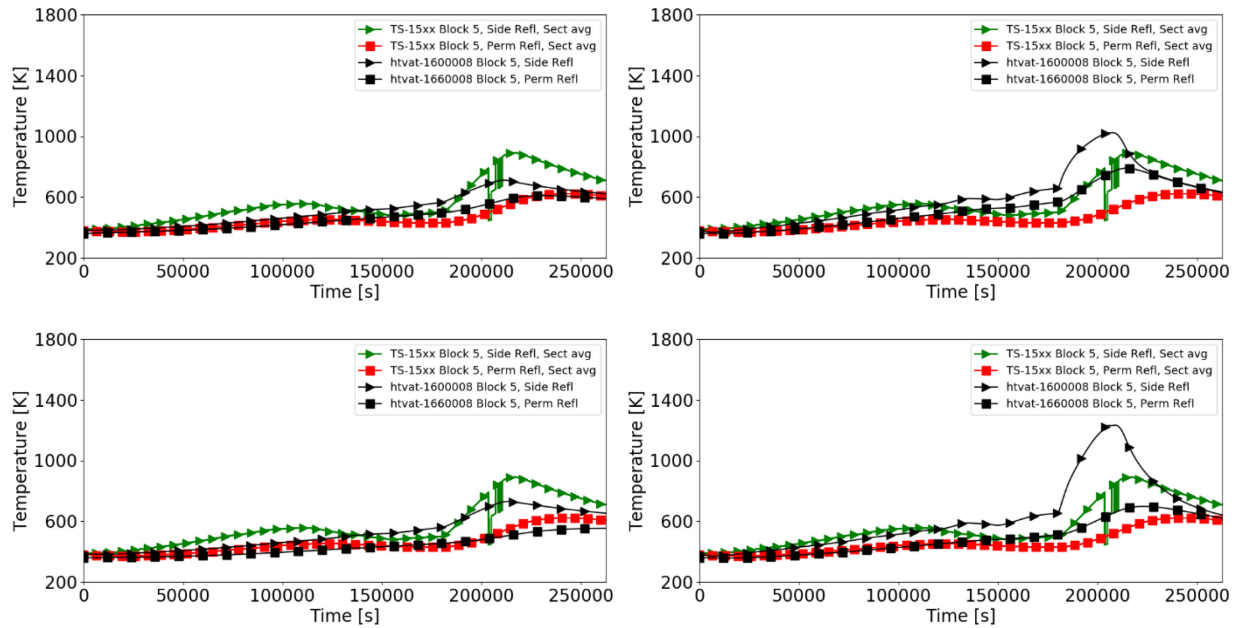


Figure 57. Whole transient, 15 g/s helium mass flow, **middle of the core (block 5) side and permanent ceramic temperatures**: upper left) original c_p and λ , upper right) $1/10 c_p$ and original λ , lower left) original c_p and $1/5 \lambda$, and lower right) $1/10 c_p$ and $1/5 \lambda$.

4.4.2 RCCS Heat Evacuation

The second sensitivity investigated was with respect to the energy evacuated by the RCCS. During the DCC, the steam generator is not operating, and the only possibilities of heat removal are through the RCCS or through direct convection from the metal structures (vessels and piping) to the environmental air. The measured RCCS water inlet and outlet temperature data indicates that very little heat has been evacuated through the RCCS (the water temperature difference across the RCCS is zero, see Figure 6) while the RELAP5-3D calculations indicate some heat removed by the RCCS. It is suspected that during the test, some heat was removed through natural convection in the air cavity between the primary vessel and the RCCS panels. This heat removal is not captured in the measured data since it escaped through the top of the cavity (this is not airtight) before being transferred to the RCCS.

This section compares the 15 g/s helium mass flow rate base case “whole transient” with a calculation that sets the RCCS water flow rate to zero to see the effect of heat removal through the RCCS on the DCC portion of the transient. Figure 58 through Figure 60 compare the RCCS water mass flow, the helium core inlet temperatures, and selected core ceramic temperatures for these two cases. The following observations are made:

- During the DCC, the riser helium temperature does not cool as fast when the RCCS is shut off (see Figure 59). This indicates that a little less energy is evacuated through the primary vessel wall than expected.
- No noticeable change in solid temperatures can be observed (see Figure 60). This confirms the hypothesis that the RCCS is not evacuating a significant amount of heat. It appears that, during the DCC, heat just goes radially into the side reflectors to equalize temperatures in the core while heat very slowly leaves the system through leakage to the environment (it cannot go through the steam generator or through the RCCS).
- It is not shown here, but there is no change in solid temperatures when the RCCS is shut off and the thermal properties of the core ceramics have been reduced. Even the higher structure temperatures with the lower properties do not lead to a significant amount of heat transported to the RCCS.

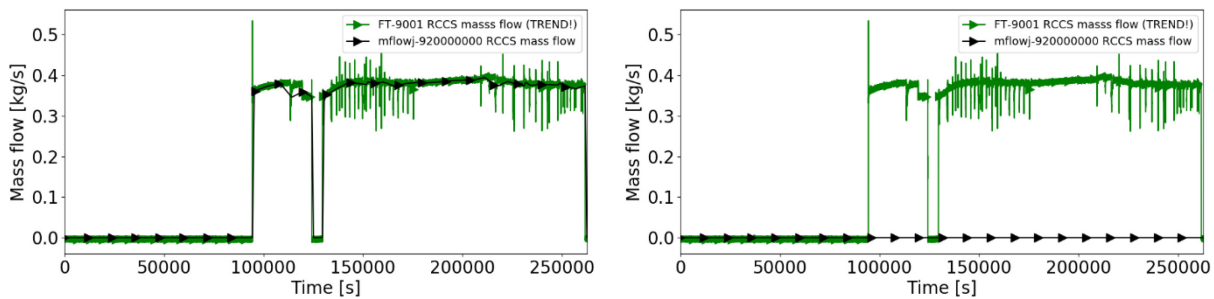


Figure 58. Whole transient, 15 g/s helium mass flow, **RCCS mass flow**: left) base case and right) “no RCCS” case.

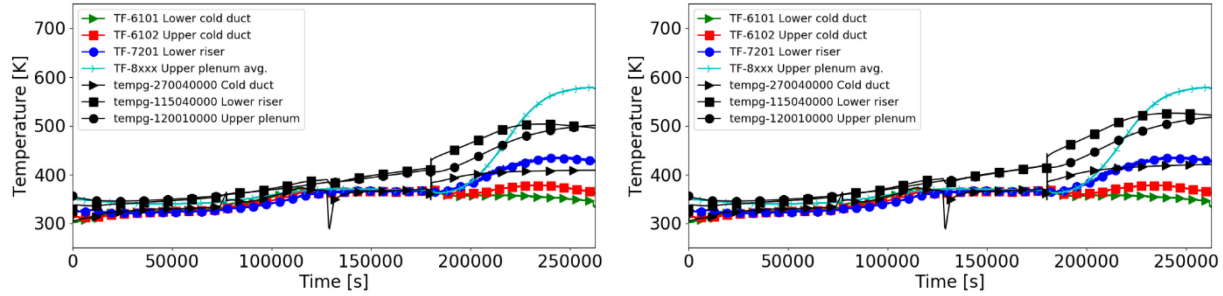


Figure 59. Whole transient, 15 g/s helium mass flow, **helium core inlet temperatures**: left) base case and right) “no RCCS” case.

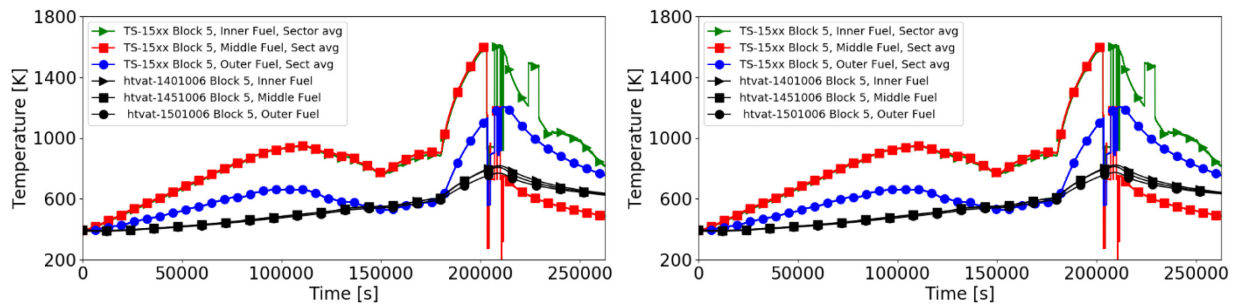


Figure 60. Whole transient, 15 g/s helium mass flow, **middle of the core (block 5) ceramic temperatures in the fuel region**: left) base case and right) “no RCCS” case.

4.4.3 Primary Loop Helium Friction

The last sensitivity investigated was with respect to the helium friction in the primary loop. During the discussion of the base calculations, it was suspected that the friction in the primary loop might be underestimated, since two natural convection flow path are established in the RELAP5-3D simulations (a) lower (outlet) plenum → upper hot duct → RCST → lower hot duct → lower outlet plenum and b) a reverse natural convection through the core (i.e., RCST → Cold duct → Core → Hot duct → RCST) that has not been observed during the test. The pressure drop in the core was measured during the test, but, since the flow rate is unknown, the friction factors that would lead to the measured pressure drop are also unknown.

This section compares two base cases (“whole transient” 5 g/s and 15 g/s helium mass flow) with cases where the friction has been amplified to match the measured value. It is assumed that most of the friction happens in the core and some happens in the hot duct. It is worth noting that different friction factors need to be used for the 5 g/s and 15 g/s cases to match the measured core pressure drop. Figure 61 through Figure 66 show comparisons of the core pressure drop and the helium mass flow rates and, as an example, the middle of the core helium temperatures. The following observations are made:

- The added friction reduces the natural convection observed in the base cases during the DCC portion of the transient. Since a larger friction factor was added to the 5 g/s case compared to the 15 g/s case (to match the measured core pressure drop during the heat up phase where the blower was running), the reduction of natural convection in the 5 g/s case is also larger compared to the 15 g/s case. In fact, natural convection through the core completely vanishes in the 5 g/s case where it is still present at a reduced rate (compared to the base case) in the 15 g/s case. Both cases

show reduced (but not eliminated) natural convection through the hot duct compared to the respective base cases.

- Helium temperatures in the core do not change noticeably between the base cases and the added friction cases. As shown previously, natural convection and heat loss through the vessel walls is not a major contributor to the core temperature distribution during the investigated phase of the DCC transient.

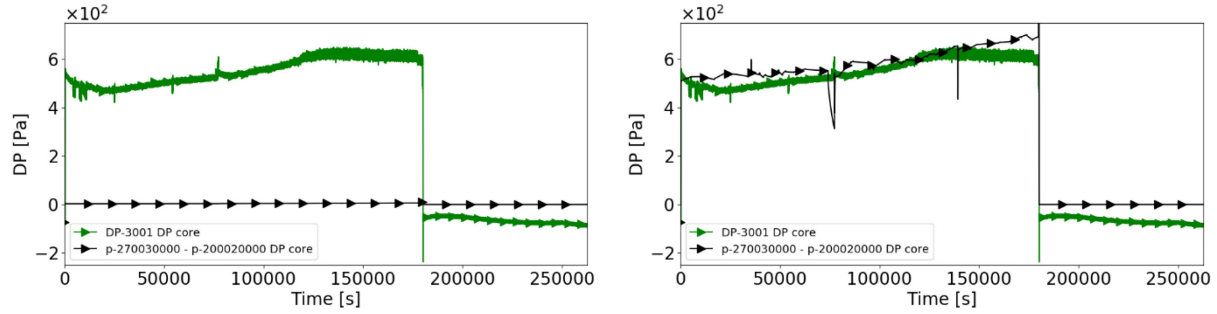


Figure 61. Whole transient, 5 g/s helium mass flow, **core pressure drops**: left) base case and right) “more friction” case.

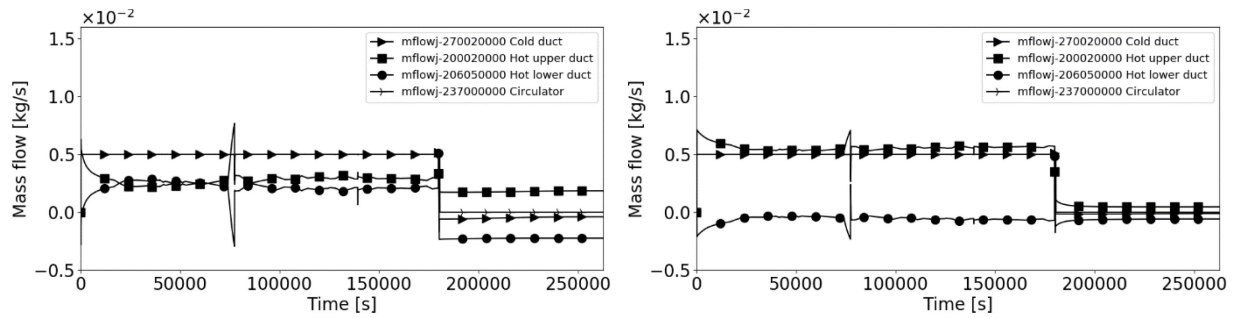


Figure 62. Whole transient, 5 g/s helium mass flow, **PCS helium mass flow rates**: left) base case and right) “more friction” case.

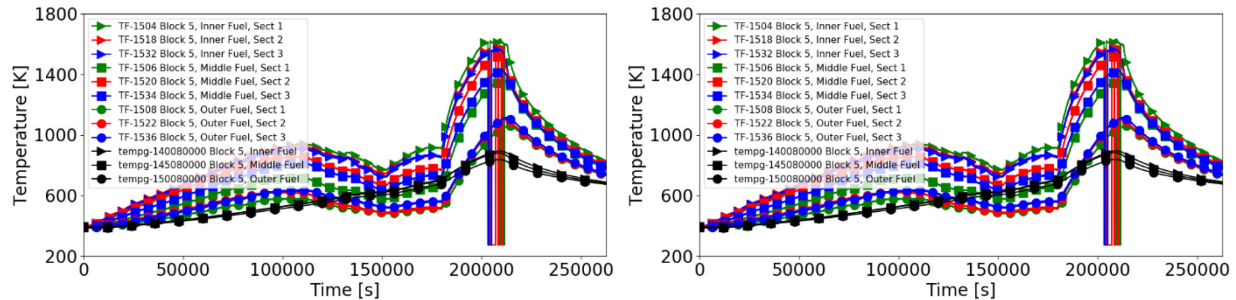


Figure 63. Whole transient, 5 g/s helium mass flow, **middle of the core (block 5) helium coolant temperatures**: left) base case and right) “more friction” case.

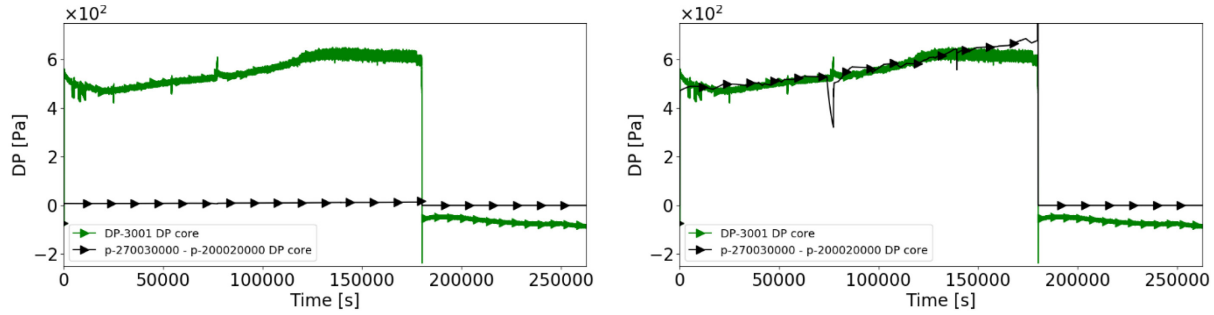


Figure 64. Whole transient, 15 g/s helium mass flow, **core pressure drops**: left) base case and right) “more friction” case.

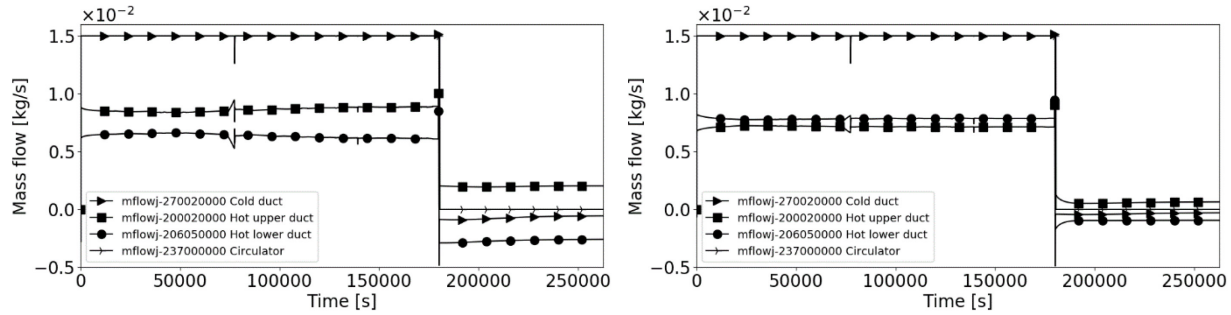


Figure 65. Whole transient, 15 g/s helium mass flow, **PCS helium mass flow rates**: left) base case and right) “more friction” case.

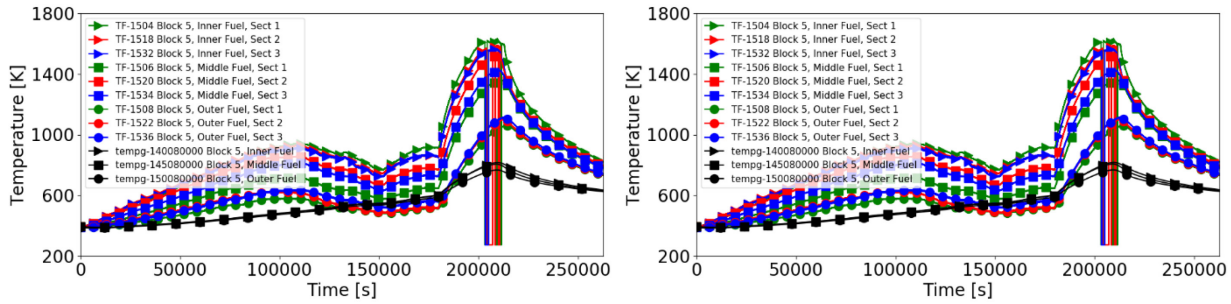


Figure 66. Whole transient, 15 g/s helium mass flow, **middle of the core (block 5) helium coolant temperatures**: left) base case and right) “more friction” case.

5. Conclusions

This section summarizes the findings and main conclusions drawn in the result sections above. For the modeling of the HTTF PG-26 test with RELAP5-3D, the following conclusions are drawn:

- Using the base model (i.e., Paul Bayless’ quality-controlled model in conjunction with the “split hot duct”) predicts a countercurrent helium flow in the hot duct observed at the beginning of the DCC, but, instead of going into a molecular diffusion mode, the RELAP5-3D model predicts the onset of natural convection through two different flow paths (recirculating flow between the outlet plenum and RCST and minimal reverse natural convection through the core). Increasing friction in the core and

hot duct prevents the natural convection from happening in some of the simulations. It is worth mentioning that constant friction factors have been used in the presented simulations which assumes that the friction underprediction in RELAP5-3D compared to measured data solely comes from abrupt area changes (misaligned core blocks, etc.) that are not represented properly in the model. It would be interesting, as part of future work, to investigate the effect of enhanced Reynolds number dependent friction. However, natural convection is not the main means of heat evacuation during the DCC transient, and calculation results with and without onset of natural convection show similar core temperature evolutions.

- Better facility characterization is needed before final conclusions can be made on phenomena during the DCC. In particular, the establishment of natural convection strongly depends on helium density differences and, therefore, temperature differences in the system as well as friction resistances in the different flow path. Therefore, in addition to the measurements of pressure drops along the flow path, it would be helpful to also know the primary helium mass flow rate.
- Although some temperatures were well predicted, the general tendency was to underpredict the ceramic and helium temperatures and heat removal rates during the DCC, resulting in many of the assessment findings being in minimal or insufficient agreement with the data. It is worth mentioning that temperatures during the heat-up portion of the transient are generally overpredicted if a steady state is calculated and underpredicted if the full heat-up transient is calculated. This indicates that heat stored in the core is not at steady-state conditions in the test and modeling the heat-up transient should lead to better predictions of the core state before the DCC start. Reducing the thermal properties (specific heat capacity and thermal conductivity) of the core ceramics leads to a better prediction of the temperature peaks and cooling rates during the DCC. However, none of the performed calculations and sensitivities predicted the radial temperature distribution as measured in the core.
 - It appears the energy balance in the core during the heat-up and DCC is not properly captured. Although the measured data is of high quality, there is not enough information to understand how much energy enters and leaves the system, and how much energy is stored in the structures. With no helium flow data, it is impossible to determine whether the problem lies with the input model (e.g., material properties, modeling choices) or with the code models (heat transfer coefficients).
 - Facility characterization data would be useful in improving and validating the input model. While the facility geometry is well known, parameters such as loop friction and material properties (in particular the core ceramic thermal properties) are not. The modeling approach used for the core blocks has not been used before with RELAP5-3D. Facility characterization data is needed to determine the appropriate values to use for parameters such as material emissivities and the region of influence of the reflector cooling holes. Those data are also needed to determine if the model discretization adequately captures the important phenomena in the test facility, namely the peak ceramic temperatures.
 - One model limitation that could be lifted in future modeling efforts is the thermal stratification apparent in the outlet plenum and hot duct during the heat-up. This is not something that a system code such as RELAP5-3D is able to model with 0D components. The 3D component might improve the phenomena prediction capability of the model in these regions.
- It is worth noting that the described discrepancies between measured data and RELAP5-3D predictions are not RELAP5-3D code limitations. They reflect limitations in boundary condition and thermal property knowledge. There is not enough information to exactly model what happens during the heat-up (helium leak from PCS into the RCST, injection of cold helium into the PCS, manual depressurization of the PCS/RCST). As mentioned, the energy balance is not known (i.e., the energy redistributing in the core or the amount of heat leaving the system through the possible different heat paths, such as the steam generator, RCCS, or leakage to environment, is not known). For example, helium mass flow rates are not measured, the amount of steam produced is not measured, and the

energy going out through the RCCS is measured as zero, but it is likely that heat escapes through the air volume in between the vessel and the RCCS, etc. In addition, having a significant uncertainty in the thermal property data allows too many variables (i.e. too many parameters to make reliable conclusions on the physical phenomena happening during the DCC).

- While the RELAP5-3D calculations of the test provide some insights into what happens during the transient, and point to missing or potentially uncertain data to which the experimenters can direct their attention, the principal conclusion is that the PG-26 test data are insufficient for a system code assessment. There is not enough information to model the heat-up of the facility and there was no steady-state before the DCC started so it is impossible to determine the conditions at the beginning of the gas exchange phase. Since the natural circulation and molecular diffusion processes are driven by coolant temperature and density differences, not knowing the heat stored in the core nor knowing the friction coefficients in the loops makes it hard to draw an accurate conclusion.

6. References

1. Woods, Brian G. 2017. "OSU High Temperature Test Facility Technical Design Report." OSU-HTTF-TECH-003-R1, Rev. 1, Oregon State University.
2. RELAP5-3D development team. 2018. "RELAP5-3D Code Manual, Volumes I-V." INL/MIS-15-36723, Rev. 4.4, Idaho National Laboratory.
3. Cadell, Seth R. 2019. "PG-26 Low Power (<350kW) Double Ended Inlet-Outlet Crossover Duct Break, 2 Heaters." OSU-HTTF-TAR-026-R0, Oregon State University.
4. Bayless, Paul D. 2018. "RELAP5-3D Input Model for the High Temperature Test Facility." INL/EXT-18-45579, Idaho National Laboratory.
5. Stone & Webster Engineering Corp. 1986. "Preliminary Safety Information Document for the Standard MHTGR." HTGR-86-024, Department of Energy.
6. Stephen C. 2018. "Instrumentation Plan for the OSU High Temperature Test Facility, Revision 4." OSU-HTTF-TECH-002-R4, Rev. 4, March 2018.
7. JAERI et al. 1993. "2D/3D Program Work Summary Report." NUREG/IA-0126, GRS-100, and MPR-1345, prepared jointly by Japan Atomic Energy Research Institute, Gesellschaft fuer Anlagen-und Reaktorsicherheit, Siemens AG, UB KWU, U.S. Nuclear Regulatory Commission, Los Alamos National Laboratory, and MPR Associates, Inc.
8. Richard R. 1993. "International Code Assessment and Applications Program: Summary of Code Assessment Studies Concerning RELAP5/MOD2, RELAP5/MOD3, and TRAC-B", NUREG/IA-0128, EGG-EAST-8719, Nuclear Regulatory Commission.
9. U.S. Nuclear Regulatory Commission. 1988. "Compendium of ECCS Research for Realistic LOCA Analysis." NUREG-1230, Nuclear Regulatory Commission.